Proceedings

11th International Workshop on Radiation Safety at Synchrotron Radiation Sources

ESRF - Grenoble - France
30 May - 2 June 2023

Table of Contents

The ESRF Extremely Brilliant Source (EBS)

Berkvens P., Colomp P.

ESRF, 71, avenue des Martyrs, 38000 Grenoble, France

Abstract

On 10 December 2018, after 25 years of User Service Mode Operation, the ESRF X-ray source was shut down for an upgrade to a brand-new storage ring, the Extremely Brilliant Source (EBS). Less than 12 months later, on 2 December 2019, the first electrons were injected in the new storage ring and 4 days later, on 6 December, the first beam was stored. On 28 February 2020, the design value of 200 mA stored beam in the new EBS storage ring was reached for the first time. User Service Mode resumed on 25 August 2020, essentially six months ahead of schedule.

The present paper briefly recalls the radiation protection challenges of the new storage ring with respect to the old one and gives an overview of the results from radiation measurements during the new storage ring commissioning and the now almost three years of User Service Mode. The results of these radiation measurements are compared with the results of the radiation shielding study for the EBS storage ring.

1 Introduction

As part of the phase 2 upgrade of the ESRF, the original storage ring was replaced by the new EBS (Extremely Brilliant Source) storage ring. Replacing the old double bend achromat by a novel hybrid 7-bend achromat resulted in a drastic reduction of the horizontal emittance: from 4000 pm·rad for the original lattice down to 150 pm·rad for the EBS. At the same time, an important reduction in the lifetime of the stored beam is expected, due to increased Touschek interactions: the design lifetime for the new lattice in 16-bunch mode, the most constraining filling pattern in terms of beam losses, was 1.8 h, compared to 16 h for the original machine. In order to cope, from a radiation protection point of view, with these increased beam losses, two dedicated beam loss collimators were designed and installed in the new storage ring, in order to concentrate more than 80 % of the beam losses in these two, over-shielded areas. A dedicated shielding assessment study, using the Monte-Carlo code FLUKA [1], has been carried out. The results of this study confirmed that with the installation of the two beam loss collimators, the expected dose estimations for the EBS facility were as low as for the original machine, therefore showing that the ESRF radiation protection policy remained valid for the new source (nobody working at the ESRF should be classified as radiation worker, by guaranteeing of the 4-hours derived dose limit of 2 μSv in all areas accessible during operation).

The commissioning of the new storage ring started on 2 December 2019. First beam storage occurred on 6 December 2019 and the nominal 200 mA stored beam current was first reached on 28 February 2020. From a radiation protection point of view, until the end of February 2020, we guaranteed the monthly dose limit for non-exposure (80 mSv). Access to the experimental hall was only authorised for staff members and for a limited number of contractors, permanently on site. From 1 March 2020, the 4-hours dose limit of 2 μSv was again guaranteed everywhere, which corresponded with respect to the French Nuclear Safety Authorities to the official end of the EBS storage ring commissioning.

The present paper describes a number of radiation measurements carried out during the first two and a half years of operation of the EBS, which are used to validate the results of the shielding assessment study.

2 Dose rates in standard cells during beam decay

From the FLUKA simulations, an effective dose rate on the roof of the storage ring tunnel of 1 $nSv \cdot h^{-1}$ was obtained during the decay of a 196 mA stored beam with 20 h of lifetime (see Figure 1, corresponding to the dose rates for a 92 mA stored beam with 1.8 h lifetime).

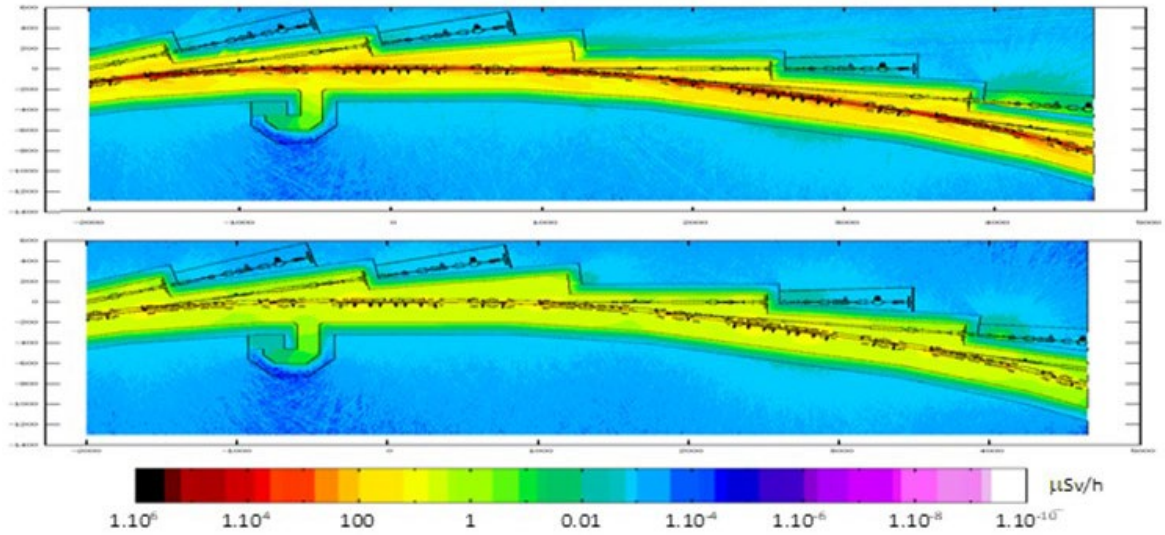

Figure 1: calculated total (top) and neutron (bottom) effective dose rates on the storage ring tunnel roof for the standard cells, during a 92 mA, 1.8 h lifetime, beam decay.

This value was calculated for the 29 standard cells, i.e. the cells other than those with the beam loss collimators and the injection cell. To validate this value, the integrated neutron doses from the corresponding 116 neutron monitors installed on the roof of the storage ring tunnel (4 per unit cell) were recorded during five 6-day user operation weeks, from 1 August to 6 October 2020. In the case of beam dumps during these periods, the corresponding measured neutron doses were subtracted. For each of the individual neutron monitors a value for the measured neutron background dose rate was obtained during the shutdown period preceding the machine run (see Figure 2). Figure 3 shows the distribution obtained for the 5-days average net effective dose rate, for the 580 individual measurements (5 periods × 116 neutron monitors). A Gaussian distribution is obtained with an average value of 1.1 $nSv \cdot h^{-1}$ and a standard deviation of 3 $nSv \cdot h^{-1}$. These measured values are clearly in good agreement with the predicted calculated value. It is also interesting to note that an average value of 11 $nSv \cdot h^{-1}$ was obtained for the neutron background, which corresponds very well to values given in the literature.

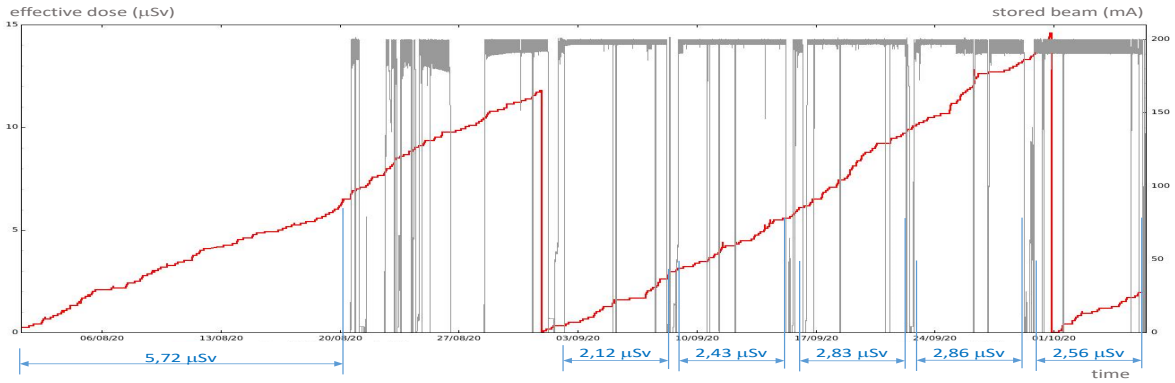

Figure 2: example of the integrated doses from one of the 116 neutron monitors on the storage ring tunnel during the concerned period.

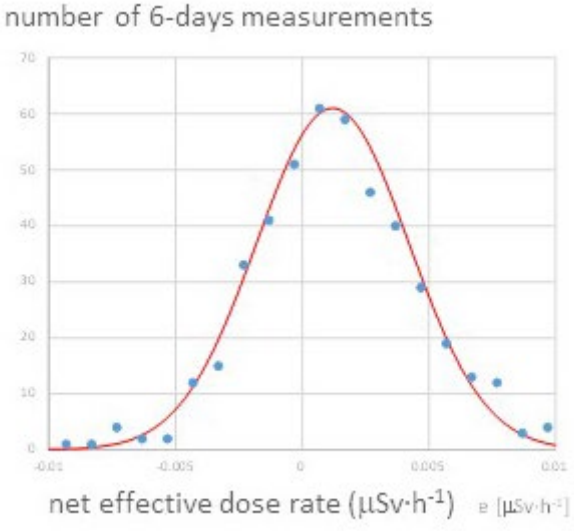

Figure 3: distribution obtained for the 5-days average net effective dose rate, for the 580 individual measurements.

3 Dose rates around the beam loss collimator cells

As mentioned before, more than 80 % of the beam losses are concentrated on the two dedicated beam loss collimators. Thanks to the installation of local shielding around the collimators, the dose rates outside these special cells remain compatible with the non-exposed worker status of the people working there. To validate the results of the shielding study, we use the doses integrated on the storage ring roof above these collimators during two 6-days user mode operation periods in April 2023. Figure 4 shows the integrated doses for the two collimators. During both periods, an average beam of 196 mA was stored with a lifetime of 24 h. During the first period, 5.66 µC were injected in the storage ring, with an average injection efficiency of 56 %; during the second period, 5.68 µC were injected in the storage ring and the average injection efficiency was 60 %. During the first period, a neutron dose of 3.05 µSv was integrated on the neutron monitor on the storage ring roof above the first collimator and a neutron dose of 2.56 µSv for the neutron monitor above the second collimator. For the second period, the corresponding neutron doses were 2.67 µC and 3.24 µC respectively.

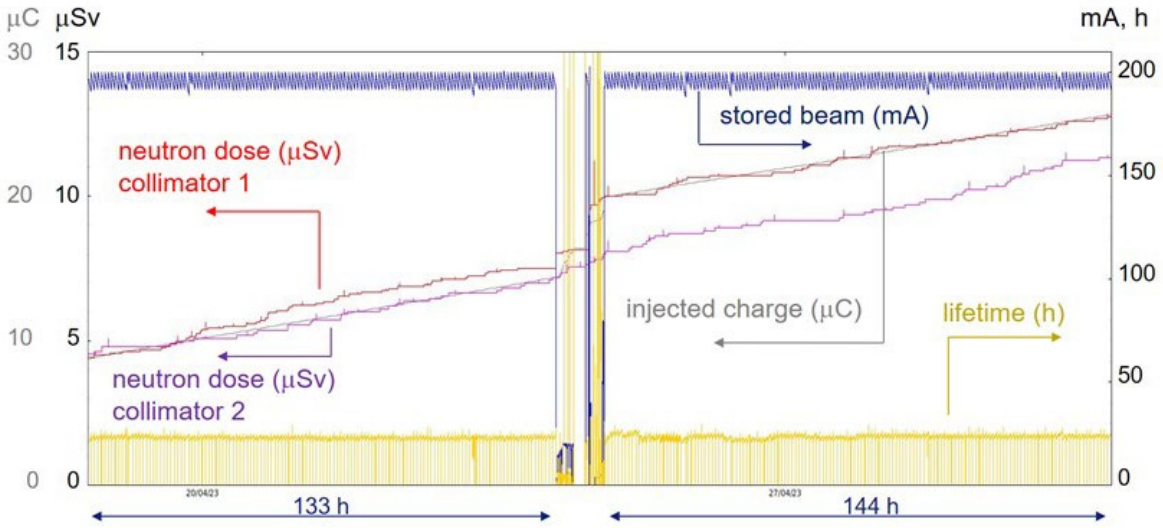

Figure 4: Neutron effective doses measured by the neutron monitors on the storage ring tunnel roof above the collimators, during two user mode operation periods.

These neutron doses were accumulated during beam decay and during injection, together with the contribution from natural background radiation. We use the results of the FLUKA simulations to calculate the expected integrated dose from the first two contributions.

Figure 5 shows the calculated dose rates above the storage ring roof, during stored beam losses. The results correspond to a stored beam of 92 mA and a lifetime of 1.8 h. At the location of the neutron monitors above the collimators, a dose rate of 0.05 $\mu Sv \cdot h^{-1}$ is calculated, corresponding to a value of 0.0082 $\mu Sv \cdot h^{-1}$ for a 196 mA, 24 h lifetime beam. The integrated neutron dose due to beam decay losses therefore corresponds to 1.063 $\mu Sv \cdot h^{-1}$ for the first period (133 h) and 1.150 $\mu Sv \cdot h^{-1}$ for the second period (144 h).

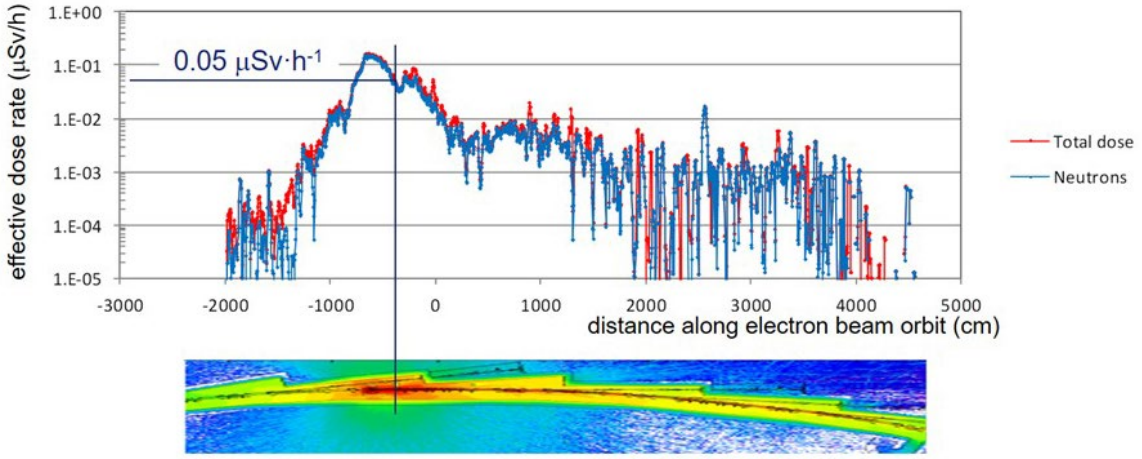

Figure 5: Calculated effective dose rates on the storage ring tunnel roof, above the beam loss collimators during a 92 mA, 1.8 h lifetime beam decay.

Figure 6 shows the calculated dose values above the storage ring roof, integrated due to injection losses. The results correspond to a full 200 mA injection with 50 % injection efficiency. Above the collimators, a value of 0.045 µSv is obtained. This corresponds to an integrated dose during injection of 0.21 µSv for the first period and of 0.22 µSv for the second period.

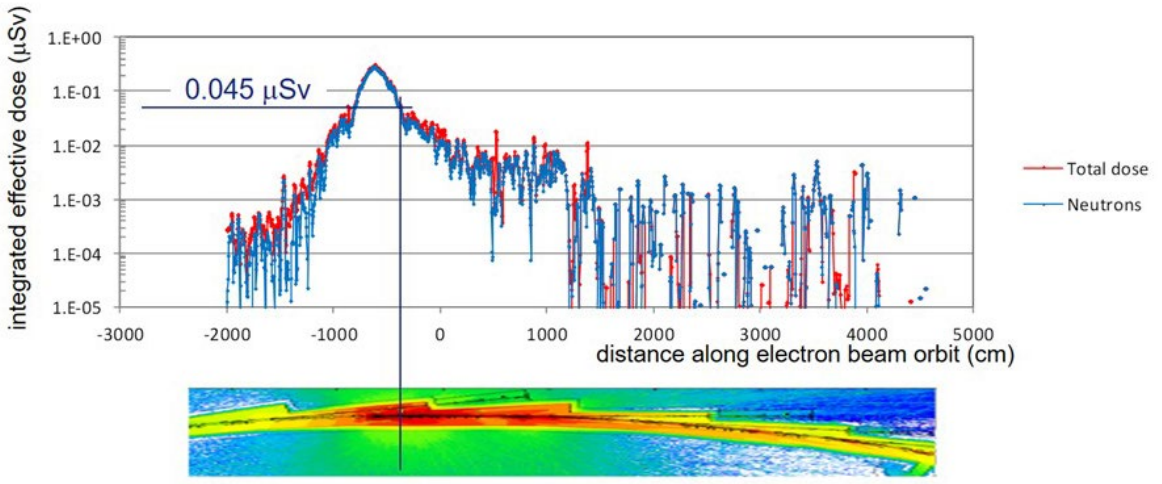

Figure 6: Calculated effective doses on the storage ring tunnel roof, above the beam loss collimators, during a 200 mA injection, with 50 % injection efficiency.

Finally, we use the value of 11 $nSv \cdot h^{-1}$ mentioned above to obtain a value for the integrated neutron dose due to natural background. We obtain an integrated dose of 1.463 µSv for the first period and an integrated dose of 1.584 µSv for the second period.

Table 1 summarises the different calculated values and the measured values. As one sees, we again obtain a very good agreement between the calculated and the measured values. This confirms the validity of the dose calculations and the reliability of the beam loss calculations used as input for the FLUKA calculations.

FLUKA model			Measurements	
	1st week	2nd week	1st week	2nd week
background (0.11 $nSv \cdot h^{-1}$)	1.463 µSv	1.584 µSv		
dose during decay	1.062 µSv	1.150 µSv		
dose during injection	0.210 µSv	0.217 µSv		
total neutron dose on tunnel roof	**2.735 µSv**	**2.951 µSv**	collimator 1: 3.05 µSv collimator 2: 2.56 µSv average: **2.81 µSv**	collimator 1: 2.67 µSv collimator 2: 3.24 µSv average: **2.95 µSv**

Table 1: summary of the measured and calculated neutron effective dose values on the storage ring tunnel roof, above the beam loss collimators.

4 Stored beam dumps

We finally look at the neutron doses above the beam loss collimators in case of a stored beam dump. We actually use the results from deliberate beam dumps, obtained by scraping the beam with one of the beam loss collimators. In this way, the interpretation of the measured integrated dose is not complicated by the correction for pulsed radiation efficiencies of the monitors.

Figure 7 shows the measured integrated doses above the first collimator, used to kill a stored beam of 186 mA and 61 mA respectively. In the first case, we get an integrated neutron effective dose of 0.96 µSv, in the second case we obtain an integrated dose of 0.31 µSv.

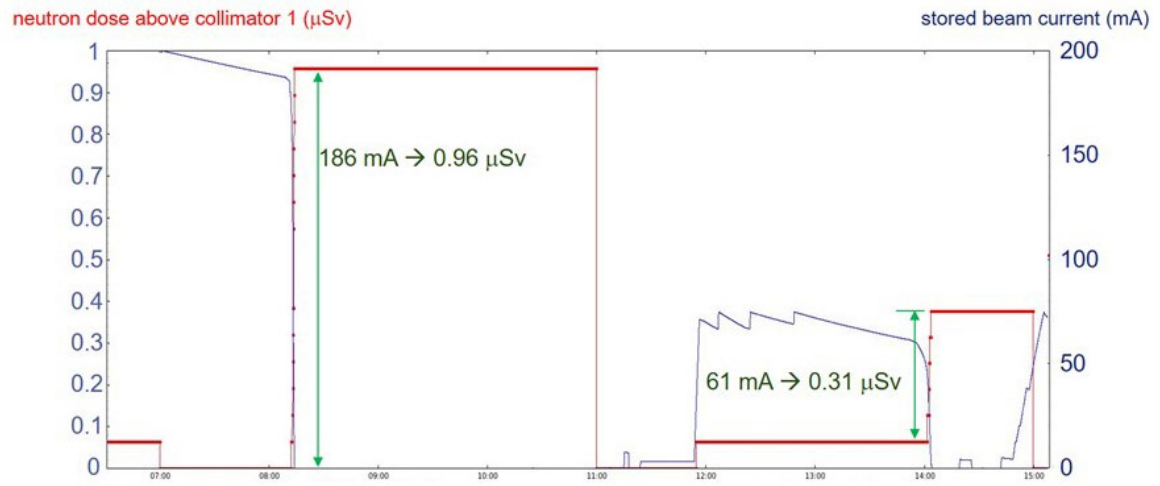

Figure 7: Neutron effective doses measured by the neutron monitor on the storage ring tunnel roof above the first collimator during two stored beam dumps, using scraping by the corresponding beam loss collimator.

Figure 8 shows the calculated doses on the storage ring roof above the collimators, integrated during a 200 mA beam dump, with 50 % of the losses on each of the collimators. A value of 0.5 µSv is obtained at the location of the neutron monitors above the collimators. This value corresponds, in the case of 100 % losses on the collimator, as occurs during the scraping down of the stored beam, to an integrated dose of 0.96 µSv for a 186 mA dump and an integrated dose of 0.305 µSv for a 61 mA beam dump. Again, these values are in very good agreement with the measured values.

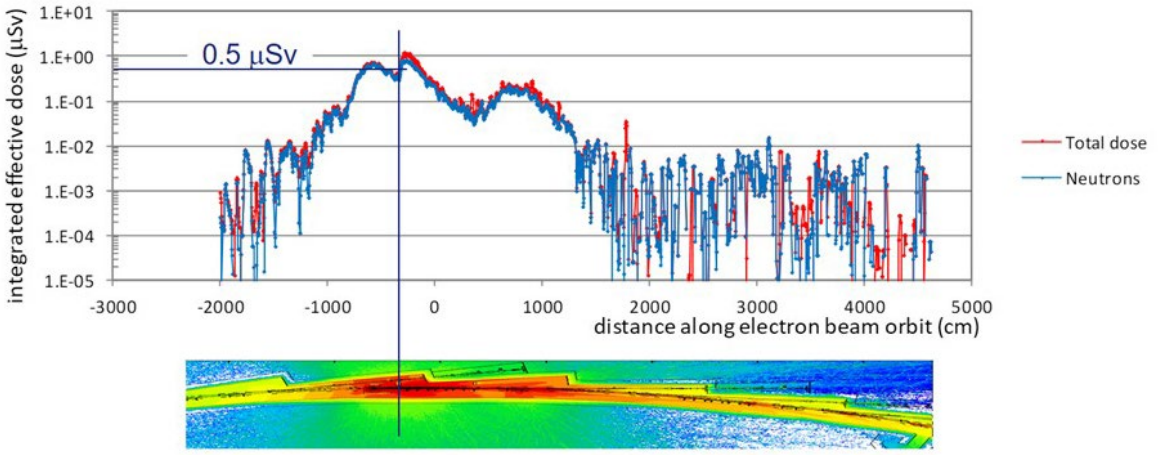

Figure 8: Calculated effective doses on the storage ring tunnel roof, above the beam loss collimators during a 200 mA beam dump, with 50 % losses on each of the two collimators.

5 Summary

The shielding assessment study for the new EBS storage ring showed that the operation of this new facility should be compatible with the existing ESRF non-exposure radiation protection policy, thanks to the installation of two, locally shielded, dedicated beam loss collimators. After nearly three years of operation of the EBS storage ring, the beam loss assumptions and shielding calculations have been conformed.

References

[1] - *"FLUKA: a multi-particle transport code",* A. Ferrari, P.R. Sala, A. Fasso`, and J. Ranft, CERN-2005-10 (2005), INFN/TC_05/11, SLAC-R-77.

Radiation Shielding Calculations for the ALS Upgrade Project

Trovati S., Liang T.*

Lawrence Berkeley National Laboratory, 1 Cyclotron Road, Berkeley CA-94720, USA
*Deutsches Elektronen-Synchrotron, Notkestraße 85, 22607 Hamburg, Germany

Abstract

The Advanced Light Source (ALS) at the Lawrence Berkeley National Laboratory is undergoing an upgrade (ALS-U), which will result in the production of much brighter and highly focused X-ray beams. The storage ring will be completely replaced by a new 9-bend achromat ring and an accumulator ring will be added to the accelerator chain. The increase in stored-beam losses due to the substantial decrease in beam lifetime, and the addition of the accumulator ring and new transfer lines, will change the dose intensity and distribution outside the shielding. ALS-U has planned to retrofit all the ratchet walls with floor-to-ceiling lead panels and to increase the thickness of the roof blocks above the injection sectors during the so-called dark time, when the current storage ring will be decommissioned and replaced with the new one.
Shielding retrofit at the ALS is challenging, due to existing space constraints and the additional infrastructure needed for the accumulator ring and the new storage ring.
This study deals with the radiological impact of the upgrade. Methods and results of the analysis performed to assess existing and planned accelerator shielding against the new electron beam parameters and losses, and to provide new requirements, are presented.
The results show that, in general, the planned retrofit of all ratchet walls is adequate to attenuate the dose below the legal requirements and the design goals set in the ALS-U shielding policy. Only the injection and collimation sectors will require additional shielding to mitigate the dose outside the walls and on the roof. Additional controls will be needed to limit the access to the roof in those sectors where a retrofit is not planned.

1 Introduction

1.1 From ALS to ALS-U: Changes in Radiological Risks

With the upgrade several changes will affect the intensity and distribution of the radiation sources in the ALS complex. The small energy increase of the electron beam from 1.9 GeV to 2 GeV will mainly affect the radiation at the beamlines.

An accumulator ring (AR) will be added to the injection chain, in between the booster and the storage ring (SR), to replenish the depleted electron bunches. It will be installed in the SR tunnel, at 40 cm from the ceiling and with a distance from the inner wall that varies between 30 cm and 60 cm, making it an important source for radiation exposure on the SR roof and in the SR pit.

A new SR will replace the existing one: all the arcs will go from triple-bend to nine-bend achromat and 2 new full-length insertion devices will be installed, becoming the synchrotron radiation sources of 2 completely new beamlines.

In order to connect SR and AR two new transfer lines will be added and the existing booster-to-storage ring transfer line will be modified to connect the booster to the AR.

All bend-magnet beamlines will be re-aligned to follow the change in source location, due to the new lattice and the existing ID beamlines that will not be upgraded will need to operate at larger gaps to withstand the increased beam power in their front-ends. In Figure 1 a pictorial comparison between the current and future facility shows the additional AR and transfer lines (top), the location of the AR on the inner walls and the new 9-bend achromat (middle) and the reduced emittance size (bottom).

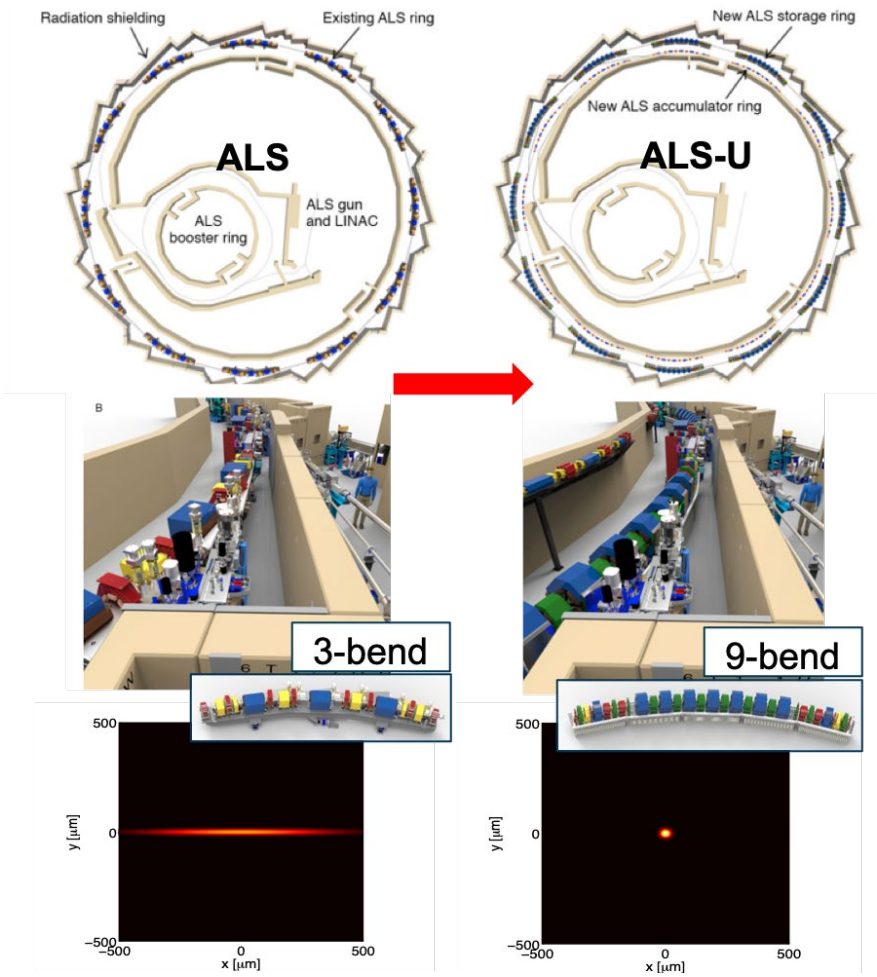

Figure 1: Summary figure showing on top the ALS facility as of now (left) and after the upgrade (right). In the middle, 3D models of the storage ring tunnel show the triple- and nine-bend achromat arcs and in the view on the right the accumulator ring. The bottom figures represent a cross section of the beam, showing the large reduction of the horizontal size.

The reduced emittance will result in a decreased beam lifetime (0.5 h from 4 h) and nearly 5 times more losses. More injected beam will be necessary to compensate for such losses, resulting in a swap-out incident charge increase, from 1 nC to 30 nC. At the same time, though, the on-axis injection method will drastically reduce injection losses, with an estimated injection efficiency of more than 99%. **Table 1** compares these key parameters for ALA and ALS-U.

Table 1 Comparison of key parameters for ALS and ALS-U

	ALS	**ALS-U**
Electron energy	1.9 GeV	2 GeV

Stored beam current	500 mA	500 mA
Injection efficiency	~50%	≥ 99%
Stored-beam losses	0.5 x 10^{12} electrons/hour	2 x 10^{12} electrons/hour
Swap-out injection shot	1 nC	30 nC

As for the distribution of the SR losses, 4 collimators, installed in the injection area, will intercept about 95% of all normal and abnormal losses, with the exception of the swap-out incident, reducing losses elsewhere to < 5%, and no more than 1% is expected at magnets and insertion devices along the arcs and straights, where there is a change in aperture.

Abnormal loss scenarios will remain the same after the upgrade: swap-out incidents, full-beam losses and injection losses away from the collimators, reduced collimator efficiency, poor vacuum and Touschek lifetime.

After commissioning, the gas bremsstrahlung produced in the SR is expected to be comparable to or less than present one, due to neg-coating of all vacuum chambers. The SR gas bremsstrahlung is shielded with lead or tungsten collimators and stops. The gas bremsstrahlung produced by the AR will be an additional source of radiation to consider for the dose on the experimental floor, as it is mainly directed towards the ratchet walls. All AR stored- and injected-beam losses will mainly be intercepted by 2 collimators and by the injection septum. Touschek loss distributions along one sector (straight section and arc) for all the AR and the SR sectors are shown in Figure 2.

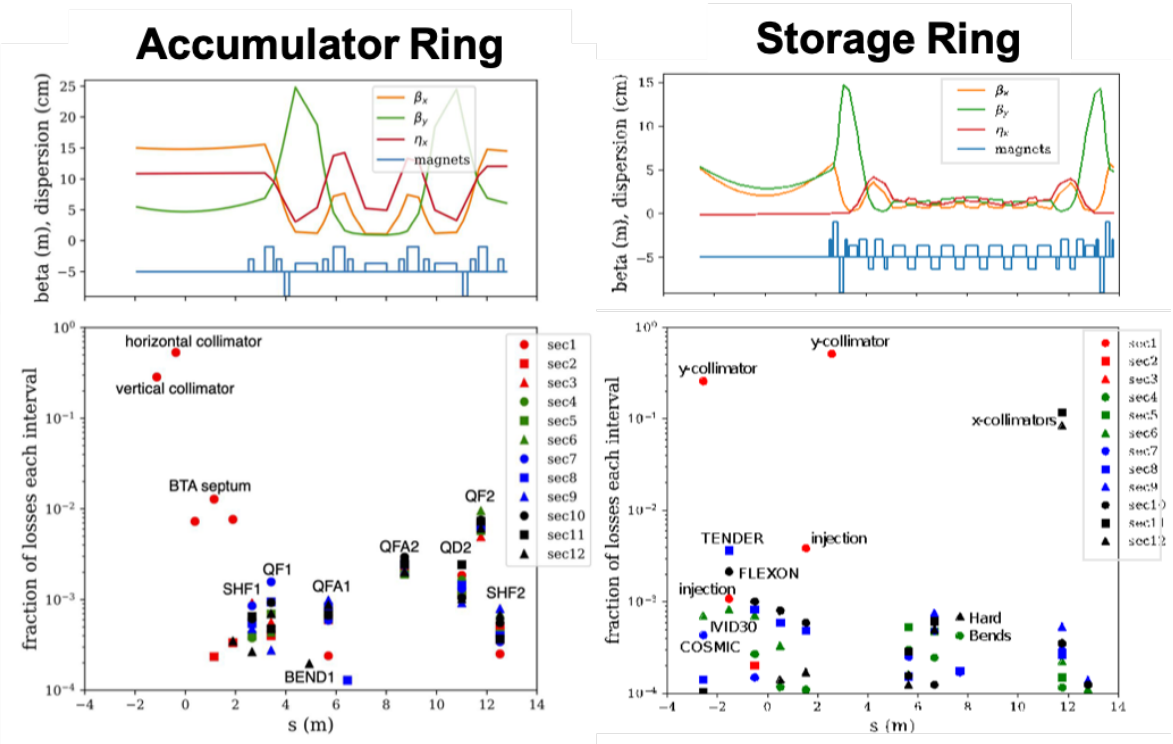

Figure 2: Accumulator ring (left) and storage ring (right) Touschek loss distribution in percentage of the total losses.

1.2 ALS-U Shielding Policy

The ALS-U shielding policy was developed to keep the designation of a low-hazard facility for the ALS, and to ensure that the annual exposure of workers and public is kept well below the regulatory and administrative limits, and as low as reasonably achievable (ALARA). An occupancy factor of 100% is used for the experimental floor and of 50% for the roofs and the inner ring areas. Based on the data collected over many years of ALS

operations, both occupancy factors are deemed to represent a conservative estimate of the actual occupancies.

Considering all the past dosimetry data and the future occupancy factors, the shielding design objectives for the ALS-U are set as follows: ≤ 5 μSv/hour in areas around the accelerators and on the experimental floor, with an ALARA goal of 0.5 μSv/hour, for routine operations; 1 mSv for the whole duration of a mis-steer event; 50 mSv/hour for the maximum credible accident scenario, defined as a credible accident scenario with the maximum or worst-case consequences.

1.3 Existing shielding and planned upgrades

The ALS complex was built at the end of the 1980's under the dome of the Lawrence's 184-inch cyclotron. It has a rather small footprint when compared to most facilities of the same energy range, as it is constrained by the landscape of the Berkeley's hills (Figure 3).

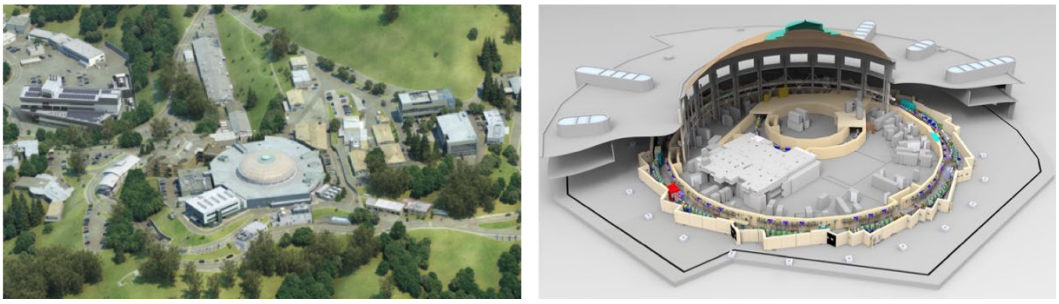

Figure 3: Aerial view of the ALS (left) and a 3D model of the upgraded facility, showing the shield walls of the storage ring and of the injector (right).

With a circumference of 197 m, the SR occupies a tunnel with a width of 4-8 m. Shielding walls (material and thickness) are not standard for all sectors: roof, inner walls and the majority of the lateral ratchet walls are made or concrete (30-60 cm thick), all transition walls and a few lateral ratchet walls have additional floor-to-ceiling lead panels, with variable width. These lead shields are most prevalent in the injection sectors. All transition walls are also equipped with and additional lead band, cantered at beam height, with a thickness that varies between 7.5 and 12.5 cm, depending on the sector (Figure 4).

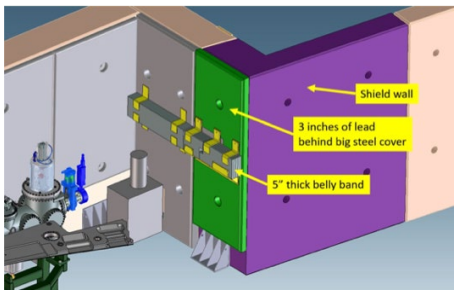

Figure 4: 3D model that shows the layout of most ALS ratchet walls, with lead panels and belly band.

ALS-U is not a green field facility and, given the many space constraints, there is no possibility to expand or rebuild the existing concrete shield walls, but with the upgrade all the ratchet walls will be lined with lead panels. The thickness will vary with location: 5 cm on all lateral walls except those in the injection/collimation sectors that will have 7.5 cm thick panels, and 7.5 cm or 10 cm on transition walls.

More flexibility is possible for the retrofit of the SR roof: the 45 cm–thick blocks will be increased to 60 cm, covering the collimation and the transfer-lines sections, where most losses occur. In all the other sectors the roof will be kept 30 cm thick.

2 Shielding calculations

2.1 Methods

A method that combines Monte Carlo simulations with analytical formulas was used to generate source terms and attenuation lengths. A cylindrical symmetry was used in the FLUKA [1][2] geometry model (Figure 5) to simulate the interaction of a 2 GeV electron beam interacting with 3 representative targets: a collimator, a thick septum and a magnet. For the shielding materials, pure concrete, pure lead, lead followed by concrete and steel followed by concrete were considered. Dose attenuation curves were calculated as a function of the angle with respect to the beam axis.

Region biasing techniques were activated in the simulations to improve the statistics. The cross-talk from neutrons generated in photonuclear (γ,n) interactions at forward angles that can lead to overestimate the neutron source term and to underestimate the attenuation length at larger angles (see Figure 6), was removed by replacing the material at angles 0-30 degrees with a completely absorbing medium ("blackhole") when scoring the dose at angles larger than 30 degrees.

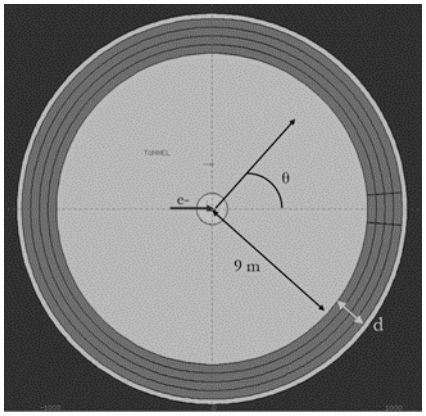

Figure 5 : Cylindrical geometry used in the MC simulations to generate the source terms.

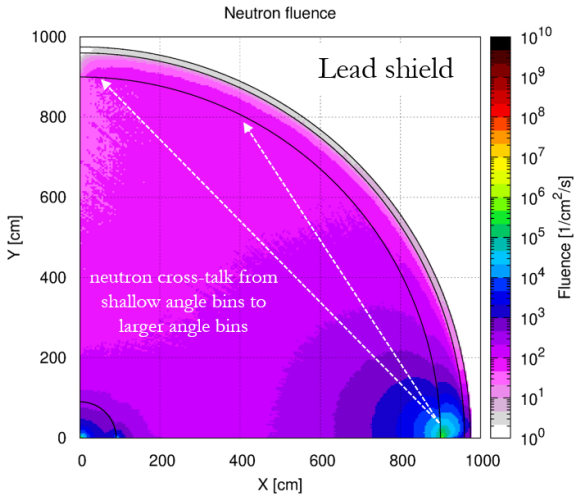

Figure 6 : Neutron cross-talk due to neutrons generated at shallow angles that are back-scattered and transported to larger angles. This leads to an overestimate of the neutron source term and an underestimate of the attenuation length at large angles.

Source terms and attenuation lengths were obtained by interpolating the dose attenuation curves with the general double-exponential function:

$$H(\theta, d, \lambda, r) = \frac{H_1(\theta)}{(r+d)^2}\exp\left[-\frac{d}{\lambda_1(\theta)}\right] + \frac{H_2(\theta)}{(r+d)^2}\exp\left[-\frac{d}{\lambda_2(\theta)}\right] \qquad (1)$$

Variations in the shield configuration and in the thickness of lead and steel that precede concrete introduce variations in the shape of the dose attenuation curves, due to build-up effects, as can be seen in Figure 7 and in Figure 8.

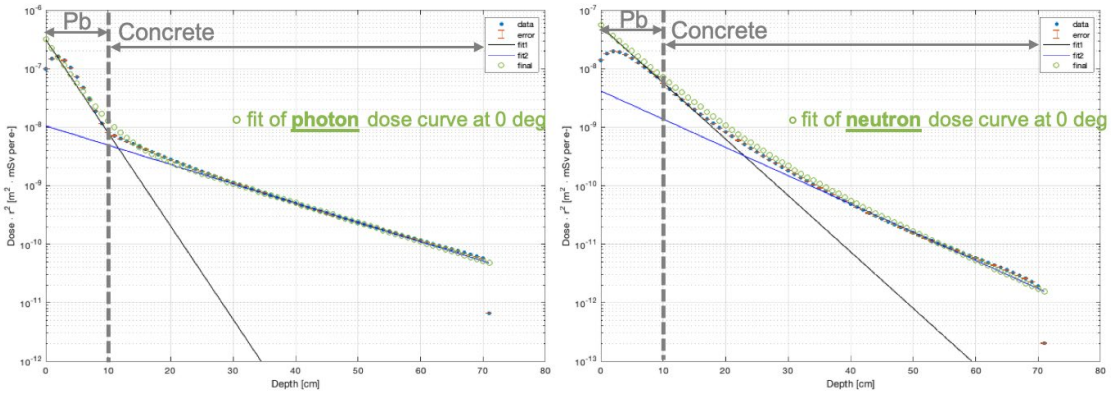

Figure 7: 0-deg dose attenuation curves for photons (left) and neutrons (right), generated in the interaction with a collimator, and their interpolation curves using the double exponential formula (1)

In some cases, the double exponential function is reduced to a single exponential term, like in the case illustrated in Figure 8, where only the attenuation length at equilibrium is used.

The shielding data, validated with measurements at the ALS, can be used to quickly and reliably calculate shielding requirements for a large number of source and shielding combinations, without the need for a Monte Carlo simulation when target type or geometry layout change. It is also very useful when determining shielding requirements for multiple sources, like in the portion of accelerator tunnel with beam-lines front-ends (see

Figure 9), where the dose through the ratchet walls is the sum of several types of losses in the SR and in the AR.

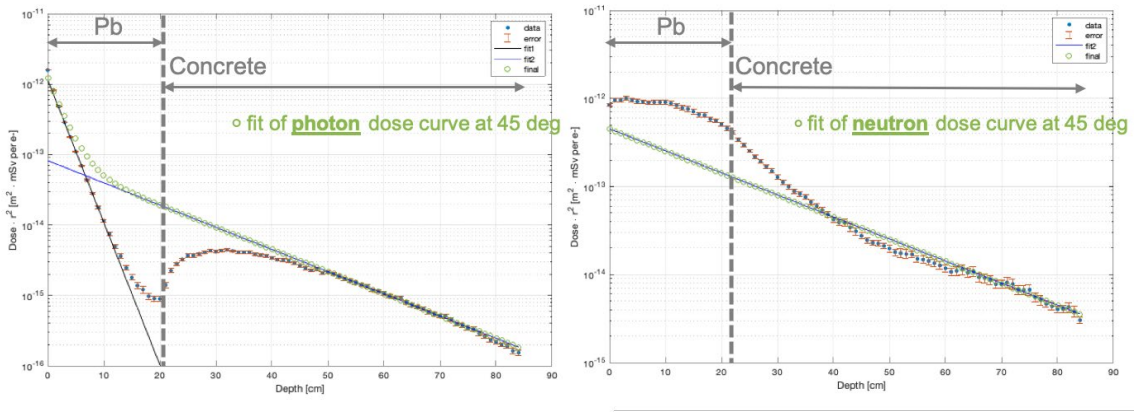

Figure 8: 45-deg dose attenuation curves for photons (left) and neutrons (right), generated in the interaction with a septum target, and their interpolation curves using the double exponential formula (1) for photons and a single exponential function for neutrons.

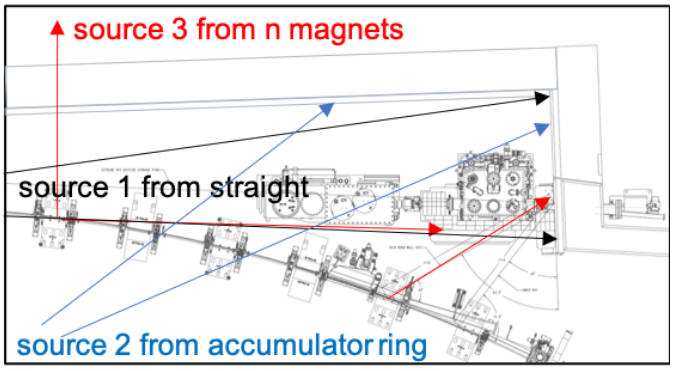

Figure 9: A top view of the portion of accelerator tunnel next to the ratchet walls, which show all sources of radiation contributing to the dose outside the shielding.

The tabulated data was also incorporated as look-up tables in a MATLAB [3] script, which calculates the dose through a shield once the following input parameters are chosen:

- beam loss intensity
- type of target
- distance of the source from the shield
- shield material and thickness
- angle

As the source terms and attenuation lengths were calculated for a finite set of shielding thicknesses of lead and steel for shielding made of lead/steel followed by concrete, the script performs also cubic interpolations using a modified Akima algorithm, to extract a continuous set of source terms and attenuation lengths for all lead shielding thicknesses. This way, new shielding requirements can be obtained without having to run simulations for each individual case when the lead or steel thickness varies.

2.2 Comparisons with the results of realistic simulations

A few comparisons were performed with the results of dose calculations with MC simulations that use realistic geometries. In particular, a scenario where the radiation sources are multiple is presented here.

The dose on the roof above the injection section caused by losses at 2 collimators and in the kicker is shown in

Figure 10, using as shielding 60 cm of concrete for the roof and a 10 cm steel plate between the accelerator and the roof, as it was estimated with the MATLAB script, where

the goal dose on the roof was set to 10 µSv/h. It can be observed that the script estimate is in good agreement with the results of the detailed simulation, where the dose above the loss points is mostly 5 µSv/h but at one spot above the septa it reaches 10 µSv/h. The dose profiles at 75 degrees were chosen as they represent the worst-case scenario.

2.3 Results

To evaluate the assumptions made by ALS-U in the shielding retrofit plan, i.e. to increase the thickness of the roof blocks above the collimation and injection sectors and to add lead panels to all ratchet walls, a combination of calculations with the script and some detailed MC simulations were used.

For the roof blocks, a concrete thickness of 60 cm will work in most locations but at the collimators additional shield is needed to bring the doses on the roof below acceptable levels.

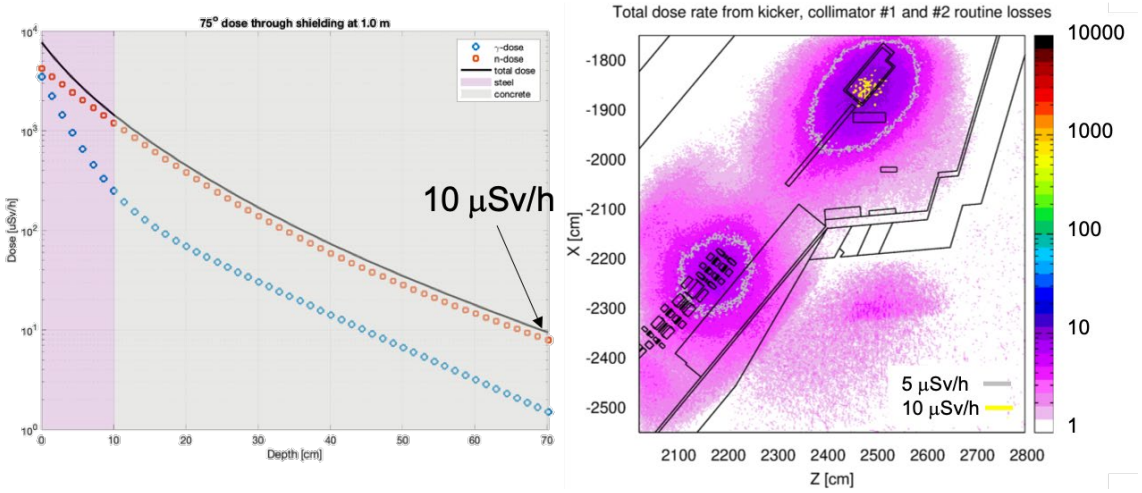

Figure 10 : Dose attenuation curves for photon, neutron and total dose through a shielding made of 10 cm of steel followed by 60 cm of concrete, at 75 degrees, as calculated with the MATLAB script (left). Dose map as calculated with FLUKA simulations for losses in the injection sections: the grey iso-dose contour line corresponds to 5 µSv/h and the yellow one to 10 µSv/h (right).

In particular, as the dose is dominated by neutrons either more concrete should be added or a material like steel should be used and placed between the loss point in the accelerator and the roof. Lead could also work but more thickness than steel would be required, making it a choice difficult to justify, considering also its nature of mixed waste.

For the ratchet walls, lead panels will also help to reduce doses in most sectors, but, again, in the collimation and injection areas, where lead panels already exist, more shielding will be needed to be installed locally at the collimators. In the injection area, where a concrete wall was excavated to remove the interference with two beamlines, the local shielding will be a 70 cm-thick concrete block, 60 cm tall and long enough to shadow the entire portion of wall which was modified. Figure 11 shows a drawing of the wall as of now and a dose map of the area when the additional concrete block is installed. At other collimator locations local steel or lead shielding will be required to reach the dose goals of the shielding policy on the experimental floor. At all transition walls where the so-called belly band is nowadays less than 12.5 cm thick, it will be required to install additional leas to meet the requirements.

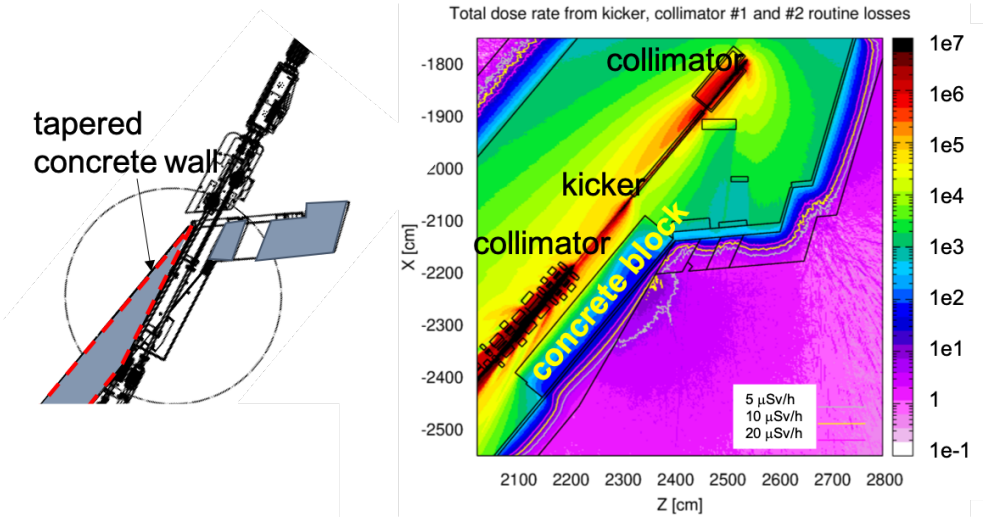

Figure 11: Layout of the injection area (left) showing the lateral shield wall as of now and results of MC simulations (right) that show the dose map with an additional concrete block, 70 cm thick, installed next to septa and a collimator.

Finally, the nominal gas pressure in the AR is estimated to reach the value of 14 nTorr in normal operation and 50 nTorr in abnormal conditions. In order to attenuate the dose generated by the gas bremsstrahlung produced in the AR, all dipoles will be equipped with a tungsten block placed at the exit of the magnets: the objective is for the tungsten to intercept and attenuate the gas bremsstrahlung that would otherwise hit the ratchet walls, as shown in Figure 12, and generate doses above 10 µSv/h on the experimental floor.

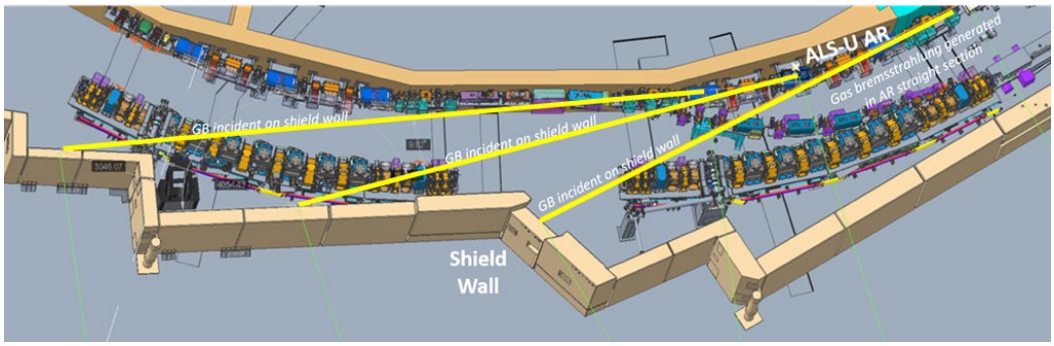

Figure 12: In the accumulator-ring straight sections, a gas pressure of 14 nTorr will generate gas bremsstrahlung directed towards the ratchet walls, as indicated by the yellow lines.

3 Conclusions

The planned shielding retrofit for the ALS upgrade will be sufficient at most locations but additional local shielding will be needed at the collimation and injection sectors. At locations where the shielding may not be retrofitted, like on the roof blocks that will remain 30 cm thick, administrative controls will be required to limit the access and the occupancy in those areas.

These conclusions are based on the results of Monte Carlo simulations and of analytical calculations. Several safety factors were included in the analysis, for instance by doubling the intensity of beam losses with respect to the assumptions, by maximizing the radiation yield from a target, and by increasing occupancy factors. The methods were benchmarked with radiation measurements at the ALS and more are planned from now until the dark time.

The ultimate confirmation of the validity of the methods used for the analysis and of the assumptions made for the beam losses will come from the results of radiation measurements during the commissioning phase.

Acknowledgments

This work was supported by the Director, Office of Science, Office of Basic Energy Sciences, of the U.S. Department of Energy under Contract No. DE-AC02-05CH11231

References

[1] C. Ahdida et al., "New Capabilities of the FLUKA Multi-Purpose Code", Frontiers in Physics 9, 788253 (2022).
[2] G. Battistoni et al., "Overview of the FLUKA code", Annals of Nuclear Energy 82, 10-18 (2015).
[3] MATLAB Version: 9.7.0.1261785 (R2019b), Natick, Massachusetts: The MathWorks Inc.

Shielding assessments for Diamond II machine upgrade

Faruk S*, Doull R

*(sanjeev.faruk@diamond.ac.uk)
Diamond Light Sources Ltd, Harwell Science & Innovation Campus, Didcot, OX11 0DE, UK

Abstract

The Diamond II machine will be upgraded to increase the brightness and coherence of the emitting synchrotron light. Linac will operate at 150 MeV, and the booster and storage ring will be operated at 3.5 GeV with a 300-mA current. However, the initial shielding calculation was done for 100 MeV for Linac and 3.0 GeV for 500 mA for other areas. We re-evaluated the shielding calculation for any potential risk of radiation hazard using empirical and semi-empirical analyses, SHIELD11[1] code and FLUKA[2,3] particle transport code. The concrete shielding around the Storage ring and the Booster were below 0.5 μSv/h in normal and abnormal loss conditions. In normal loss conditions, we have observed a possible high radiation dose rate of 90 μSv/h between the Linac and Booster wall in Booster Zone 1. However, abnormal loss conditions due to beam miss-steering in a quadrupole corrector magnet can lead to a dose rate of 90 μSv/h around the Linac rear entrance and 30 μSv/h on the primary entrance side. The LTB dipole could lead to a dose rate of 90 mSv/h in the Booster on the other side of the Linac back wall, and abnormal loss in the Faraday cup in the Linac enclosure could, in principle, lead to a dose rate of up to 30 μSv/h around the Linac rear entrance and one μSv/h on the main entrance. Additional lead shielding was proposed to reduce the dose rate to 0.5 μSv/h.

1 Radiation Protection

The current Diamond linear accelerator operates at 100 MeV but will be upgraded to 150 MeV. The Booster and Storage ring run at an energy of 3.0 GeV, which will be increased to 3.5 GeV. However, the Storage ring current (300 mA) will be less than the value for which the shielding was designed (500 mA). This section assesses whether the current radiation shielding protection is adequate for Diamond-II operating conditions and identifies where additional control measures are required.

1.1 Shielding Assessment Methods

Some methods have been used as other accelerators/synchrotrons to assess the current shielding:

1. Known expressions were used to assess photon fluxes and, thus, shielding requirements.
2. Established computer-modelling codes were used for the dose rate in a semi-empirical manner, such as SHIELD11.
3. The well-known FLUKA particle physics Monte Carlo simulation code.
4. Los Alamos Monte Carlo N-Particle Transport code (MCNP)[4] simulations by an external contractor.

1.2 Electron Losses

Electron losses were divided into two types - “normal losses”, which persist over long periods, months and years, and “abnormal losses”, which occur under test or fault

conditions and which last for only a short period, typically < 1 hour, in the case of faults until automatic systems and/or operators intervene.

Radiation doses outside the shielding for normal losses should be compared to the limit adopted by Diamond of 1 mSv/year, where a working year is defined as 2000 hours and hence, on average, the limit is 0.5 μSv/hour. For abnormal losses, they should be compared to the statutory limit for a Supervised Area of 7.5 μSv/hour, averaged over an 8-hour day.

1.2.1 Normal Losses

A model has been created to estimate the electron losses in the Diamond-II Storage ring, considering:

- The nominal beam currents.
- The beam lifetime.
- The top-up interval.
- The number of user-mode hours.
- The mean time between failures (MTBF) and the number of beam trips.
- The number of machine start-up and machine development days.
- The estimated number of machine refills during the above.
- The injection efficiency.

The model has been checked against archive data of the total charge injected into the Storage ring over three pre-pandemic years, 2017-2019[5]. The model and archive data agreement are excellent, with only a single fitting parameter. The total losses in the Storage ring were very similar over the three years with an average of 4.6 $x10^{15}$ electrons/year, or on average over the machine operational hours of 2.1 $x10^{8}$ electrons/s. The variation year-by-year was very small, within 5% of the average.

Loss location	Losses e^-/s
Linac	1.6 10^8
LTB1	2.9 10^8
Booster injection	4.7 10^8
Booster extraction	7.3 10^7
Storage ring	4.2 10^8

Table 1: Estimated average electron losses at various points in Diamond-II under normal conditions.

1.2.2 Abnormal Losses

Table 2 lists the abnormal loss scenarios that have been considered. In estimating the loss rates, higher transfer efficiencies have been assumed than for normal losses to be more pessimistic: 80% Linac end to LTB end, 90% Booster injection, 100% BR acceleration, 100% BR extraction, and 100% SR injection. This results in the maximum abnormal losses of Table 5.1.4, based on the maximum achieved Linac multi-bunch charge of 9 nC at the maximum repetition rate of 5 Hz.

Location	Cause of abnormal loss
Linac	Mis-steering occurring due to corrector errors/failures in-between linac sections.
LTB	Linac beam directed into Faraday cup or mis-steered into the collimator.
Booster	Linac beam mis-steered, either hitting the injection septum or where it enters the narrow aperture vessels in the arcs.
Booster	3.5 GeV beam hits extraction septum.
BTS	Booster beam directed into Faraday cup or mis-steered into the collimator.
Storage Ring	Mis-steering of injected beam, hitting a collimator.
	Loss of stored beam through various mechanisms.

Table 2: Abnormal loss scenarios.

Loss location	Charge (nC)	Losses e^-/s
Linac	9 nC	$2.8\ 10^{11}$
LTB	9 nC	$2.8\ 10^{11}$
Booster injection	7.2 nC	$2.3\ 10^{11}$
Booster extraction	7.2 nC	$2.3\ 10^{11}$
Storage ring injection	6.5 nC	$2.0\ 10^{11}$

Table 3: Estimated maximum abnormal electron losses at various points in Diamond-II.

1.3 Linac and LTB

1.3.1 Linac Normal Losses

Electron losses were simulated along the Linac and the first LTB dipole magnet with losses of 1.6×10^8 and 2.9×10^8 electrons/s, respectively, and the results are shown in Fig. 1.

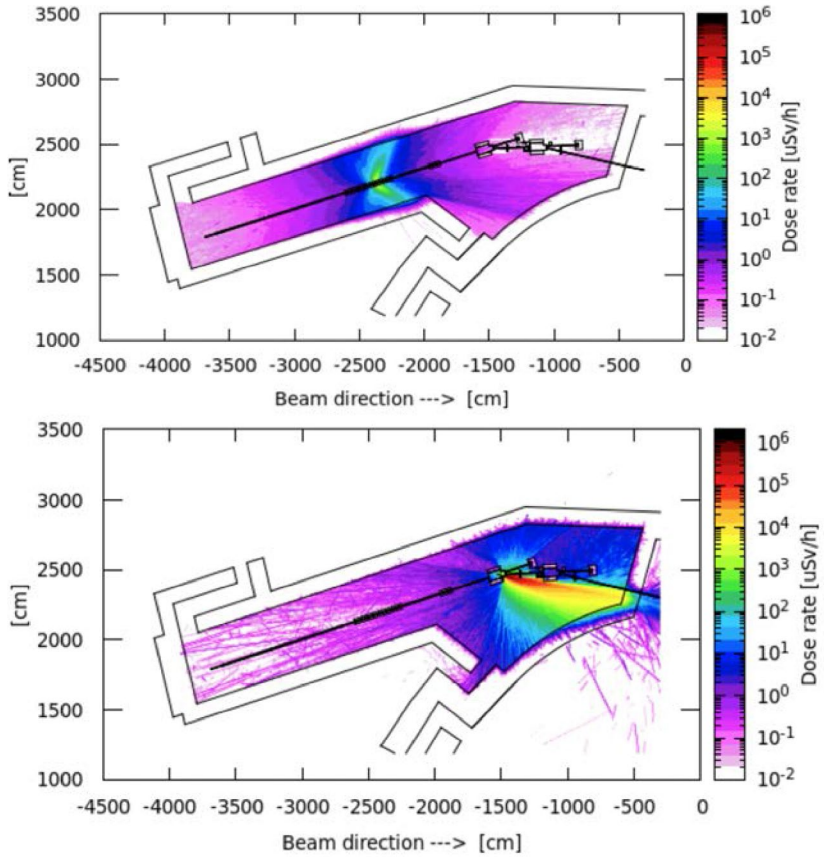

Figure 13 FLUKA models showing dose rate (electrons, neutrons & X-ray) outside the Linac shield wall due to 1.6 x10^8 electron loss/s along the Linac (upper) and 2.9 x10^8 electron loss/s at the first LTB dipole magnet (lower).

Table 4 summarises the results. In the case of normal losses in the Linac, the dose rates are <0.03 µSv/h; hence, no additional measures are necessary. Losses at the first LTB dipole could lead to 90 µSv/h in the Booster on the other side of the back wall of the Linac. Although this area is rarely occupied, the Personnel Safety System (PSS) will be configured so that the Linac can only operate when Booster Zone 1 is searched and locked.

Loss location	Losses e^-/s	Dose rate outside shielding µSv/h	Comments
Linac	1.6 10^8	< 0.1	Shielding is adequate
LTB dipole	2.9 10^8	90	PSS will restrict access to booster when the Linac is in operation.

Table 4: FLUKA calculated maximum dose rates due to normal electron losses at various points in the Diamond-II Linac.

1.3.2 Linac Abnormal Losses

Electron losses were simulated due to mis-steering in the dipole corrector magnets, losses at the LTB first dipole magnet and Faraday cup with abnormal losses of 2.6 x10^{11} electrons/s in each area, and the results are shown in Fig. 2.

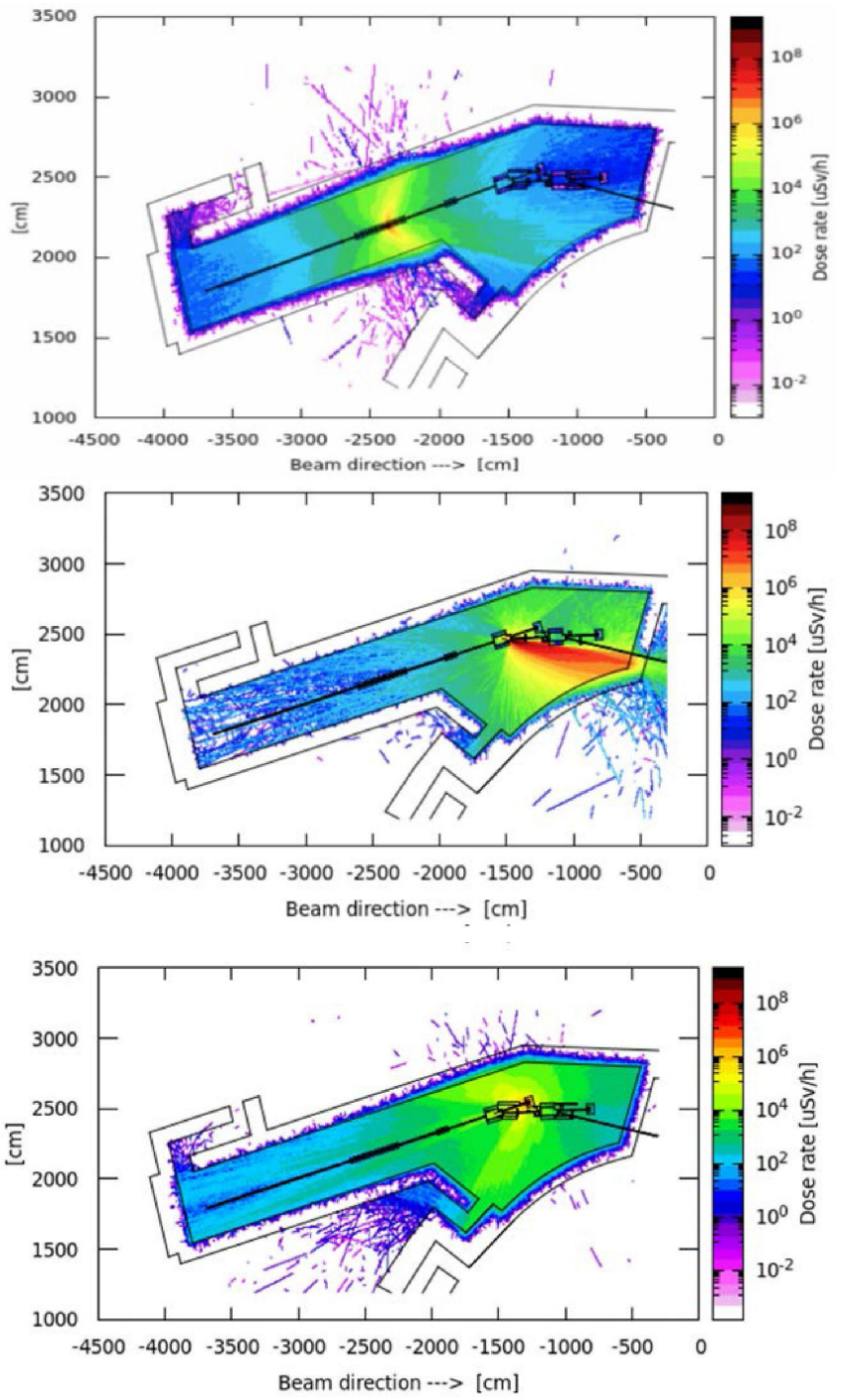

Figure 14 FLUKA models showing dose rate (electrons, neutrons & X-ray) outside the Linac shield wall due to 2.8 x10^{11} electron loss/s due to mis-steering at a quadrupole corrector magnet (upper), at the LTB dipole magnet (centre) and in the Faraday cup (lower).

The results are summarised in Table 5.

Loss location	Losses e^-/s	Dose rate outside shielding (µSv/h)	Additional lead shielding required to reduce dose rates to 7.5 µSv/h
Linac	2.8 10^{11}	90 & 30	23 mm & 13 mm
LTB dipole	2.8 10^{11}	90000	N/A - PSS will restrict access to Booster Zone 1
Faraday cup	2.8 10^{11}	30	13 mm

Table 5: FLUKA calculated the maximum dose rate due to abnormal electron losses at various points in the Diamond-II Linac enclosure.

Abnormal losses due to mis-steering in a quadrupole corrector magnet can lead to dose rates of 90 µSv/h around the Linac rear entrance and 30 µSv/h on the main entrance side. 23 mm of Pb shall be installed parallel to the corrector magnets on the rear entrance side, and 13 mm Pb shall be installed on the main entrance side to reduce the dose rate to 7.5 µSv/h. Abnormal losses in the LTB dipole could lead, in principle, to dose rates of 90 mSv/h in the Booster on the other side of the back wall of the Linac.

Abnormal losses in the Faraday cup in the Linac enclosure could, in principle, lead to dose rates of up to 30 µSv/h in the area of the Linac rear entrance and 1 µSv/h on the main entrance side. An additional 13 mm Pb shall be installed on the Rear entrance side of the Faraday cup.

1.4 Booster

1.4.1 Booster Normal Losses

Electron losses were simulated in the injection and the extraction areas with a loss of 4.7 x10^8 and 7.3 x10^7 electrons/s, respectively. The results are presented in Fig. 3 and 4.

1.4.1.1 Injection septum

The average dose rate outside the side wall and roof for losses in the injection septum is <1 µSv/h. It can be assumed that for any person, less than 1000 hours per year would be spent in these areas accessed infrequently; therefore, the annual dose would be less than 1 mSv/y, and hence, no additional controls are necessary. However, access to the roof will be controlled to manage possible abnormal losses, as described in Section 1.4.2.

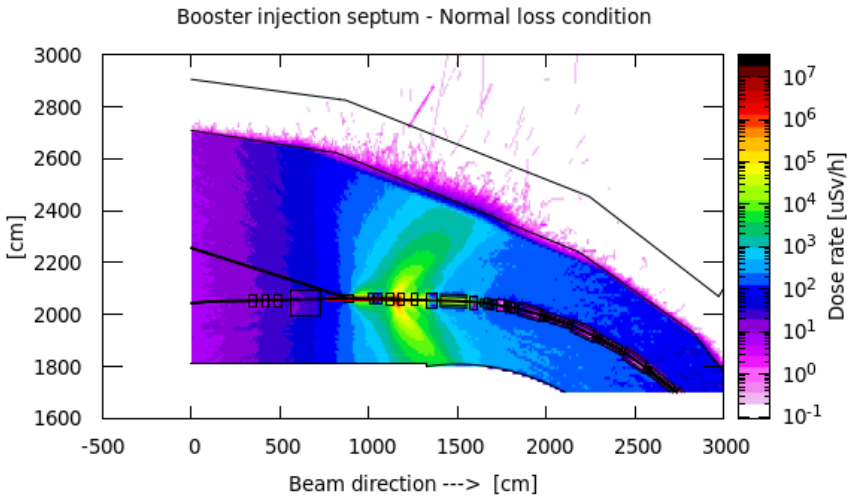

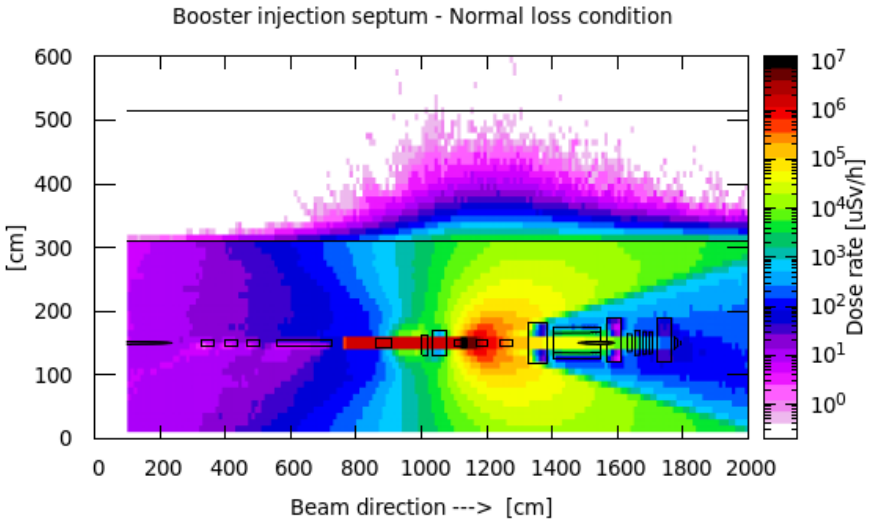

Figure 15 FLUKA models showing dose rate (electrons, neutrons & X-ray) outside the Booster shield wall (upper) and roof (lower) due to 4.7 x10^8 electron loss/s at the injection septum magnet.

1.4.1.2 Extraction septum

The average dose rate outside the side wall for losses in the extraction septum is <0.5 µSv/h; for the roof, it is about 1 µSv/h. This would not require additional controls. However, access to the roof will be controlled to manage possible abnormal losses, as described in Section 1.4.2.

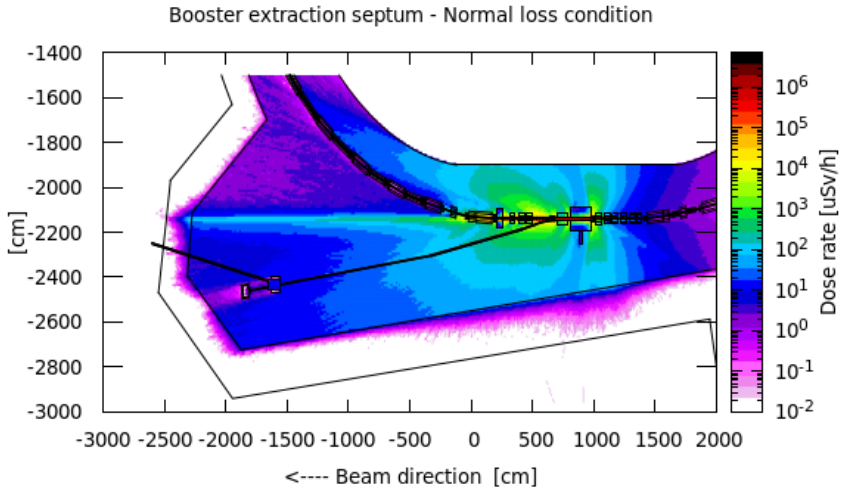

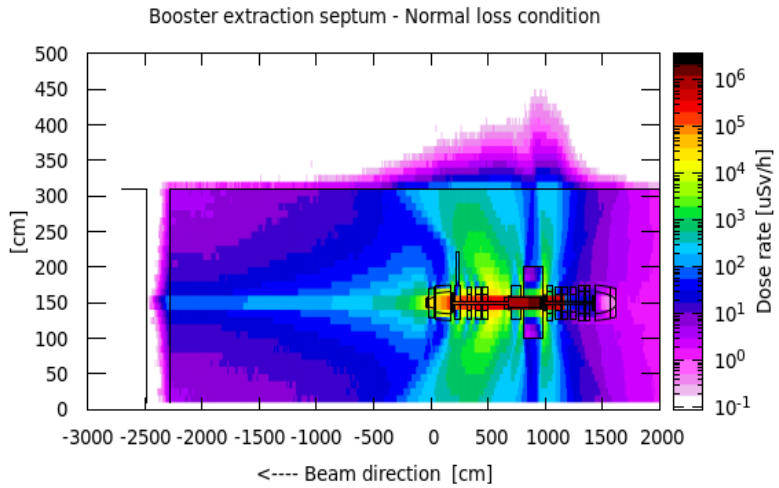

Figure 16 FLUKA models showing dose rate (electrons, neutrons & X-ray) outside the Booster shield wall (upper) and roof (lower) due to 7.3 x10^7 electron loss/s at the extraction septum magnet.

1.4.2 Booster Abnormal Losses

Electron losses were simulated in the injection septum, extraction septum and the BTS Faraday cup within the Booster shield wall, with an electron loss of 2.3 x1011 in the injection septum and extraction septum and 2.0 x1011 in the Faraday cup. The results are shown in Fig. 5, 6 and 7, respectively. In all cases, doses above the Booster roof exceed 7.5 mSv/h, so access to the roof will be restricted and only possible under a Permit-to-work procedure that ensures the Booster is off.

1.4.2.1. Injection Septum

The average dose rate outside the side wall and roof for abnormal losses in the injection septum is <300 µSv/h. An additional 34mm of Pb shall be installed parallel to the septum magnet to reduce the dose rate outside the shield wall to 7.5 µSv/h. In addition, access to the roof will be restricted, as described above.

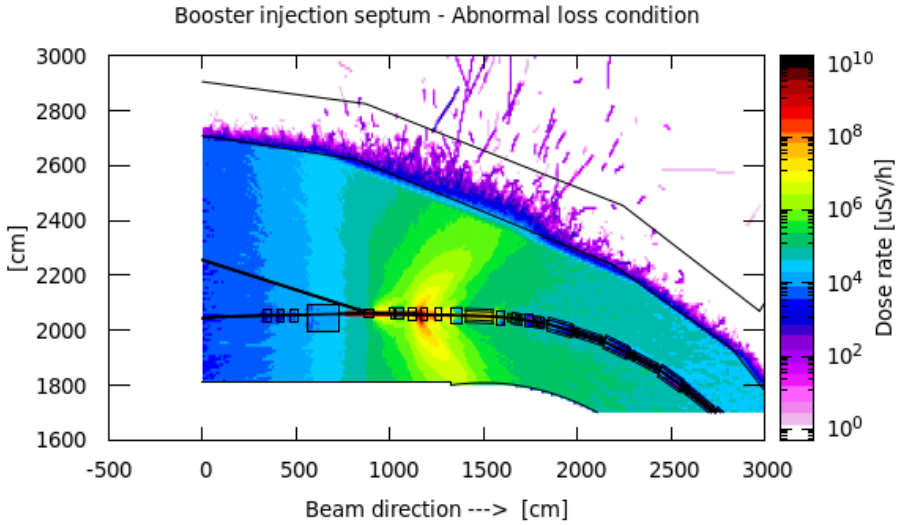

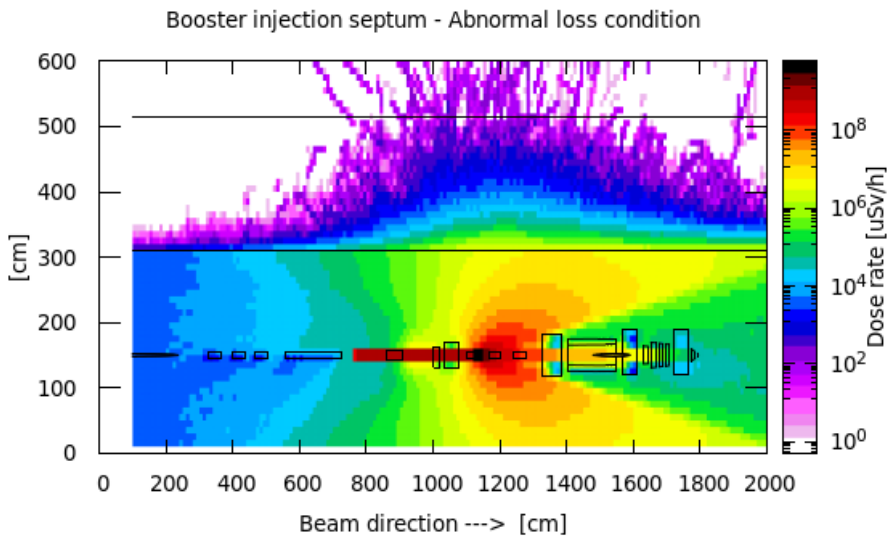

Figure 17 FLUKA models showing dose rate (electrons, neutrons, X-ray) outside the Booster shield wall (upper) and roof (lower) due to 2.3 x10^{11} electron loss/s at the injection septum magnet.

1.4.2.2 Extraction Septum

The average dose rate outside the side wall for abnormal losses in the extraction septum is <50 µSv/h. For the roof, it is <150 µSv/h. Local lead shielding (~17 mm) shall be placed around the septum to reduce the dose rate to less than 7.5 µSv/h. Access to the roof will be restricted as described above.

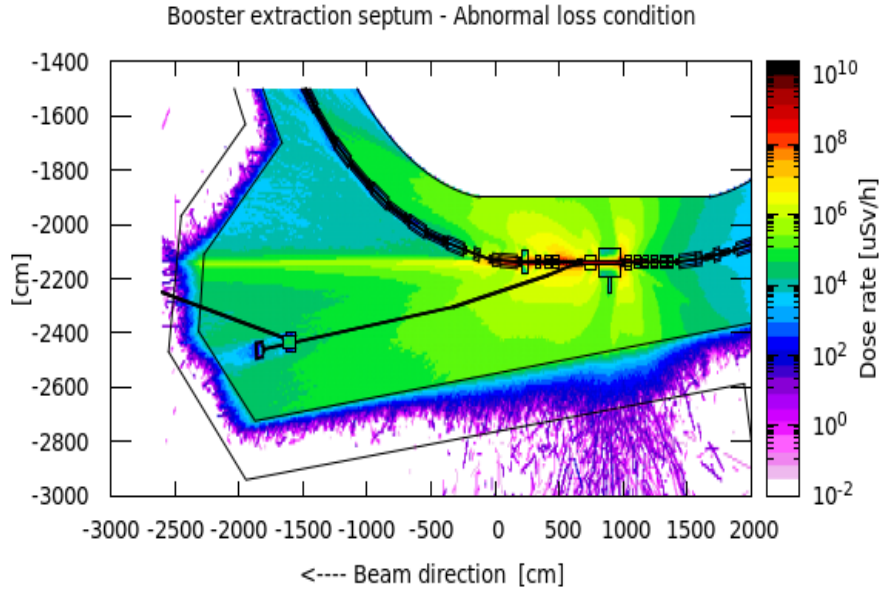

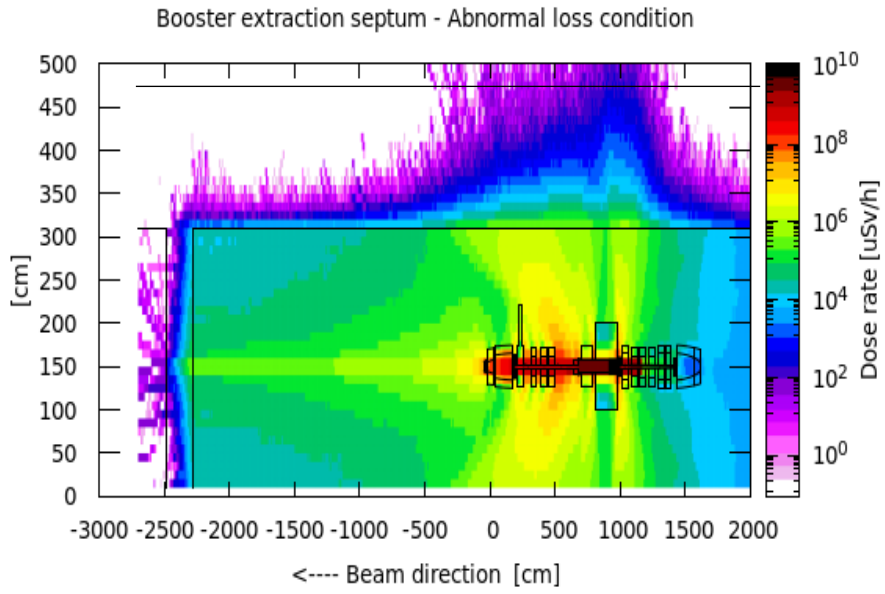

Figure 18 FLUKA models showing dose rate (electrons, neutrons, X-ray) outside the Booster shield wall (upper) and roof (lower) due to 2.3 x10^{11} electron loss/s at the extraction septum magnet.

1.4.2.3 BTS Faraday Cup

The average dose rate outside the side wall and roof for losses in the BTS Faraday cup is <100 µSv/h. Additional local lead shielding (~24 mm) shall be placed around the Faraday cup to reduce the dose rate to less than 7.5 µSv/h. Access to the roof will be restricted as described before.

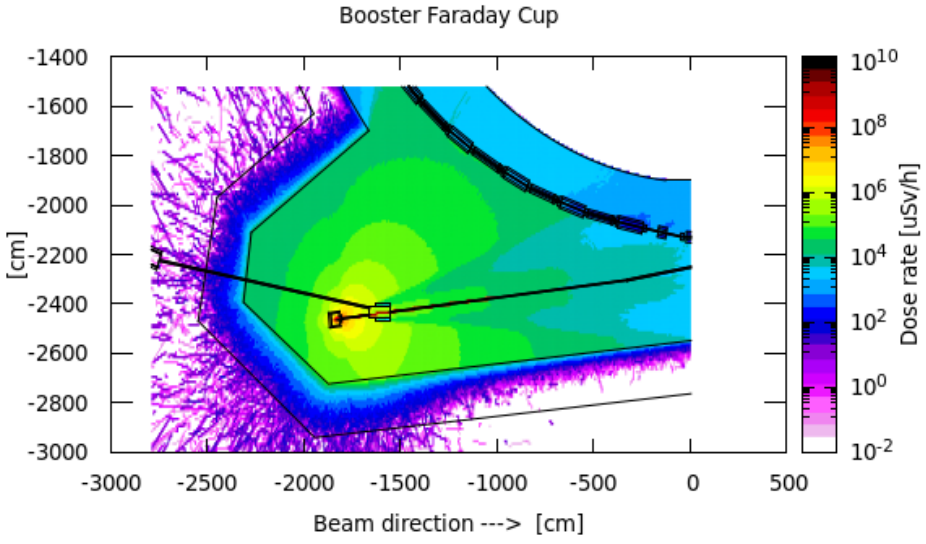

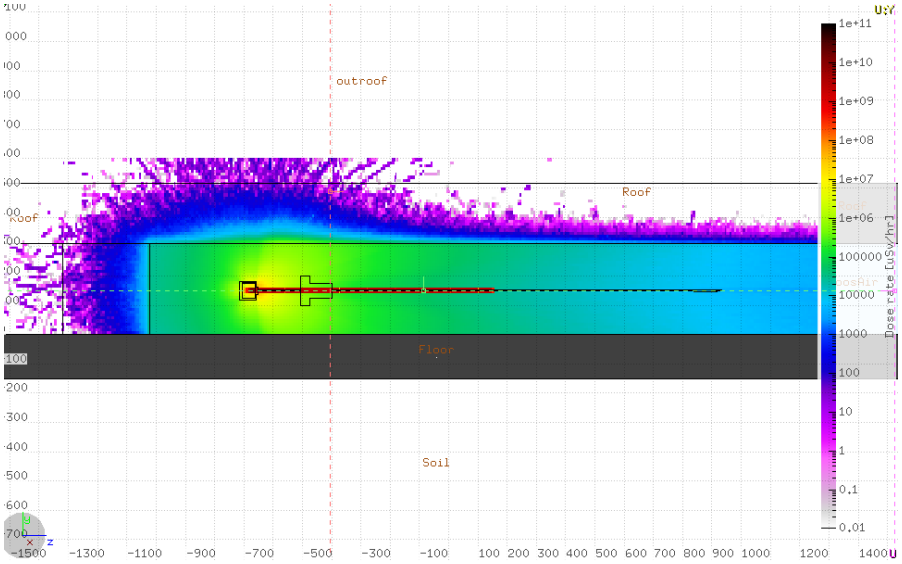

Figure 19 FLUKA models showing dose rate (electrons, neutrons, X-ray) outside the Booster shield wall (upper) and roof (lower) due to 2.3 x10^{11} electron loss/s in the BTS Faraday cup.

1.5 Storage Ring

1.5.1 Normal Losses

Diamond-II will employ a distributed collimation scheme rather than single horizontal and vertical collimators in the injection straight. Based on detailed simulations of where particles are lost due to various mechanisms and given the losses predicted by the model, the resulting losses are:

- 75.3% lost at the collimators (3.2 x10^{8} e-/s).
- A maximum of 25% is lost at any single collimator (8.2 x10^{7} e-/s).
- The rest of the losses (1.0 x10^{8} e-/s) are distributed around the ring.

Figure 8 shows that the maximum dose rate outside the side wall and roof in the vicinity of a collimator is <0.02 µSv/h even in the extreme case that all the normal losses (4.2 x10^{8}) occur at a single collimator, which is well within the required limits.

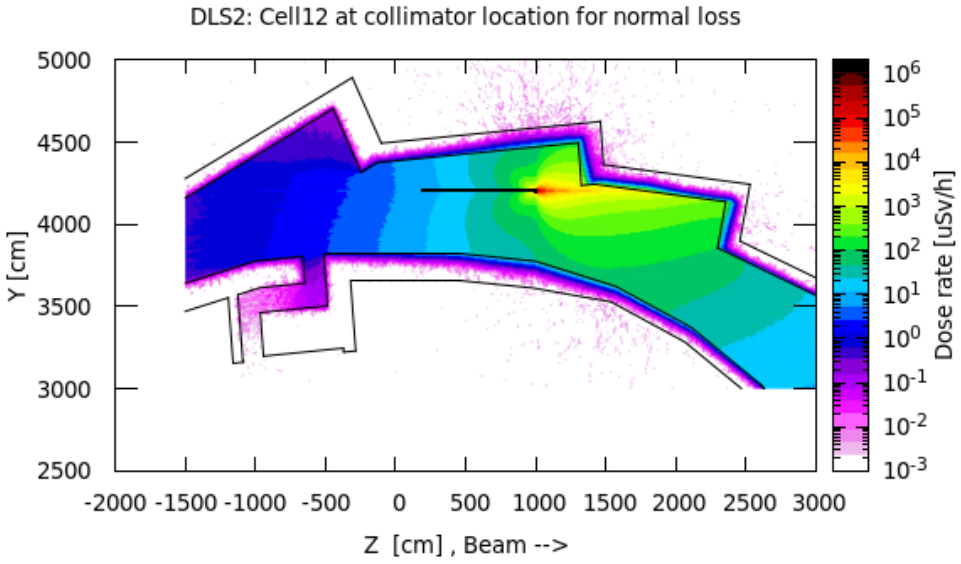

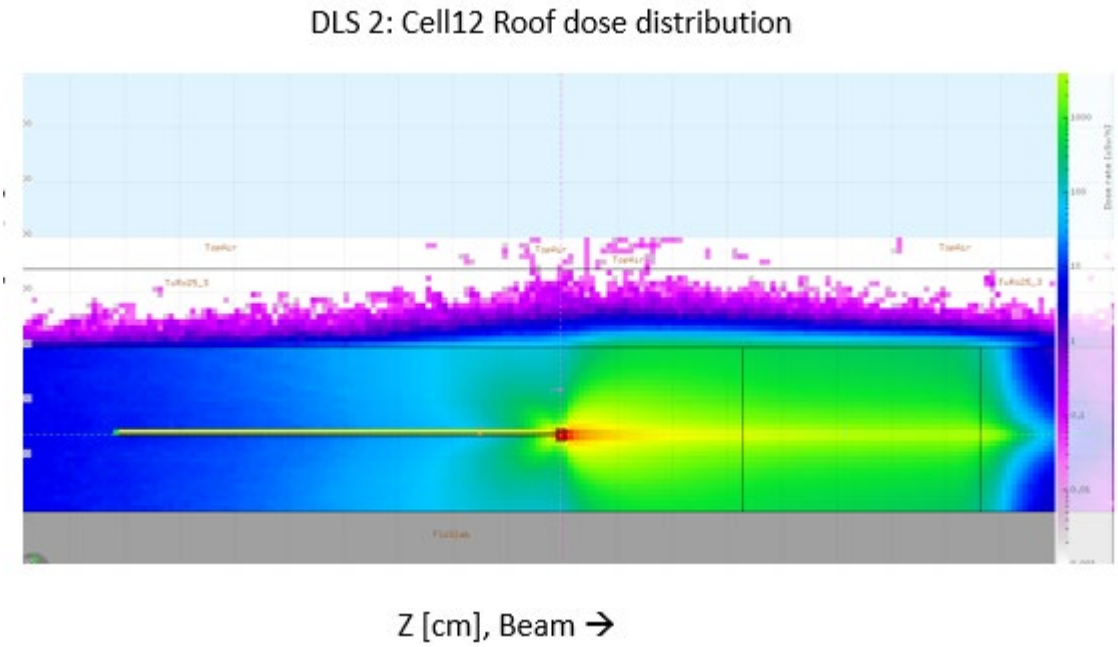

Figure 20 FLUKA models showing dose rate (electrons, neutrons, X-ray) outside the shield wall (upper) and roof (lower) due to 4.2 x10^{8} electron loss/s at a collimator.

1.5.2 Abnormal Losses

The most likely abnormal loss of electrons is a loss of stored beam (3.5 x10^{12} electrons). However, even if this is lost at a single collimator, the instantaneous dose outside the shielding (based on the results of Section 1.5.1) is < 0.05 μSv, and hence negligible, and even if every beam dump (either deliberate or through a fault) would lead to complete loss at the same collimator over a whole year, the dose outside the shield wall would still be < 0.02 mSv.

The most likely continuous loss of electrons over any significant period due to fault conditions will be if the injected beam is lost entirely at a single collimator, e.g. due to mis-steered beams from the BTS or mis-setting of injection elements. In this case, according to Table 3, the maximum loss rate could be 2.0 x10^{11} electrons/s.

Figure 9 shows that the average dose rate outside the side wall is <0.5 μSv/h; therefore, no additional controls are needed. The average dose rate outside the roof is <2.5 μSv/h, so no other controls are required as the dose rate is below 7.5 μSv/h, and such conditions will not persist for very long.

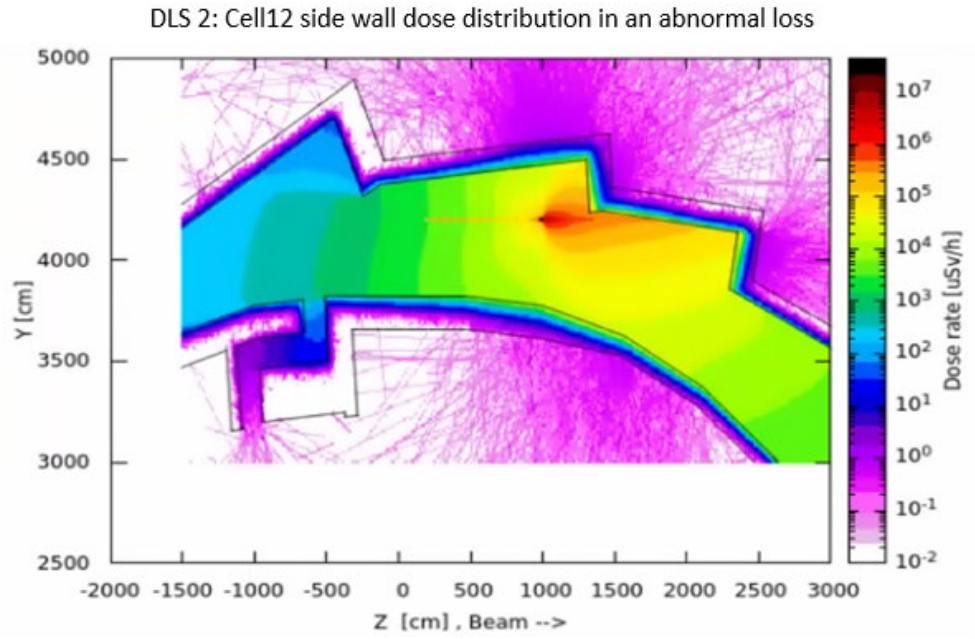

Figure 21 FLUKA models showing dose rate (electrons, neutrons, X-ray) outside the shielding wall (upper) and roof (lower) due to 2.0 x10^{11} electron loss/s at a collimator.

1.6 Storage Ring Injection Area

The storage ring shielding in the injection area has a thicker wall and roof than anywhere else. The simulation for two conditions did not indicate any requirements for further control Table 6.

Loss Location	Losses e^-/s	Dose rate outside shielding µSv/h	Comments
Injection Area	$4.2\ 10^8$	<0.02 [SW & R]	No additional controls are necessary for the hall area.
Injection Area	$2.0\ 10^{11}$	<0.5 [SW] <2.5 [R]	No additional roof controls are needed as the dose rate is below 7.5 µSv/h, and such conditions will not persist for a very long period.

SW = Side wall; R = Roof

Table 6: FLUKA calculated the maximum dose rate due to normal and abnormal electron losses at injection in the storage ring.

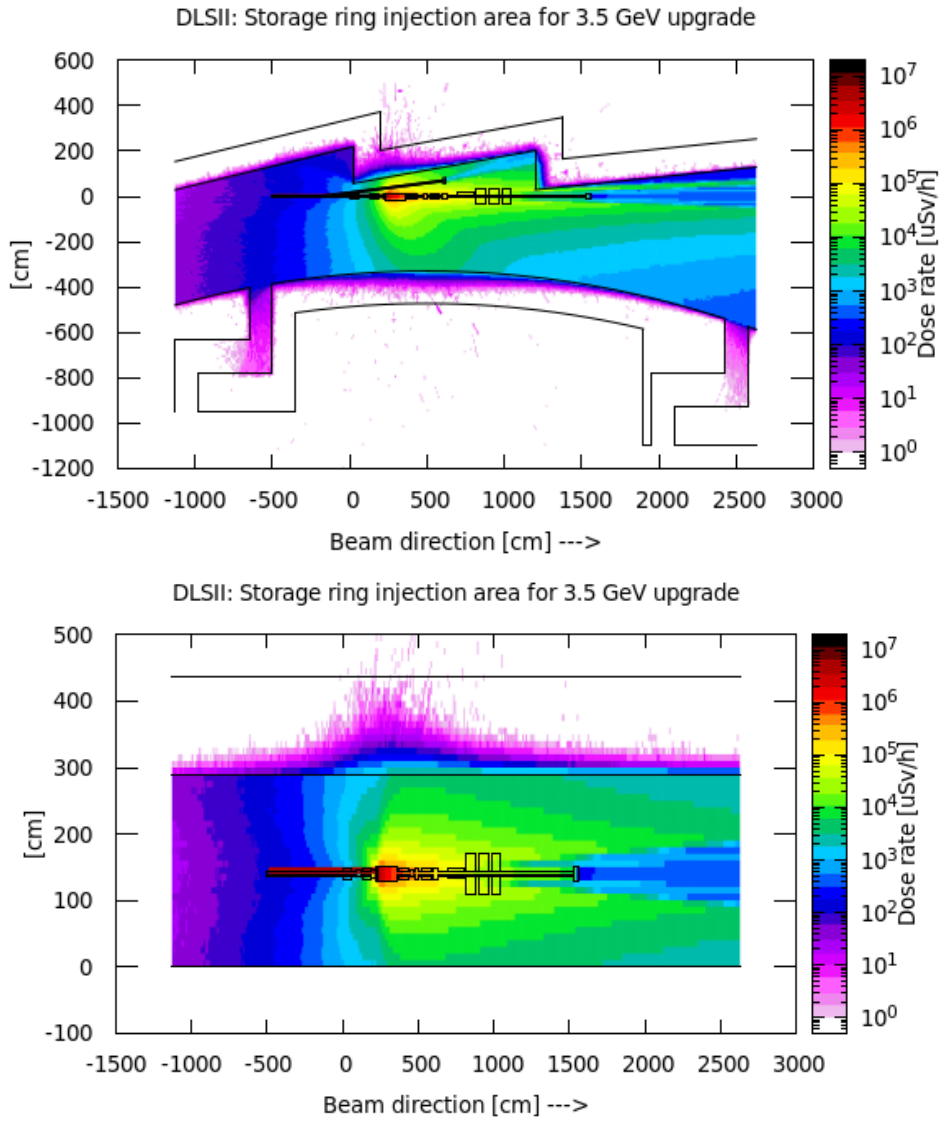

Figure 22 FLUKA model showing dose rate (electrons, neutrons, X-ray) outside the shielding wall (upper) and roof (lower) at the injection area.

1.7 Permanent Magnet Dose

Diamond II will have permanent dipole Sm_2Co_{17} magnet modules next to the collimator. The Fluka model determined the radiation exposure dose to these magnets for potential magnetic flux loss using the following conditions –

1. Electron beam to target closed collimator.
2. Electron beam to target open collimator at normal state.
3. Gas bremsstrahlung (GB) to target closed collimator.

4. GB to target open collimator at normal state.

When the collimator was open (Fig 11), it was observed that the maximum dose rate of 1400 µSv/s on the face of the first magnet module dropped to 200 µSv/s as it was leaving the module.

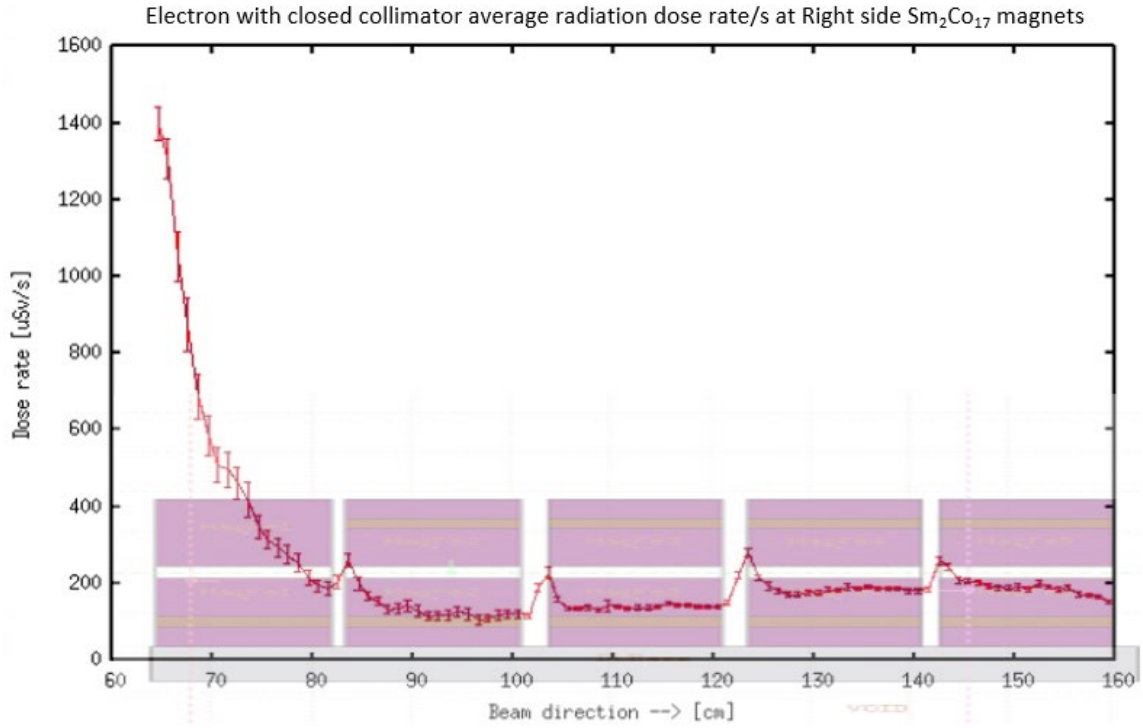

Figure 23 Electron dose rate with open collimator.

Due to the magnetic force, each module was exposed to a higher dose on the face of each module than on the back of the module (Table 7).

Module	Face	Back
	(µSv/s)	
First	1400	200
Second	260	120
Third	230	140
Forth	280	190
Fifth	260	155

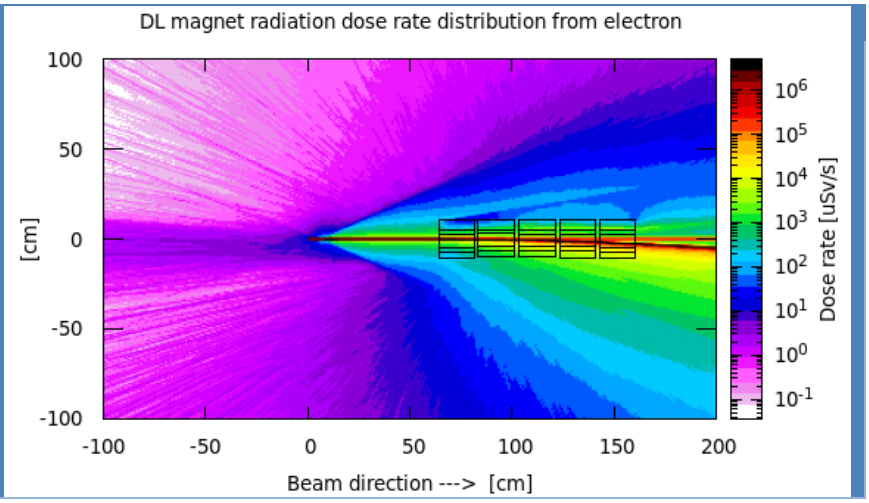

Table 7: DL magnet Dose distribution from electron with collimator open.

The radiation dose rate contribution from GB with open and closed collimator was observed to be 150 and 216 µSv/s on the first module and reduced to an average of 10 µSv/s on the last module end. We recommend using localised lead (Pb) shielding to save from radiation damage in front of the DL dipole magnet. For example, a thickness of 21 mm of Pb will reduce the dose rate to 1/10th of its effect.

1.8 Conclusions

Diamond Light Source Storage ring, Booster and the Linac shielding were initially designed to withstand 3.0 GeV energy of electrons with 500 mA currents. However, the upgrade to Diamond II will be 3.5 GeV energy and 300 mA current. The monte-carlo calculations indicated that there are areas that will need some additional shielding. It was proposed that local additional shielding be installed where possible, and in other places, it will be controlled using personal safety system (PSS) access control.

References

[1] - W. Nelson, "The SHIELD11 computer code," (2005).
[2] – "The FLUKA code: Description and benchmarking" G. Battistoni, S. Muraro, P.R. Sala, F. Cerutti, A. Ferrari, S. Roesler, A. Fasso`, J. Ranft, Proceedings of the Hadronic Shower Simulation Workshop 2006, Fermilab 6--8 September 2006, M. Albrow, R. Raja eds., AIP Conference Proceeding **896**, 31-49, (2007)
[3] - "FLUKA: a multi-particle transport code" A. Ferrari, P.R. Sala, A. Fasso`, and J. Ranft, CERN-2005-10 (2005), INFN/TC_05/11, SLAC-R-77.
[4] - J. T. Goorley et al., "Initial MCNP6 release overview - MCNP6 version 1.0," (2013).
[5] - I. Martin et al., "Electron losses in Diamond-II," Diamond internal report AP-DII-REP-0025, 2022.

Shielding Design and Current Status of New Compact Synchrotron Facility at PAL

Lee. H. S.*, Bakhtiari. M[2]., Lee. U.[1]

[1] Pohang Accelerator Laboratory, Pohang University of Science and Technology, Pohang 37673, Republic of Korea
[2] Div. of Advanced Nuclear Engineering, POSTECH, Pohang, 37673, South Korea
* lee@postech.ac.kr

Abstract

A compact synchrotron facility with a EUV (Extreme Ultra-Violet) beamline has been constructed at Pohang Accelerator Laboratory. PAL-EUV consists of a linac, booster, and storage ring. Electrons are accelerated up to 20 MeV in the linac and are injected into the booster to gain energy up to 400 MeV and finally are injected into the storage ring with 140 mA stored current. The injection frequency is 0.5 Hz and the injected charge is 20 pC/injection. Beam loss occurs at injection points, during the boosting as well as in the storage ring. The literature information or operation experience of Pohang Light Source (PLS-II) was applied to assume an injection or extraction efficiency. The radiation shielding calculations were performed using the PHITS Monte Carlo code considering such beam losses. Normal and accident operating scenarios were assumed in the shielding analysis. It was shown that the current shielding walls meet the shielding criteria for PAL-EUV. The facility has started the commissioning since Feb. 2023. The radiation level has been monitored using the area radiation monitoring system and periodic survey procedure.

1 Introduction

A compact synchrotron facility to generate EUV radiation with 13.5 nm wavelength has been designed and constructed at Pohang Accelerator Laboratory. In February 2023, its commissioning started. Figure 1 shows the photographs of PAL-EUV construction and commissioning status. The layout of the PAL-EUV facility is also shown in Figure 2. It includes a linear accelerator (height of 100 cm), a booster (height of 220 cm), and a storage ring (120 cm). The electron beam is accelerated up to 20 MeV in the linac and then injected into the booster. After accelerating its energy up to 400 MeV in the booster, the electron beam is injected into the storage ring, and the EUV radiation is generated via the undulator and through the beamlines are transported to the experimental hutch. Currently, one EUV beamline is ready for the semiconductor industry.

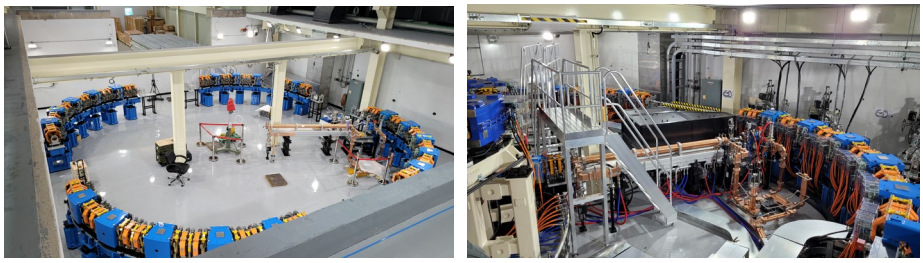

Figure 1: PAL-EUV on (a) construction, and (b) on commissioning period.

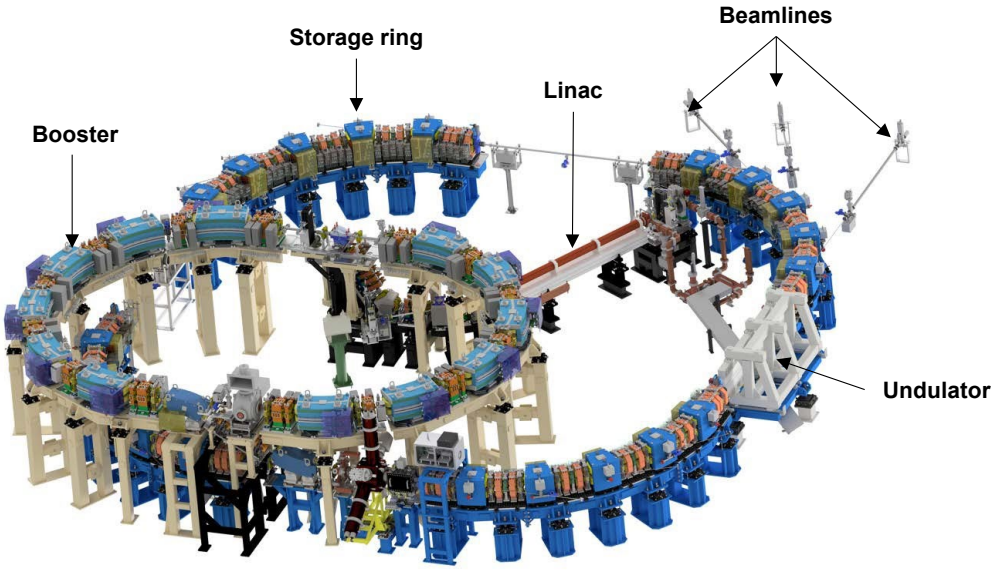

Figure 2: General layout of the PAL-EUV.

The stored current in the storage ring is 140 mA which is equivalent to 1.05×10^{11} stored electron or 16.8 nC. The circumference of the storage ring is 36 m. The injection frequency is 0.5 Hz and the injected charge is 20 pC/injection. Table 1 lists the storage ring parameters.

Beam energy (MeV)	400
Beam current (mA)	140
Beam lifetime (min)	30
Circumference (m)	36
Stored charge (nC)	16.8
Stored electrons	1.05×10^{11}
Stored energy (J)	42
Beam loss (pC/s)	~10
Beam loss (e/s)	5.83×10^{7}

Table 1: PAL-EUV storage ring parameters.

2 Methods

The dose rate was calculated using the PHITS-3.3 code [1]. In the PHITS calculations, the electron and photon transport were handled by EGS5 [2]. The JENDL-4.0 [3] library was used for the neutron interactions below 20 MeV, and the INCL-4.6 [4] was used for those above 20 MeV. A 3-D model of the tunnel simulated by the PHITS code is illustrated in Figure 3. The tunnel walls were made of ordinary concrete and three walls were 40 cm thick. One wall was in common with the building outside which was a public access zone and its thickness was 60 cm. The ceiling thickness was 20 and 35 cm depending on the position.

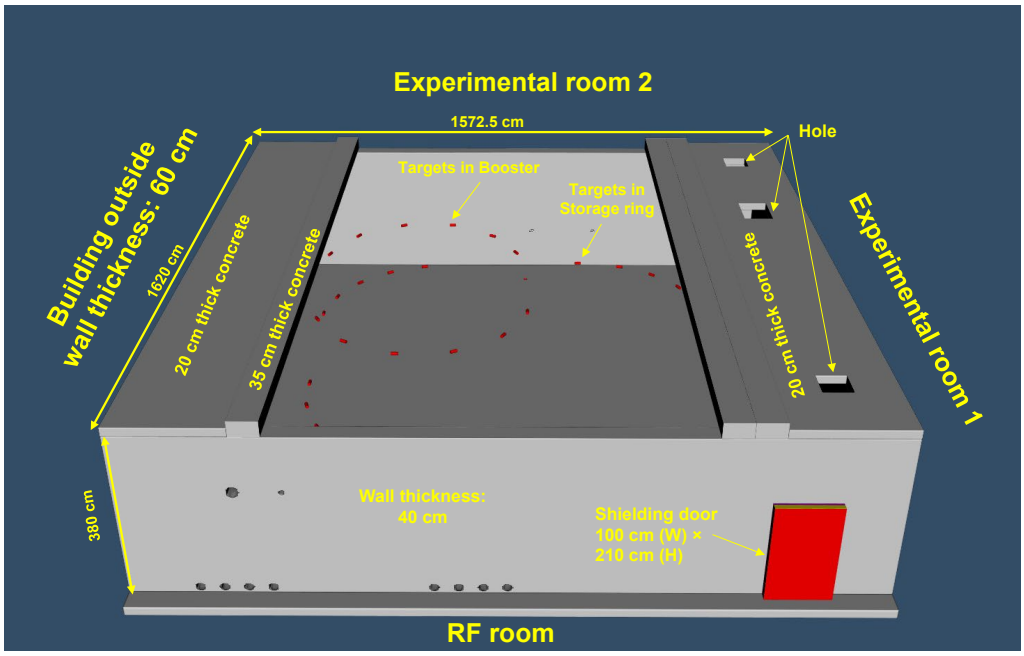

Figure 3: A 3-D model of the PAL-EUV tunnel simulated in the PHITS code.

The shielding calculations were performed for normal and accidental operation scenarios. Thick cylindrical Fe targets (Φ=8 cm, thickness=17.6 cm) were assumed at each dipole magnet position in the storage ring (20 dipole magnets) and booster (12 dipole magnets). The multi-source option was used in the PHITS code to irradiate each target to simulate a uniformly distributed beam loss situation. The dose conversion factors of ICRP-116 [5] were used in the antero-posterior (AP) direction to calculate the effective dose rate.

The injection efficiency is an important factor in determining the shielding structure and to estimate the dose rate. In this analysis, the literature information or operation experience of PLS-II were applied to assume an injection or extraction efficiency. During normal operation, a 20-pC electron beam is injected into the booster from linac with a frequency of 0.5 Hz. The beam loss amount and positions are assumed as follows during normal operation:

1. 20 pC/injection is lost during 2 seconds in the storage ring.
2. A 10% beam loss (90% injection efficiency) was assumed during the injection from booster to storage ring of which 5% loss occurs locally and 5% distributed loss in storage ring.
3. A 20% distributed loss was assumed during boosting.
4. A 20% beam loss (80% injection efficiency) was assumed during the injection from linac to booster of which 10% loss occurs locally and 10% distributed in booster.

The beam losses are also schematically shown in Figure 4. In the PHITS calculations, each beam loss scenario mentioned above was simulated and the dose rates were calculated separately. Afterwards, the dose rate from 4 scenarios were summed up to obtain the total dose rate in the full normal operation mode of the facility.

In addition to the normal operation, accidental cases were also investigated as follows:

1- Total loss of stored beam current of 140 mA was assumed.

2- Continuous loss was assumed at one point during injection.

3- Beam loss by failures of magnets for injection or dipole magnets was assumed.

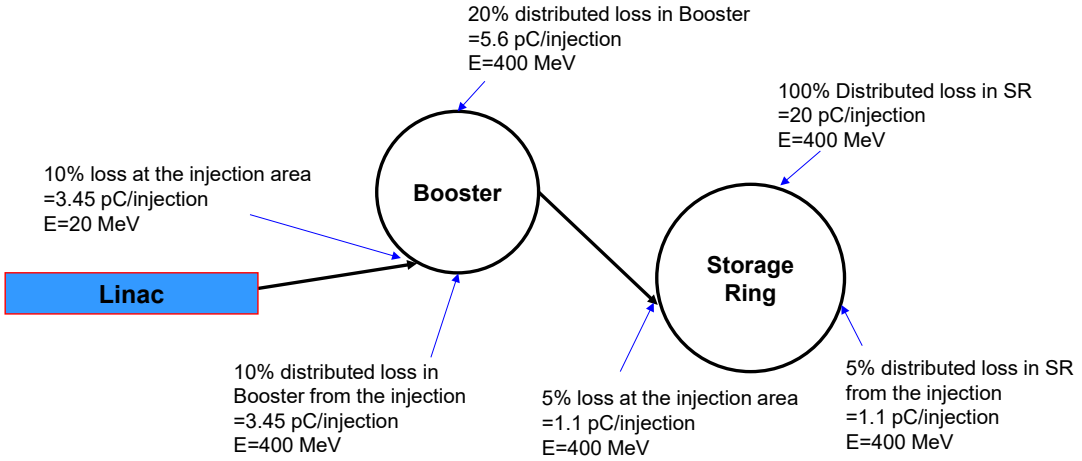

Figure 4: Schematic drawing of the normal beam loss scenario of PAL-EUV.

The PAL radiation control policy aligns with the regulations outlined in the Nuclear Safety Act of Korea [6]. However, the shielding criteria based on the As Low As Reasonably Achievable (ALARA) principle are being managed. According to Korean regulations, specific dose limits have been established for various groups. Radiation workers operating within the facility are subject to an annual dose limit of 20 mSv. Frequent visitors have a set annual dose limit of 6 mSv. The dose limit for the public, including facility users, is 1 mSv. Furthermore, comprehensive monitoring ensures that the radiation dose at the site boundary remains well below the permissible limit, which is 0.25 mSv/year. In PAL, the dose rate limit at the exterior surface of the shielding is 10 mSv/year, which is half of the annual effective dose limit for occupational workers and it is equivalent to 5 μSv/h by considering annual working time of 2000 h.

The areas are classified as Restricted Area, Generally-Controlled Area, Radiologically-Controlled Area, and High Radiation Area. The criteria for area classifications are shown in Table 2.

Classification	Dose
Restricted Area	0.25 mSv/y < Dose < 1 mSv/y
Generally-Controlled Area	1 mSv/y < Dose < 20 mSv/y
Radiologically-Controlled Area	20 mSv/y < Dose < 1 mSv/h
High Radiation Area (No Access)	Dose > 1 mSv/h

Table 2. Criteria for the area classification of PAL [6].

The shielding calculations were performed for normal and accidental scenarios to ensure the dose limit criteria for a specific area discussed above.

3 Results and discussions

The shielding calculations were performed for the normal and accidental beam loss scenarios mentioned above. The results of each scenario are shown and discussed below.

3.1 Normal beam loss scenario

During normal operation of PAL-EUV, a beam loss occurs locally at injection areas as well as uniformly-distributed in the booster and storage ring. Figure 5 illustrates the

calculated dose rate distributions in the top view of the PAL-EUV at the storage ring height of 120 cm. Figure 5(a) is the dose rate distribution from distributed loss of stored beam in storage ring. Figure 5(b) shows the dose rate distribution during injection from booster to storage ring. Figures 5(c,d) indicate the dose rate distributions from distributed beam loss during boosting, and during injection from linac to booster, respectively. According to the PHITS calculations, the dose rate contribution from the ditributed loss of stored beam in the storage (Figure 5(a)) ring was dominant. Total dose rate was estimated by adding the dose rate from 4 cases and the results are shown in Figure 6.

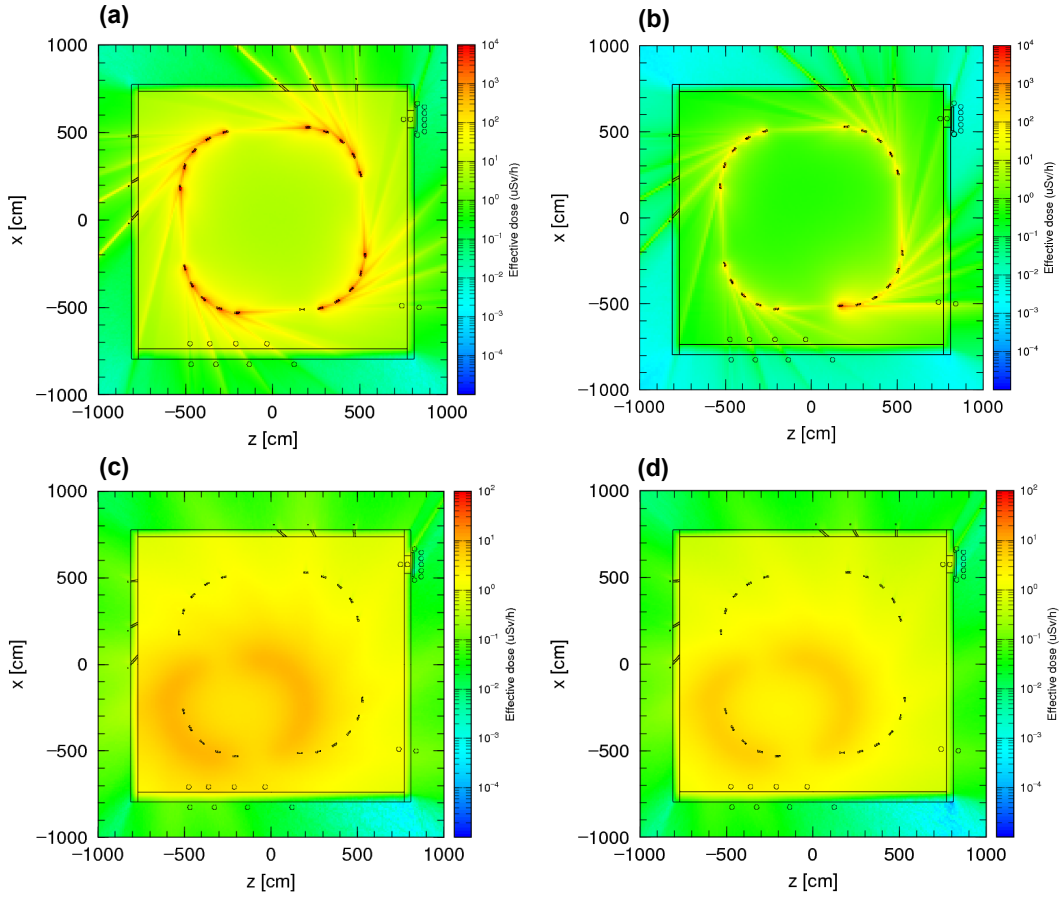

Figure 5: Dose rate distributions at the height of 120 cm for normal beam loss cases, (a) distributed loss of stored beam in storage ring, (b) during injection from booster to storage ring, (c) distributed beam loss during boosting, and (d) during injection from linac to booster.

The 2-D distribution of the total dose rate is indicated in Figure 6(a) at the height of 120 cm which is the storage ring height. The dose level at each area outside of the tunnel e.g. radiofrequency (RF) room, experimental rooms, and building outside are also shown in the 1-D plots in Figures. 6(b-e). It should be mentioned that these calculations are very conservative as very thick targets are used and also the electron energy in the booster is considered to be 400 MeV. The results show that the dose rate of the outside tunnel building reaches 2.2 μSv/h (Figure 6(e)) which is higher than the dose limit of 0.5 μSv/h by a factor of 4.4. An extra shielding needs to be considered to reduce the dose level. The dose rate in other areas around the tunnel is lower than the dose limit during normal operation.

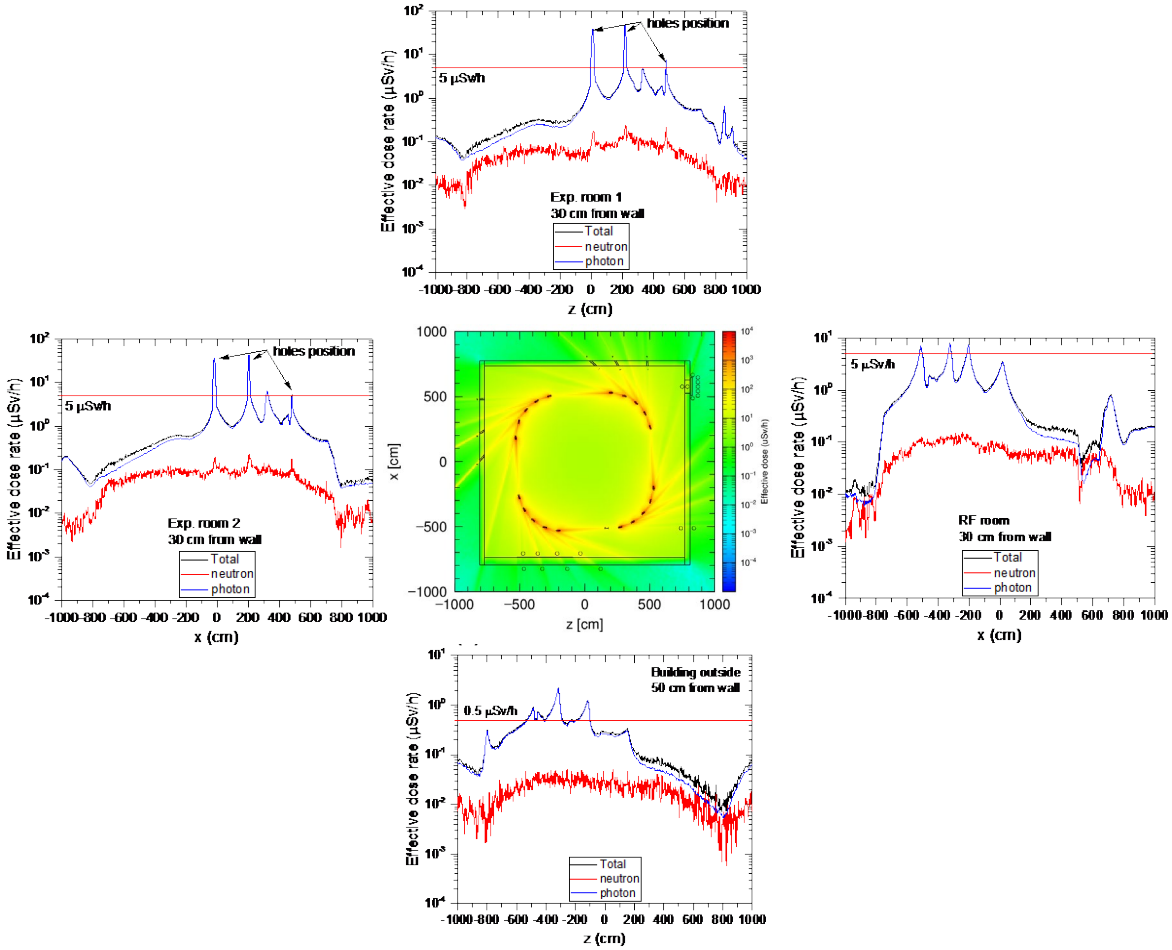

Figure 6: Radiation dose distribution outside of the tunnel for normal beam loss conditions and at the height of 120 cm.

Because the photon dose contribution is dominant, Pb or Fe are reasonable candidates to be used as the extra shielding to reduce the dose rate outside of the building. Figure 7 shows the effect of 3 and 5.06 cm-thick Pb and Fe on the dose rate. A Fe block was installed inside the tunnel, due to its handling simplicity than Pb, to reduce the dose rate.

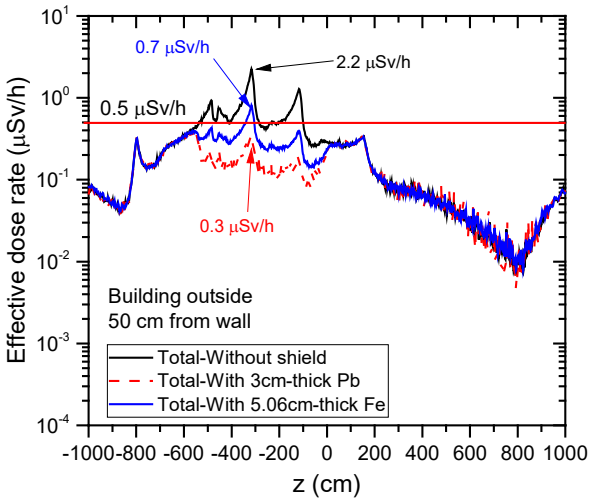

Figure 7: Effect of the Pb and Fe extra shields on the radiation dose level outside of the building.

3.2 Accidental beam loss scenario

For the accidental case scenario (one of several cases), it was assumed that the 140-mA stored electron beam is lost at the dipole magnet position shown in Figure 8(a) so that the bremsstrahlung radiation enters the experimental room. The calculations showed that the dose of this event would be 35 μSv after the beamline hole in the experimental room. This dose value is far below the criterion of 1 mSv/event for the accidental case. Figure 8(a) shows the 2-D distribution of dose resulting from this accidental case. Figure 8(b) shows the 1-D plot of the dose in the experimental room indicated by the dashed line at a distance of 30 cm from the wall. It is concluded that the dose from the accidental case is not severe and is below the limit.

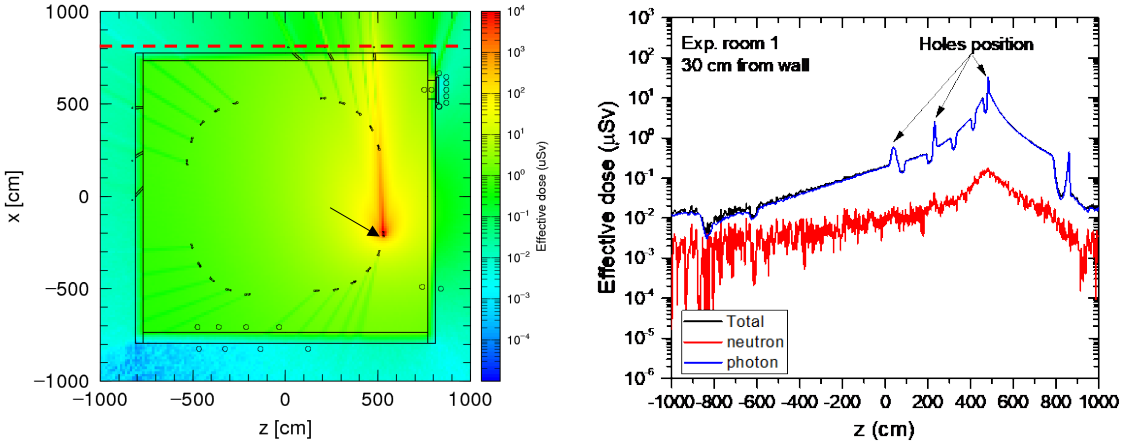

Figure 8: Radiation dose rate distribution at the point for the accidental case beam loss, (a) 2-D distribution, (b) 1-D plot in the experimental room 1 shown by the dashed line in (a).

4 Commissioning status

The commissioning had started in Feb. of 2023 and it was observed that the first beam was accelerated up to 400 MeV stored in the booster synchrotron. The personal safety and interlock system (PSIS) for securing workers was performed perfectively from the e-beam extraction step of the photo-cathode gun and the area radiation monitoring system of PAL-EUV also showed low dose level during whole commissioning period. The monitoring system structure are shown in Figure 9.

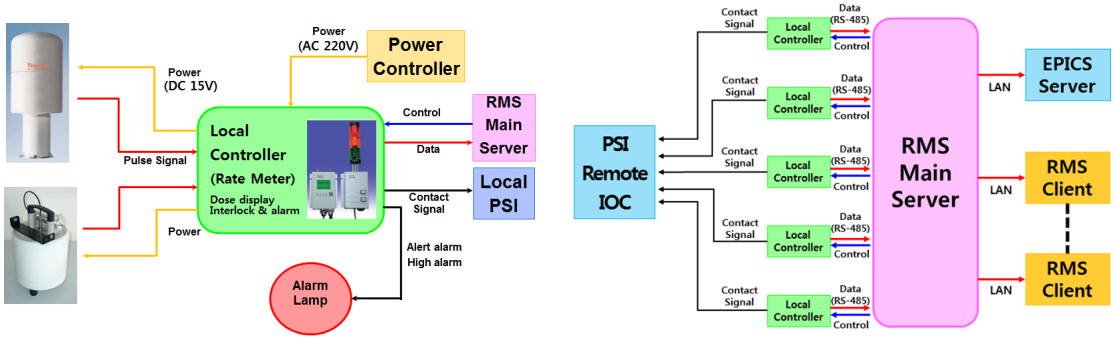

Figure 9: Area radiation monitoring system of PAL-EUV: the combination of pressured ion chamber and wide-energy rem He-3 detector and operating network and interlock connections.

5 Conclusion

Radiation shielding analysis was carried out by PHITS-3.30 for the newly launched PAL-EUV synchrotron facility. The normal and accidental scenarios of operation were considered. The results above show that the current concrete shielding for the storage ring and booster is adequate for operation at 400 MeV to shield the highly penetrating bremsstrahlung radiations. An additional Fe shield was installed to reduce the dose rate outside of the tunnel building which is accessed by the public. Because of the power supply system of dipole magnet at the storage ring, a safety magnet will be also installed to protect workers from the accident electron beam path to a beamline due to the power fail of main dipole magnet.

The radiation control during the commissioning period was carried out safely. The measured dose level showed to confirm the shielding analysis and to ensure the radiation levels are aligned with the ALARA concept.

References

[1] T. Sato, Y. Iwamoto, S. Hashimoto, T. Ogawa, T. Furuta, S. I. Abe, T. Kai, P.-E. Tsai, N. Matsuda, H. Iwase, N. Shigyo, L. Sihver, and K. Niita, J. Nucl. Sci. Technol. **55**, 684 (2018).

[2] H. Hirayama, Y. Namito, A. F. Bielajew, S. J. Wilderman, U. Michigan, W. R. Nelson, and others, The EGS5 Code System, 2005.

[3] N. Kishida, T. Murata, T. Asami, K. Kosako, K. Maki, H. Harada, Y. O. Lee, J. Chang, S. Chiba, and T. Fukahori, AIP Conf. Proc. **769**, 199 (2005).

[4] A. Boudard, J. Cugnon, J. C. David, S. Leray, and D. Mancusi, Phys. Rev. C **87**, 014606 (2013).

[5] N. Petoussi-Henss, W. E. Bolch, K. F. Eckerman, A. Endo, N. Hertel, J. Hunt, M. Pelliccioni, H. Schlattl, and M. Zankl , Ann. ICRP **40**, 1 (2010).

[6] N. S. Jung, H. S. Lee, J. H. Oh, and B. J. Kim, J. Korean Phys. Soc. **66**, 425 (2015).

Personnel Safety Systems for PETRA IV

Dressel M.

Deutsches Elektronen Synchrotron (DESY)
Notkestraße 85, 22607 Hamburg, Germany

Abstract

In the planed DESY project PETRA IV the PSSs for the whole accelerator chain Linac 4, Booster, PETRA 4 storage ring and the 31 beamlines with a total of about 100 experiments and optics hutches will be replaced or newly build based on PLC technology. Here we outline the strategy for developing a functional safety concept and some of the methods envisioned for the requirements assessment, design and development of safety functions.

1 PETRA IV project overview

The PETRA IV project [1] upgrades the PETRA III storage ring to a 4th generation synchrotron source with

- ultra-low emittance, providing
- high brightness with brilliance in excess of 10^{22} [ph/s/mm^2/mr^2/0.001BW],
- hard x-rays in the energy range of 10-50 keV.

Figure 1 gives a schematic overview of the PETRA 4 storage ring, pre-accelerators and experiment halls, including the new hall PXW to be built. Linac 4, the booster and the PETRA 4 storage ring will be built into existing tunnels.

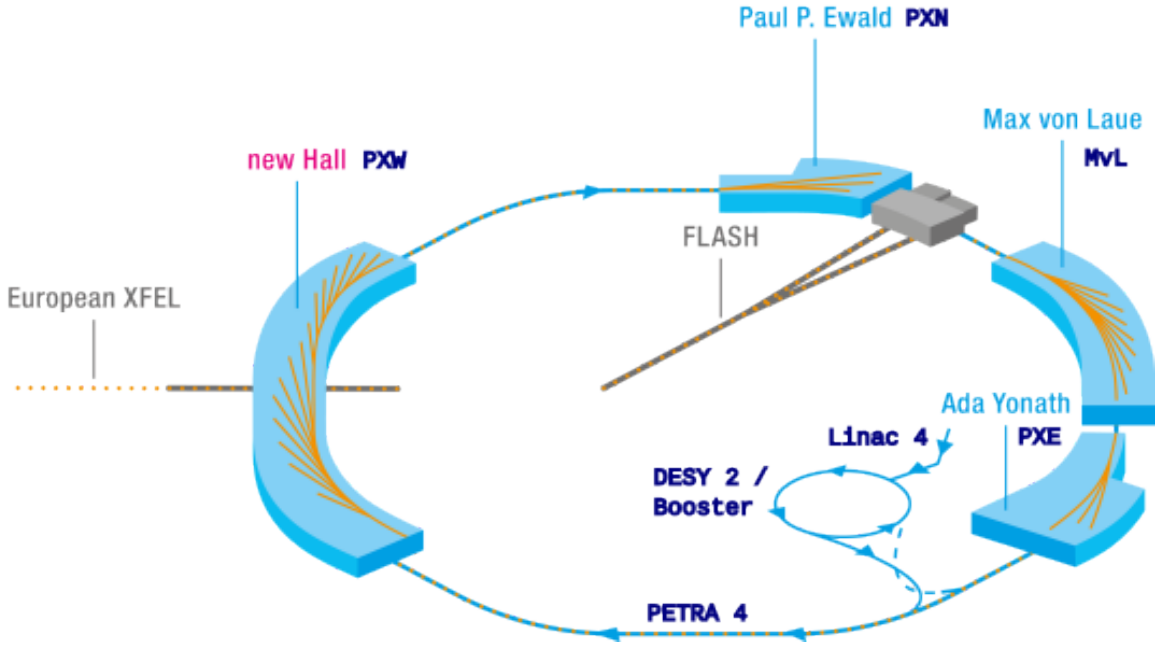

Figure 24: PETRA IV overview (Courtesy of PETRA IV project).

Table 1 and Table 2 list numbers of interlock components related to the door interlock for the three accelerators and the four experiment halls respectively. To support restricted access (ZZ) for a limited amount of personnel to searched (interlocked) accelerator areas without repeating the search procedure, a safety key system is provided. The ZZ procedure makes sure, every person entering the searched area takes a safety key with them. Beam permission can not be granted before all safety keys are returned. The key-locks provide

safety signals to the interlock control. The ZZ procedure is supervised by the operators from the central control room via video and intercom systems.

	Linac	Booster	PETRA	total
interlock-areas	2	2	6	10
ZZ-doors	3	4	17	24
other doors	4	16	15	35
PLC systems	1	1	2 (interlock, and ZZ)	4
PC	1	3	5	9
el. cabinet (el. room)	2	3	8	13
el. cabinet (doors)	5	19	24	48

Table 2: Number of interlock areas, ZZ- and other doors, PLC systems and PCs of the three accelerators. In total 10 accelerator interlock areas with 24 ZZ-doors and 35 other doors will be controlled by 4 PLCs and 9 PCs. The listed 13 and 48 electronics cabinets are related to the electronics rooms and interlock doors respectively.

	PXN	MvL	PXE	PXW	total
beam-lines	3	11	4	13 (+5)	36
optics, hutches	3	15	4	13 (+5)	40
exp. hutches	6	24	9	23	62
(main+back) doors ~	11	60	13	50	134
PLC system and PC	3	11	4	18	36
el. cabinet (el. room)	1	2	1	2	6
el. cabinet (beam-line)	3	11	4	18	36
el. cabinet (door)	9	39	13	41	102

Table 3: Number of beam-lines (parenthesis indicate free slots in PXW), hutches (interlock areas), main- plus back-doors in the PETRA 4 experiments halls: PXN: PETRA-Extension-North. MvL: Max-von-Laue hall. PXE: PETRA-Extension-East, PXW: PETRA-Extension-West. In total about 31 (+5) beam-lines with about 102 areas with about 134 doors will be interlocked. The 6, 36 and 102 electronics cabinets are related to the electronics rooms, beam-lines and to the area doors, respectively.

2. Safety functions

The usual safety function structure can be sketched as a chain with links belonging to the three categories:

Sensor - Logic - Actuator

The overall safety function and all subsystems have to be designed for fulfilling the safety requirements. The total Probability of dangerous Failures per Hour (PFH_d) is the sum of all the subsystem PFH_d.

Examples for requirements on PFH_d of sub-systems and on the overall safety function, a.o. are:

- sub-system and overall architecture,
- Diagnosis Coverage (DC) and test interval,

- Common Cause Failures (CCF),
- failure rate λ_d of the elements,
- useful lifetime (commonly: 20 years),
- Safety Integrity Level (SIL according to IEC 62061) or Performance Level (PL according to ISO 13849).

Below some typical sensors, logics and actuators are listed.

Sensors

- door contacts,
- key locks or switches (for door latching, restricted access (ZZ), beam permission),
- beam shutter position switches,
- magnet current sensors or position switches of movable permanent magnets,
- emergency-off switches,
- light barrier, etc.

Logics

- safety PLC for permissions,
- safety-relays for emergency-off,
- safety diagnostics
- safety network

Actuators

- contactors (circuit breaker) of RF-modulators,
- contactors of high voltage (HV) power supplies,
- safety signals to solid state amplifiers,
- switches of HV getter pumps, etc.

2 Architecture for safety and supplementary functions

Figure 2 depicts the logical view of the architecture relating the components in safety functions (upper part) and in supplementary functions (lower part). The safety PLC is used for both safety and supplementary functions. In addition, PCs are used to provide remote control panels, announcements, logging and support for maintenance.

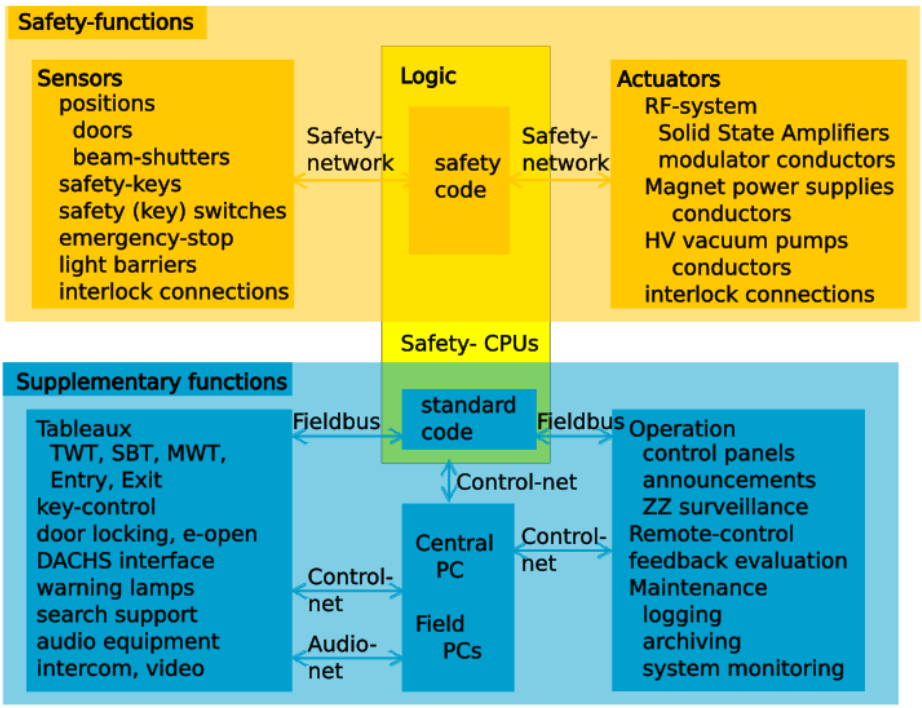

Figure 25: Overview of components within safety functions (upper part) and related supplementary functions (lower part) categories. There will be several distinct functions in both categories. The tableaux: TWT (door in interlock), SBT (radiation prohibited area), MWT (magnet current warning) and the Entry and Exit tableaux, related to the ZZ functions are LED-illuminated text-based signs.

Figure 3 gives a logical view of the architecture used in the access control system DACHS. DACHS is used for authentication. Authentication is required for access to certain areas as well as for conducting search procedures in experiment hutches. Access is granted based on work permits assigned by the area responsible, instructions or trainings required and the possession of dosimeters. The data is managed in the DESY developed DarfDACHS database.

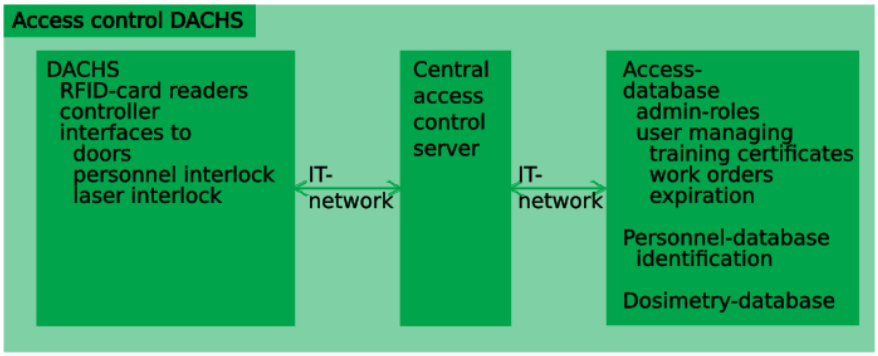

Figure 26: Overview of the access control system DACHS (DESY-Access-Control-System) structured in field devices, central access control server and the databases for managing personnel identification, up-to-date trainings and work orders and dosimetry bookkeeping.

3 Legal requirements

The obligations for manufacturers, very generally, are addressed in the EU directive for machinery 2006/42/EC covering e.g. the requirements for safety components and devices producing ionizing and other radiations. Occupational regulations, in Germany e.g. TRBS 1115, do also address functional safety.

Both refer to the same standards:

- ISO 12100 (risk assessment),
- ISO 13849 (functional safety),
- IEC 62061 (functional safety),
- (TRBS 1115 also to IEC 61511 (process industry) organization etc.).

It should be realized that the directive and the standards, listed above, provide state-of-the-art means for assessing safety requirements, designing safety systems as well as evaluating the achieved safety. No other state-of-the-art frameworks is known to the author that would provide quantifiable and qualifiable safety measures.

A top-down-initiated iterative approach is followed within the standards. The overall risk assessment should be started already with the development of the facility concept. In case it is found that risk reduction by safety functions is required, depending on the complexity of a system or facility, a Management of Functional Safety (MFS) should be implemented.

The Management of Functional Safety addresses:

- organizational responsibilities e.g. roles and their relations and limitations,
- qualification and competence of personnel assigned to roles,
- processes for safety strategy and system development,
- evaluation of appropriateness, effectiveness, compliance etc. to finally provide the basis for granting the permission to operate by the organizational responsible people.

3.1 Risk assessment in General

A risk assessment should be conducted according to ISO 12100. In case measures are required for risk reduction:

- Safety concepts have to be developed respecting the required independence given by the amount of risk reduction to be achieved.
- All safety measures have to be appropriate and effective for their safety tasks.
- The concept and safety measures have to follow the reasoning and have to be evaluated.
- All activities have to be traceable and documented.

3.2 Basic MFS goals

In case functional safety is required to reduce risks, a MFS should be implemented. The MFS must make sure that

- methods,
- work flows (processes) as well as,
- the safety systems

reach the following goals permanently:

- appropriateness,
- effectiveness,
- traceability,

- and maintainability.

3.3 Top-Down-initiated iterative procedure

Systematic identification of all hazards of the overall system is based on a top-down initiated iterative procedure that passes top-level safety requirements on to subsystems.

Some reasons for this approach are e.g.:

- Essential hazards of the overall system are evident from start, e.g. accelerators are to deliver electron beams and undulators are to deliver photon beams with high brightness. This already puts demands on subsystems such as e.g. beam shutters.
- Additional hazards occur by combining subsystems. E.g. RF-system produces additional ionizing radiation when combined with cavities. This puts additional safety requirements on the RF-system with respect to the electrons accelerated by the cavities.

Controlling these hazards puts requirements on subsystems that cannot be derived from the subsystems alone. E.g. SIL-requirement on shutting off the modulators.

Hazards of the overall system and hazards occurring by combining subsystems generate additional requirements on the overall system and the subsystems in turn.

The top-down setup allows to add these requirements as soon as possible to the requirements of the subsystems.

In turn, the subsystems as well as the combination of subsystems can create new hazards not immanent in the top-level concept. Controlling these hazards may also put increased demands on safety functions and their subsystems, in reverse.

Therefore, the risk assessment, risk analysis and MFS are iterative processes.

3.4 The two basic types of safety requirements

For the development and implementation of safety functions and components two basic types of safety requirements are distinguished: systematic and hardware safety integrity. Both safety integrity demands increase with increasing required SIL_r or PL_r.

Functional safety demands both kinds of integrities, see table 3.

	Systematic Safety Integrity	**Hardware Safety Integrity**
to:	prevent systematic failures	cope / master random failures
by:	robust process	robust design

Table 4: Two kinds of integrities required (Courtesy of A. Cords).

Higher safety levels put increasing demands on the qualities listed in table Table 4

Systematic Safety Integrity	**Hardware Safety Integrity**
management	reliability
planning	diagnoses
documentation	architecture
quality	failure modes
V&V	redundancy
independence	

Table 5: Required qualities separated for the two kind of integrities (Courtesy of A. Cords).

4 Glance on a process under development for the group MPS at DESY

Figure 4 shows the process map related to the part of the PSS the group MPS is responsible for. The process is currently under development.

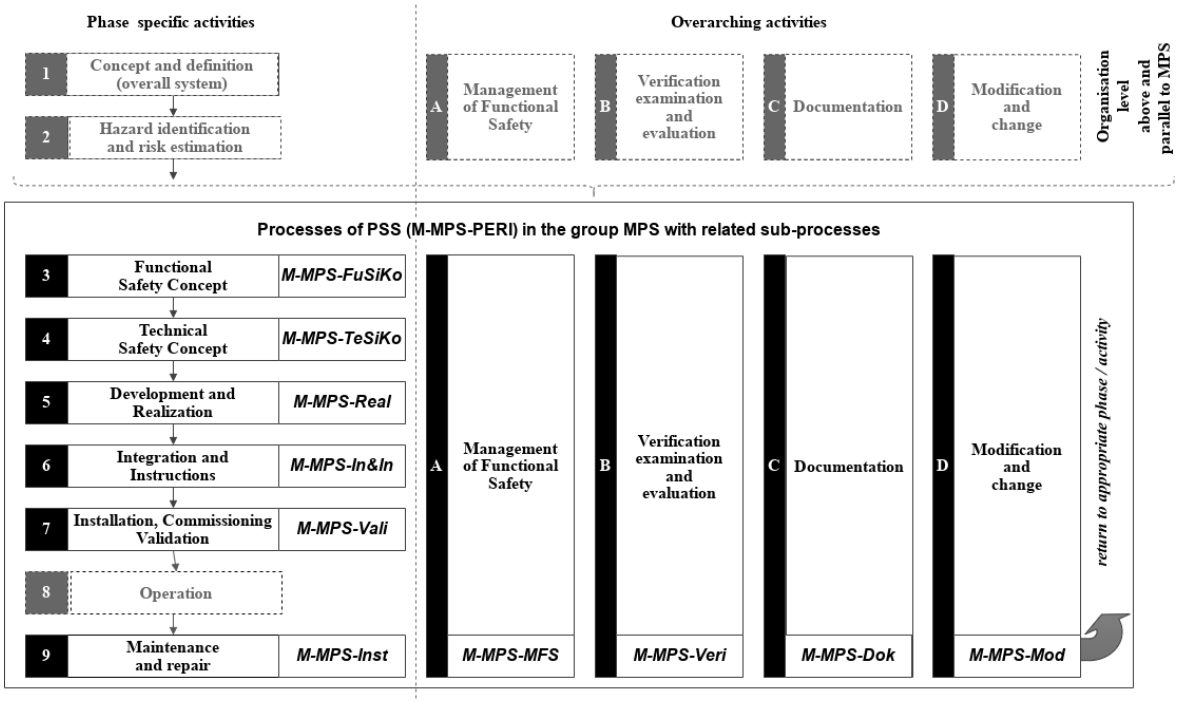

Figure 27: MFS process within group MPS (Courtesy of A. Cords).

The process (M-MPS-PERI) is started in case the overall hazard analysis and risk assessment require the reduction of risks due to ionizing radiation by means of safety functions. Practically, already during the risk assessment the group MPS is involved.

The process displayed in Figure 4 is divided in the sub-processes 1 to 9 accompanied by the overarching activities A-D.

For each of these sub-processes and activities exist dedicated descriptions defining roles, responsibilities, the required input and the to be delivered results.

The roles have to be assigned to personnel in agreement with the required independence according to the safety level required.

5 Example implementation methods

The PETRA IV project comprising three accelerators and 31 (initially) beam lines to be equipped with new PSS systems requires a high level of modularization and automation in order to manage the large number and variety of systems to be produced.

The modularization should already start at the very beginning of the development i.e. during the concept phase and risk assessment.

In this section the strategy for implementing the parts of the safety functions the group MPS is responsible for is briefly outlined.

The overall concept of the implementation is based on the organization sketched in Figure 5.

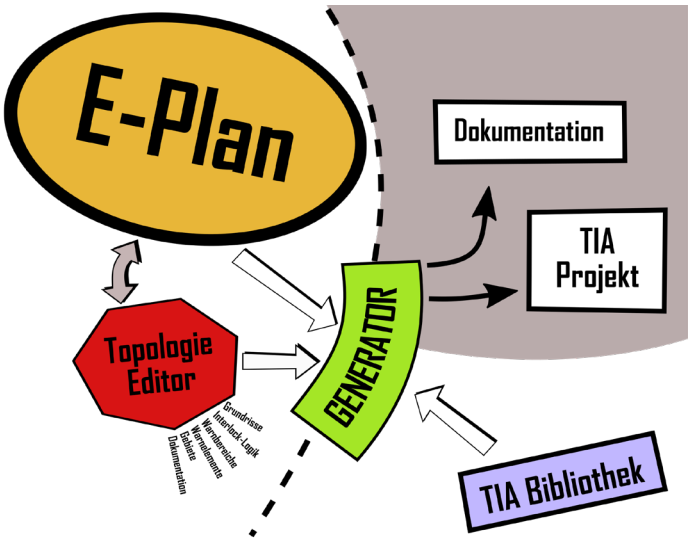

Figure 28: Code generation based on certified third party modules as well as self-verified and -qualified modules (Courtesy of S. May and A. Kropmanns).

From the electronical construction (done with EPLAN), see Figure 6, lists of components, I/Os, connections etc. are exported providing the first input to a generator developed for the automated generation of PLC code.

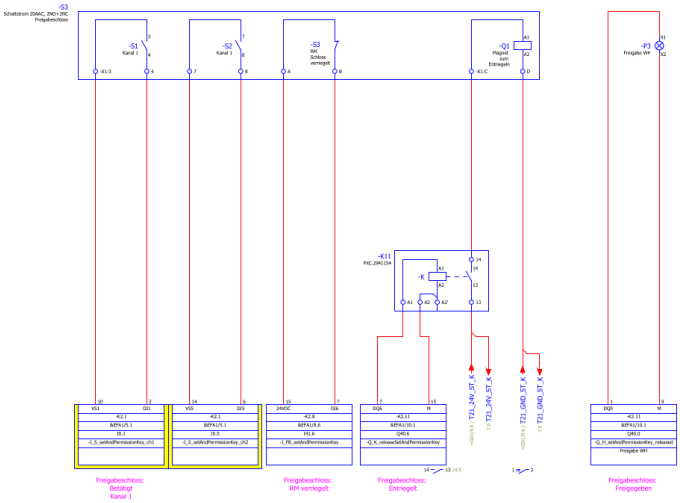

Figure 29: Snapshot of an example using EPLAN. Electrical construction providing input to the generator (Courtesy of A. Kropmanns).

The generator is developed by the group MPS using C# and the TIA openness interface from Siemens. Custom modules are developed and added to a library being used by the generator. The module and application software development are done using the so-called matrix method [2], supported by the tool SOFTEMA [3], see Figure 7.

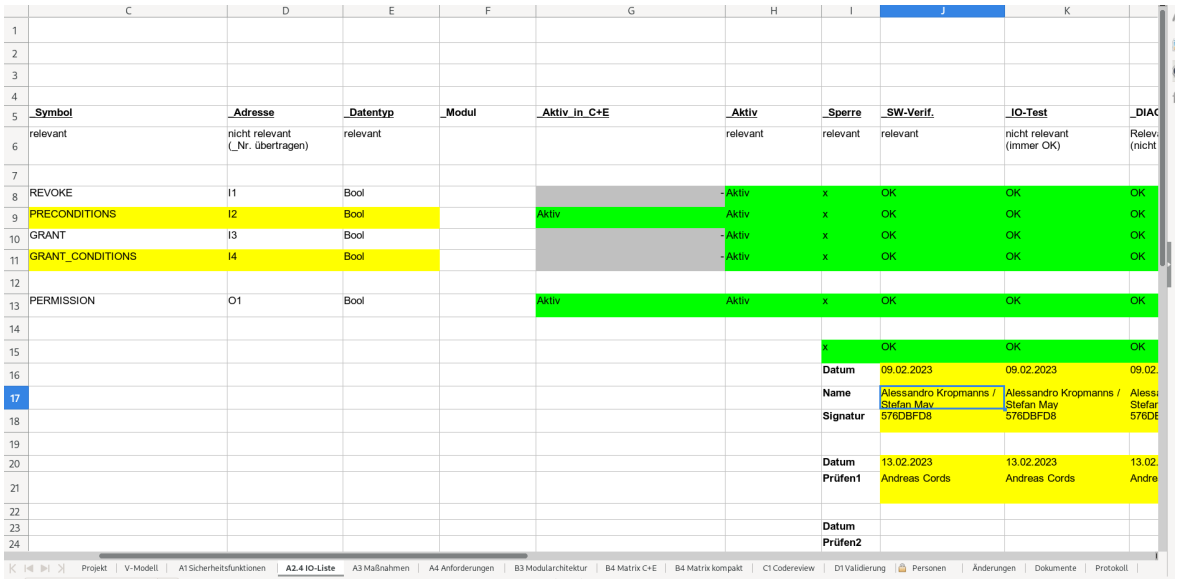

	C	D	E	F	G	H	I	J	K	
1										
2										
3										
4										
5	_Symbol	_Adresse	_Datentyp	_Modul	_Aktiv_in_C+E	_Aktiv	_Sperre	_SW-Verif.	_IO-Test	_DIAC
6	relevant	nicht relevant (_Nr. übertragen)	relevant			relevant	relevant	relevant	nicht relevant (immer OK)	Relev (nicht
7										
8	REVOKE	I1	Bool		-	Aktiv	x	OK	OK	OK
9	PRECONDITIONS	I2	Bool		Aktiv	Aktiv	x	OK	OK	OK
10	GRANT	I3	Bool		-	Aktiv	x	OK	OK	OK
11	GRANT_CONDITIONS	I4	Bool		-	Aktiv	x	OK	OK	OK
12										
13	PERMISSION	O1	Bool		Aktiv	Aktiv	x	OK	OK	OK
14										
15							x	OK	OK	OK
16							Datum	09.02.2023	09.02.2023	09.02.
17							Name	Alessandro Kropmanns / Stefan May	Alessandro Kropmanns / Stefan May	Alessa Stefar
18							Signatur	576DBFD8	576DBFD8	576DE
19										
20							Datum	13.02.2023	13.02.2023	13.02.
21							Prüfen1	Andreas Cords	Andreas Cords	Andre
22										
23							Datum			
24							Prüfen2			

Projekt | V-Modell | A1 Sicherheitsfunktionen | A2.4 IO-Liste | A3 Maßnahmen | A4 Anforderungen | B3 Modularchitektur | B4 Matrix C+E | B4 Matrix kompakt | C1 Codereview | D1 Validierung | Personen | Änderungen | Dokumente | Protokoll

Figure 30: Snapshot of an example using the matrix method tool SOFTEMA (Courtesy of A. Cords).

The individual configuration of a project is programmed in an XML format. As an example, Figure 8 shows an XML snippet used by the generator together with library modules to create the PLC code displayed in Figure 9

```
<permission id="HfPermission">
  <preconditions>
    <or>
      <and>
        <internal>ShortingPlate1</internal>
        <internal>ShortingPlate2</internal>
      </and>
      <and>
        <internal>BeamWarning</internal>
        <internal>RadiationMonitor</internal>
      </and>
    </or>
    <internal>EmergencyStop</internal>
  </preconditions>
  <grantconditions>
    <input>I_S_modulatorOff_HF</input>
    <input>I_S_modulatorOff_HV</input>
  </grantconditions>
</permission>
```

Figure 31: Generator code snippet (Courtesy of S. May).

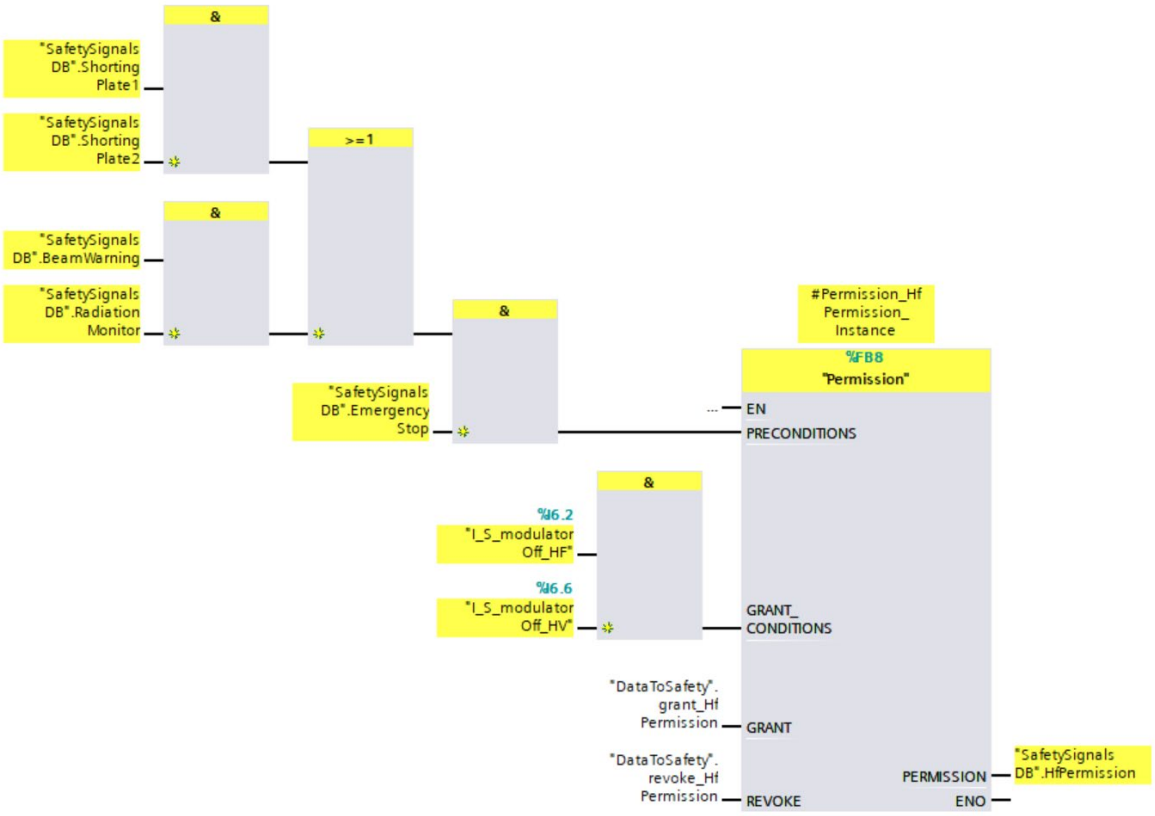

Figure 32: Generated code example (Courtesy of S. May).

6 Summary

The PSS for PETRA IV aims to be safe and compliant with the safety standards. Processes are developed and implemented to manage functional safety. Software tools are used to support the documentation and verification from specification to validation. Modularization and automated project generation is developed in order to deal with the large variability of accelerators and experiments safety systems.

References

[1] PETRA IV: Upgrade of PETRA III to the Ultimate 3D X-ray Microscope.
Conceptual Design Report.
Schroer, C. G. et al. 2019, ISBN: 9783945931264,
http://dx.doi.org/10.3204/PUBDB-2019-03613

[2] Huelke, M.; Becker, N.; Eggeling, M.: Sicherheitsbezogene Anwendungssoftware von Maschinen – Die Matrixmethode des IFA (IFA Report 2/2016). Ed.: Deutsche Gesetzliche Unfallversicherung e. V. (DGUV), Berlin 2016 ISBN (print): 978-3-86423-165-0
(https://dguv.de/ifa/fachinfos/arbeiten-4.0/industrie-4.0/sicherheitsbezogene-maschinensoftware/index-2.jsp)

[3] Software-Assistent SOFTEMA: Spezifikation zur IFA-Matrixmethode bei sicherheitsbezogener Anwendungssoftware. Hrsg.: Institut für Arbeitsschutz der Deutschen Gesetzlichen Unfallversicherung (IFA), Sankt Augustin

Shielding Considerations for BEATS beamline (SESAME)

Zahran I.Y*, García-Fusté M.J [1], Hamad A.M*.

* SESAME (Synchrotron-Light for Experimental Science and Applications in the Middle East), Allan 19252, Jordan. [1]ALBA Synchrotron Light Source, 08290 Cerdanyola del Vallès, Barcelona, Spain.

Abstract

BEATS (BEAmline for Tomography at SESAME) beamline has a 3T 3-pole-wiggler as insertion device located on a short straight section of the SESAME storage ring. The beamline aims at producing synchrotron beams in the range of hard X-ray for tomography techniques.
This work gives the recommendation for the shielding of BEATS hutches: material and thickness for the different walls. Those requirements have been checked by FLUKA Monte Carlo simulation to ensure that the outside contact radiation levels are below the guideline of 0.5 μSv/h limit when considering a vacuum chamber pressure of 5×10-9 mbar. All the calculations were done under the supervision of Radiation Protection Service of ALBA synchrotron.

1 Introduction

The Synchrotron-Light for Experimental Science and Applications in the Middle East (SESAME) is an independent laboratory located in Allan in the Balqa governorate of Jordan.
SESAME is composed of:

- A 22.5 MeV microtron,
- A 800 MeV booster synchrotron, with a repetition rate of 1 Hz,
- A 2.5 GeV, 400 mA electron storage ring, with a circumference of 133.2 m,
- Beamlines utilizing radiation extracted by the storage ring through bending magnet (BM) and insertion device (ID) sources.

To date, three beamlines are operative at SESAME: IR, XAFS/XRF and Material Science. Two new beamlines dedicated to hard X-ray tomography and soft X-ray spectroscopy are under final research commissioning procedures.

BEATS project has received funding from the EU's H2020 frame work programme for research and innovation under grant agreement n°822535. BEATS involves leading research facilities in the Middle East (SESAME and the Cyprus Institute), and European synchrotron radiation facilities ALBA-CELLS (Spain), DESY(Germany), the ESRF (France), Elettra (Italy), INFN (Italy), PSI (Switzerland), SESAME (Jordan) and SOLARIS (Poland). BEATS beamline has a 3T 3-pole-wiggler as insertion device located on a short straight section of the SESAME storage ring.

1.1 Objective

The objective of this document is to describe the results of the shielding calculations made for BEATS Beamline at SESAME to guarantee public zone outside BEATS shielding in operation with dose rates below 0.5 μSv/h (derived from the dose limit for non-exposed workers, assuming 2000 working hours per year).

1.2 Hypothesis for the shielding calculations

The Monte Carlo code used for these calculations is FLUKA code [1], [2], the following parameters are used for the calculations:

- Electron energy: 2.5 GeV
- Stored beam current: 400 mA
- Average pressure in the straight section: 5.0×10^{-9} mbar, with the residual gas composition given in Table 1.

Molecule	Relative pressure (%)	Partial pressure (mbar)
H_2	80	1.12×10^{-9}
CO	10	1.4×10^{-10}
CO_2	5	7×10^{-11}
Noble gases	3	4.2×10^{-11}
H_2O	2	2.8×10^{-11}

Table 6: Residual gas composition in the straight sections, used for the bremsstrahlung shielding calculations. The partial pressures in the third column correspond to a total pressure of 1.4×10^{-9} mbar[3].

Figure 1 and Figure 2 show BEATS beamline components in SESAME. The shielding elements are shown in Table 2 and table 3. The maximum permitted total dose rates outside BEATS shielding should be below 0.5 μSv/h. To achieve this aim, the Beamline was allowed to operate at higher pressure value without surpassing the public access classification. All the shielding calculations for BEATS Beamline are performed with an average pressure in the straight section of 5×10-9 mbar, this will guarantee that at the design pressure of 1.4×10-9 mbar, will be within our guidelines.

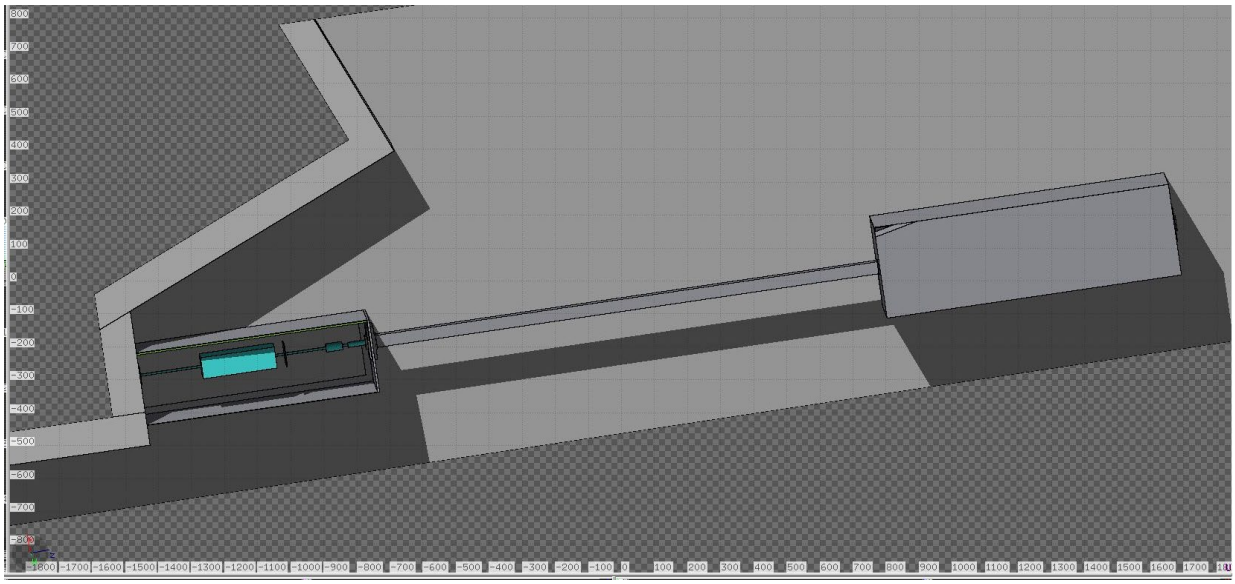

Figure 1: 3D top view of BEATS beamline

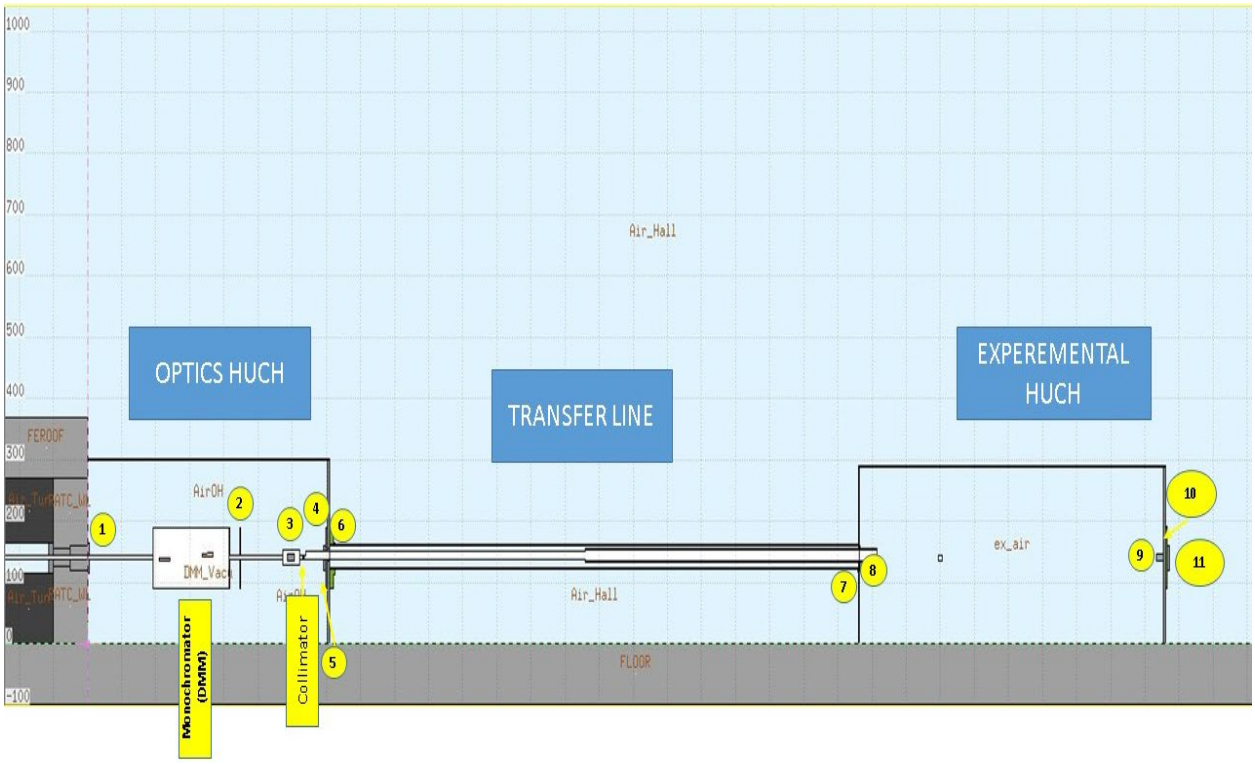

Figure 2: Side view of BEATS beamline.

2 BEATS shielding elements

2.1 Structural shielding

Table 2 summaries the recommendation for the shielding of BEATS hutches: material and thickness for the different walls. Those requirements have been checked by Monte Carlo simulation to ensure that the outside radiation levels are close to the background when considering a vacuum chamber pressure of 5×10-9 mbar.

Element	Material and thickness
Sidewall OH-I	Pb 15 mm +PE 50 mm
Sidewall OH-0	Pb 10 mm
Backwall OH	Pb 60 mm +PE 100+Pb 5
Roof OH	Pb 5 mm
Frontwall EH Sidewall EH-I Sidewall EH-O	Pb 20 mm
Backwall EH	Pb 60 mm
Roof EH	Pb 20 mm

Table 2: Structural shielding elements

2.2 Non-structural shielding

As it has been done with the other beamlines currently in operation at ALBA, non-structural shielding elements are also needed to cope with the scattered radiation produced by the different optic elements. Among them: Lead screens, guillotines, beam stops and chicane entrances to allow feeding the instruments with adequate supplies (power supplies,

data acquisition, fluids, etc.). Table 3 provides the characteristics of these BEATS local shielding elements, such as their minimum dimensions and construction material.

#	**Shielding Elements**	**Height (cm)**	**Width (cm)**	**Thickness (cm)**	**Material**
1	Tunnel-to-OH guillotine	50	50	5	Pb
2	Local Pb screen behind DMM	100	70	2	Pb
3	Safety Shutter			20	W
4	OH_backwall-to-TL guillotine	40	40	6.5	Pb
5	OH backwall central reinforcement	100	100	5	Pb
6	OH-backwall neutron central shield	100	100	10+0.5	PE + Pb
	Extension of OH-backwall neutron shield over the TL collar	Along the first 15.5 cm of TL		5+0.5	PE + Pb
7	ExpHall-to-EH guillotine	54	42	2	Pb
8	TL to EX guillotine	40	40	2	Pb
9	EH-B beamstop	20	12	20	W
10	EH-B neutron central reinforcement on outer side	100	100	5+0.5	PE + Pb
11	EH-B central reinforcement after neutron shield	40	40	5	Pb
12	Collar around TL	-	-	2	Pb

Table 3: Non- structural shielding elements.

2.2.1 Collimator

To ensure that no ray will hit the TL and reduce the total photon flux reaching the Experimental Hutch.

Single tungsten collimator placed 29.3 cm upstream the OH back wall. Aperture of 22 (h) x 26 (v) mm2 and fill the entire vacuum chamber, figure 3.

The use of a collimator adds a scattering element inside the OH, thus incrementing the radiation level at this hutch, but allows for a dose rate reduction of a factor 5 inside the Experimental Hutch.

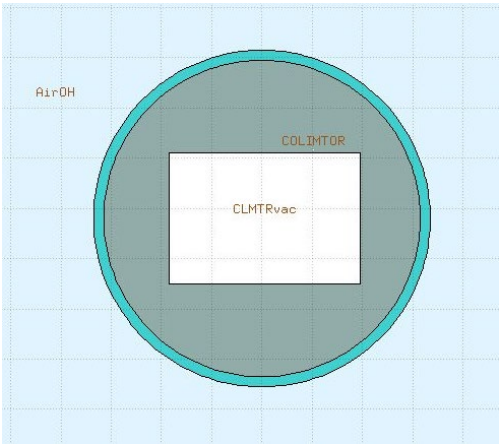

Figure 3: Collimator geometry by FLUKA.

2.2.2 Safety Shutter

Located at the end of the optical hutch, to allow access to the experimental hutch when there is beam inside the optics hutch, Figure 4.

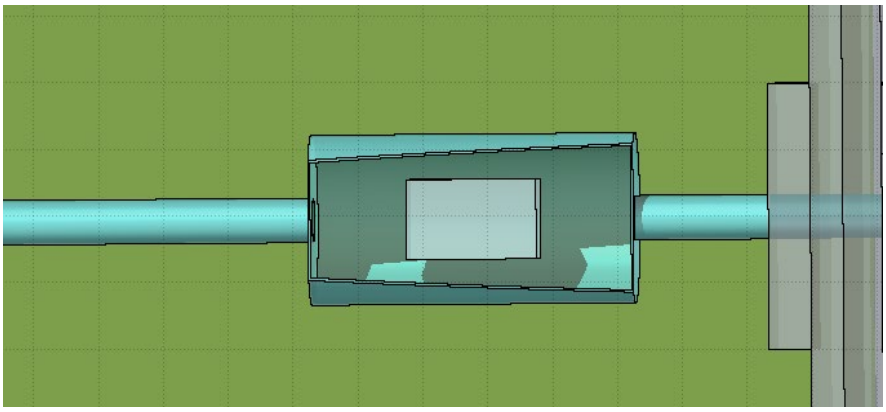

Figure 4: Safety Shutter geometry by FLUKA.

2.2.3 Beam Stopper

A bremsstrahlung stop is needed at the end of the experimental hutch to absorb all the flux coming from the OH through the TL in any beamline configuration. This beam stop must deal with the neutrons production induced by the primary photons.

A 200 mm × 120 mm × 200 mm (h × w × t) Tungsten beamstop must installed inside EH on EH-Backwall at the nominal beam height of 1400 mm (Figurer 5).

On the outer side of EH-B, a central 50-mm-thick neutron shielding in polyethylene with a surface of

1 m × 1 m must be installed at the nominal beam height of 1400 mm (Figurer 5).

The neutrons reinforcement is followed by a 400 mm × 400 mm rectangular screen with minimum lead thickness of 50 mm (Figurer 5).

The surface of the polyethylene layer which is not in contact with the lead screen must be covered with a 5-mm-thick lead wrapping (Figure 5).

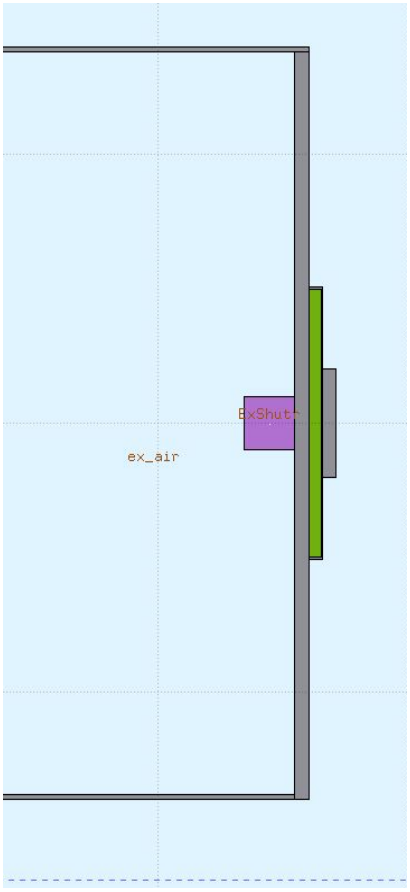

Figure 5: Back wall of experimental hutch with non-structural elements, by FLUKA geometry.

3 Shielding calculation results

We will discuss the dose rate caused by both bremsstrahlung and Synchrotron radiation from insertion devices (ID).

Noting that, the working angle (θ) (figure 6) is between 0.23 degree (maximum energy of 50 keV) and 1.1 degree.

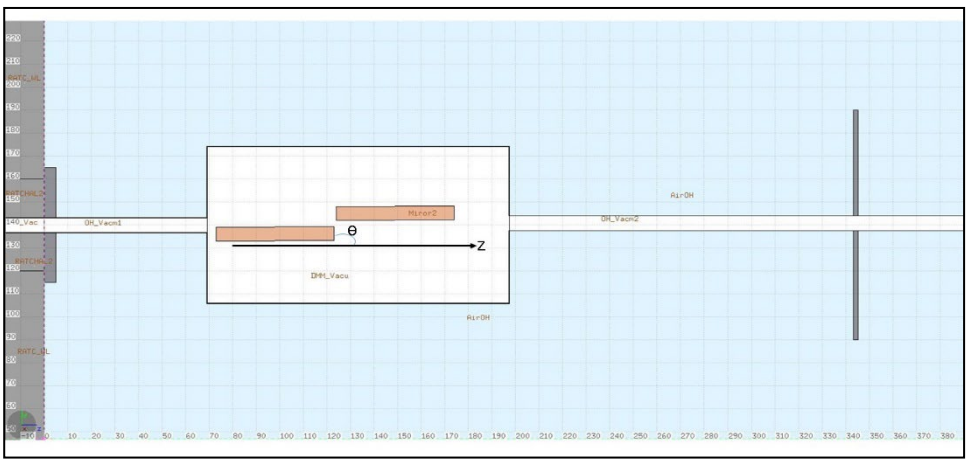

Figure 6: The working angle (θ) of the two mirrors.

We classified the scenarios for three classes: high priority scenarios, medium priority scenarios and low priority scenarios. In this paper we will display some scenarios of the high priority.

3.1 Scattered bremsstrahlung case

This section details the Monte Carlo simulation results used to calculate dose rate for scattered bremsstrahlung, describing the BEATS Beamline optical elements. The geometry used for the calculation was BEATS Beamline geometry (Figure 2) including Tables 1, 2 and 3 for shielding elements, and using the gas bremsstrahlung source. The following scenarios will be studied:

3.1.1 Accident with white beam (OH mirrorless down to EH) with TL pipe at atmospheric pressure.

Figures 7,8 and 9, show respectively the total dose rates (in µSv/h) for OH, TL and EH, at 140 cm height for OH and 144cm for TL and EH (primary beam level). It can be observed that the maximum total dose rate outside BEATS Optical Hutch, Transfer line and Experimental Hutch are less than 0.1 µSv/h (for 5.0×10^{-9} mbar).

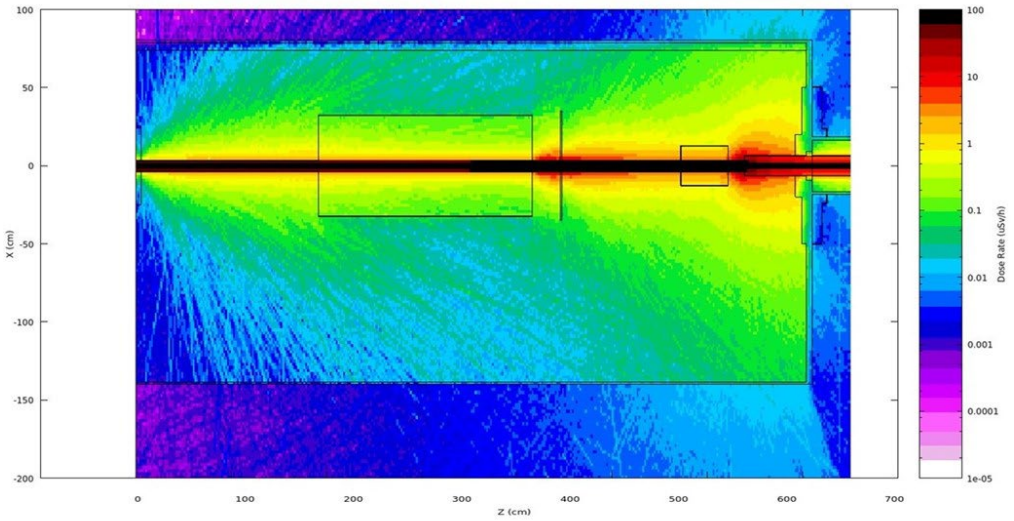

Figure 7: Total Dose Rate (µSv/h) from scattered bremsstrahlung for Optical Hutch.

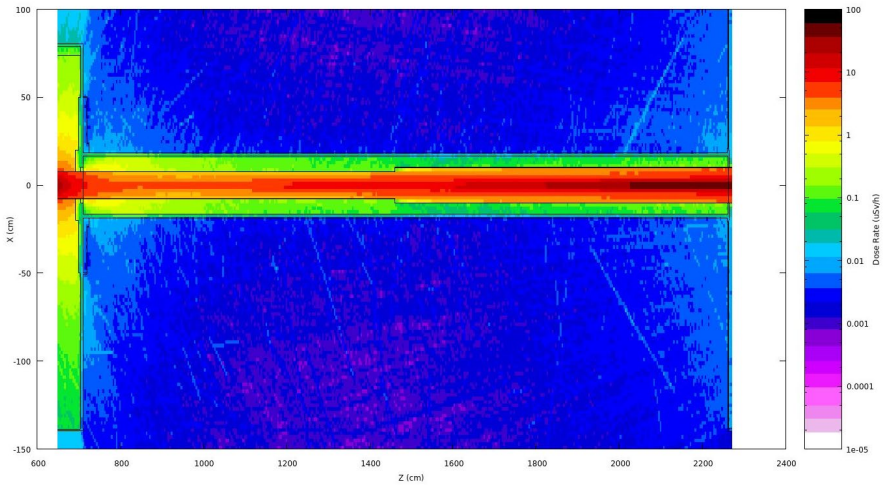

Figure 8: Total Dose Rate (µSv/h) from scattered bremsstrahlung for transfer line.

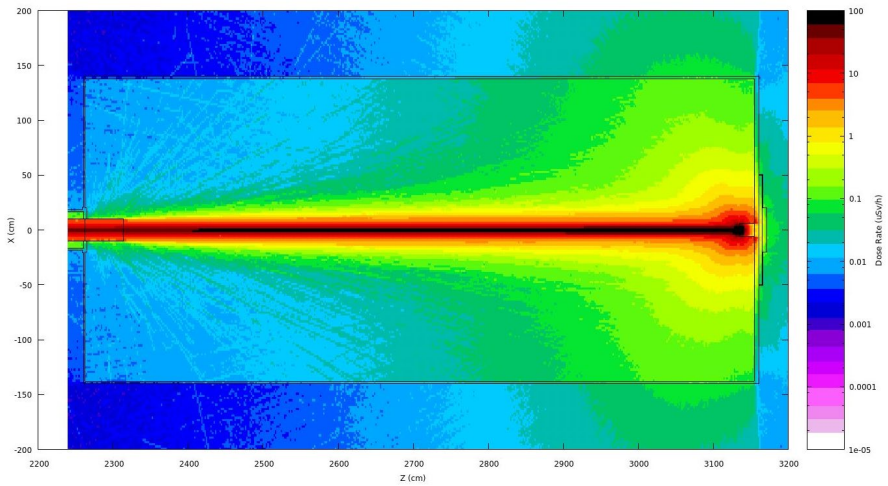

Figure 9: Total Dose Rate (µSv/h) from scattered bremsstrahlung for Experimental Hutch.

3.1.2 White beam (OH Mirrorless down piece of NEAR Cu as sample holder)

Figures 10, 11 and 12, show respectively the total dose rates (in µSv/h) for OH, TL and EH, at 140 cm height for OH and 144cm for TL and EH (primary beam level).. It can be observed that the maximum total dose rate outside BEATS Optical Hutch, Transfer line and Experimental Hutch are less than 0.1 µSv/h (for 5.0×10^{-9} mbar).

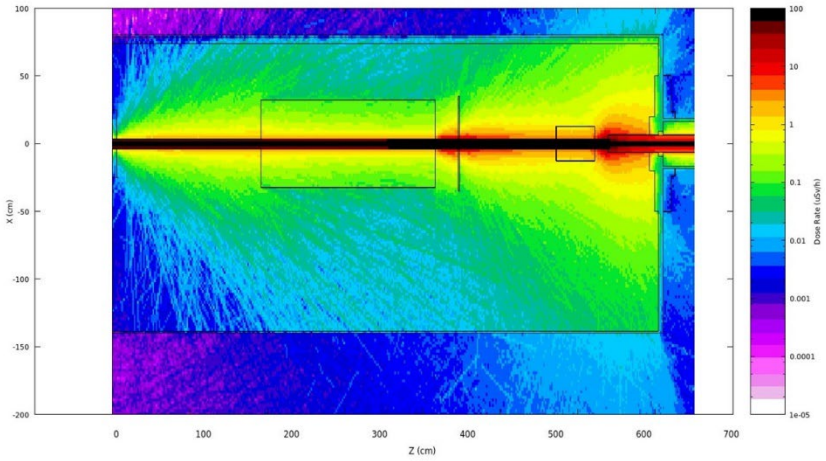

Figure 10: Total Dose Rate (µSv/h) from scattered bremsstrahlung for Optical Hutch.

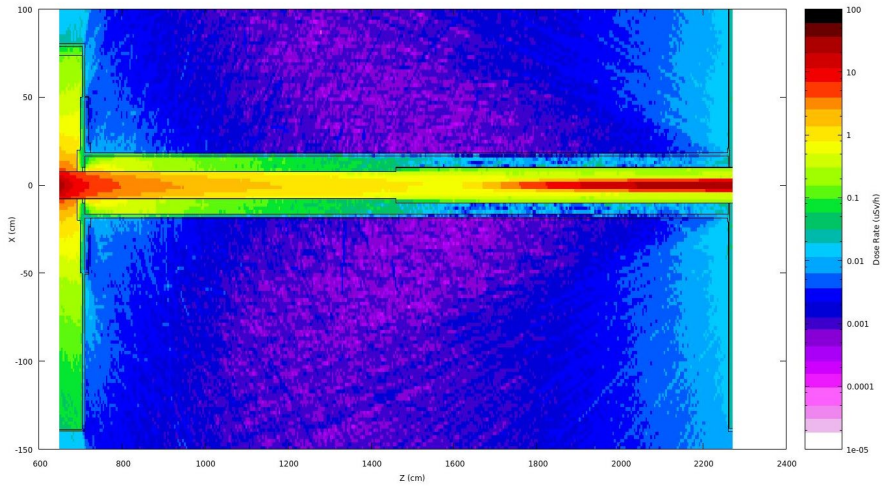

Figure 11: Total Dose Rate (µSv/h) from scattered bremsstrahlung for transfer line.

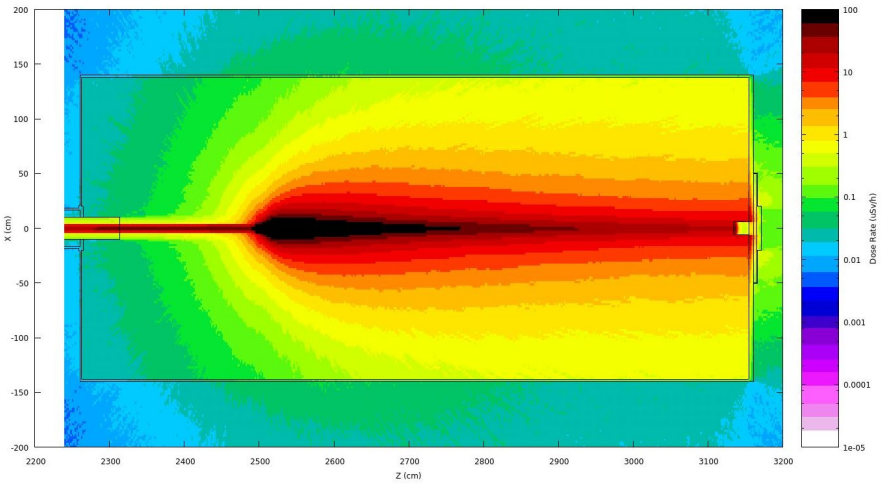

Figure 12: Total Dose Rate (µSv/h) from scattered bremsstrahlung for Experimental Hutch.

3.2 Synchrotron radiation from ID case

Considering wiggler ID, and using the Flux file from the wiggler and FLUKA code, the simulation was carried out for the two cases:

3.2.1 For the first case (OH mirrorless with open safety shutter and no samples)

Figure 13,14 and 15, show respectively the total equivalent dose rates around OH, TL and EH, at 140 cm height (primary beam level) (µSv/h) from ID source photons with BEATS geometry and shielding. The results show effective dose rates below background level outside the hutches.

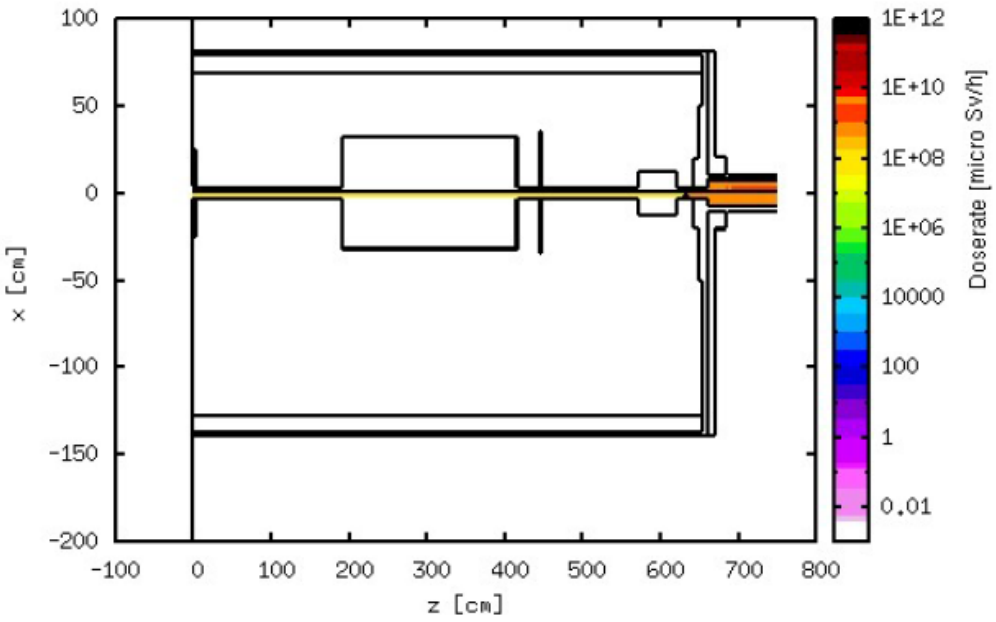

Figure 13: Total dose rate map (in µSv/h) around OH from ID source photons with BEATS geometry and shielding.

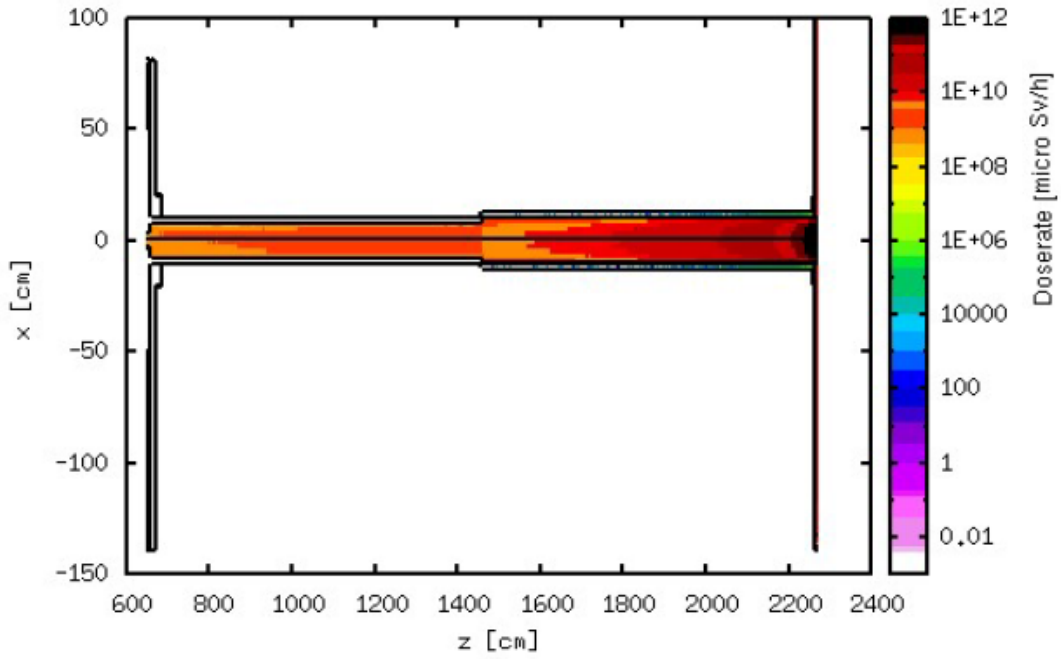

Figure 14: Total dose rate map (in µSv/h) around TL from ID source photons with BEATS geometry and shielding.

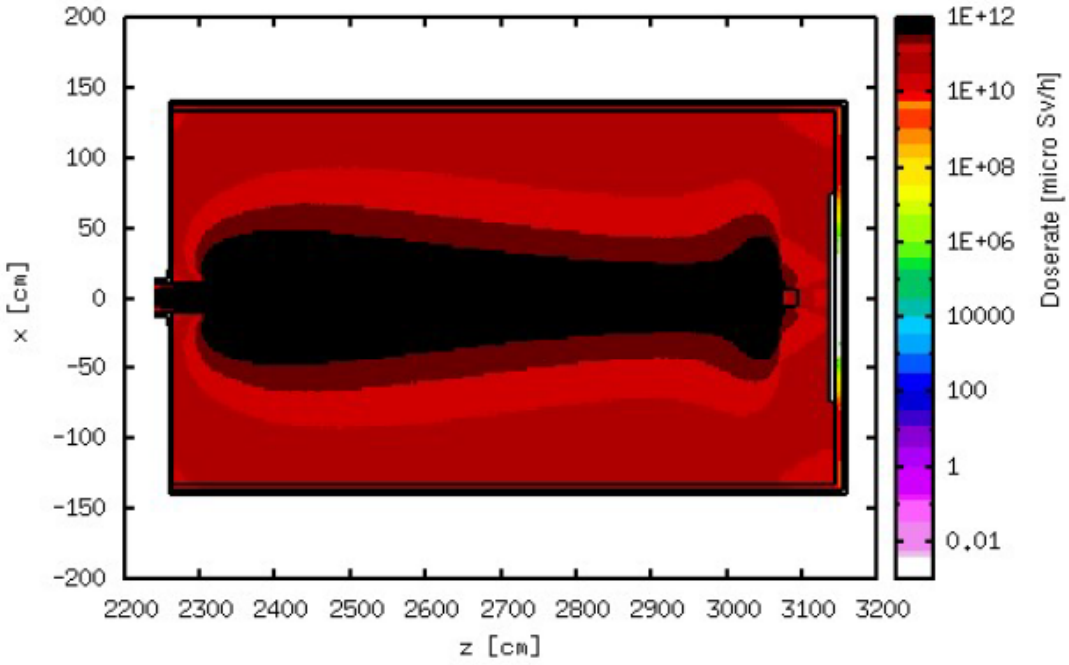

Figure 15: Total dose rate map (in µSv/h) around EH from ID source photons with BEATS geometry and shielding.

3.2.2 For the second case (all mirrors are installed with open safety shutter and no samples)

Figure 16, 17 and 18, show respectively the total equivalent dose rates around OH, TL and EX at 140 cm height (primary beam level) (µSv/h) from ID source photons with BEATS geometry and shielding. The results show effective dose rates below background level outside the hutches, confirming that the shielding requirements for scattered synchrotron radiation are largely met by the shielding thicknesses required for scattered bremsstrahlung.

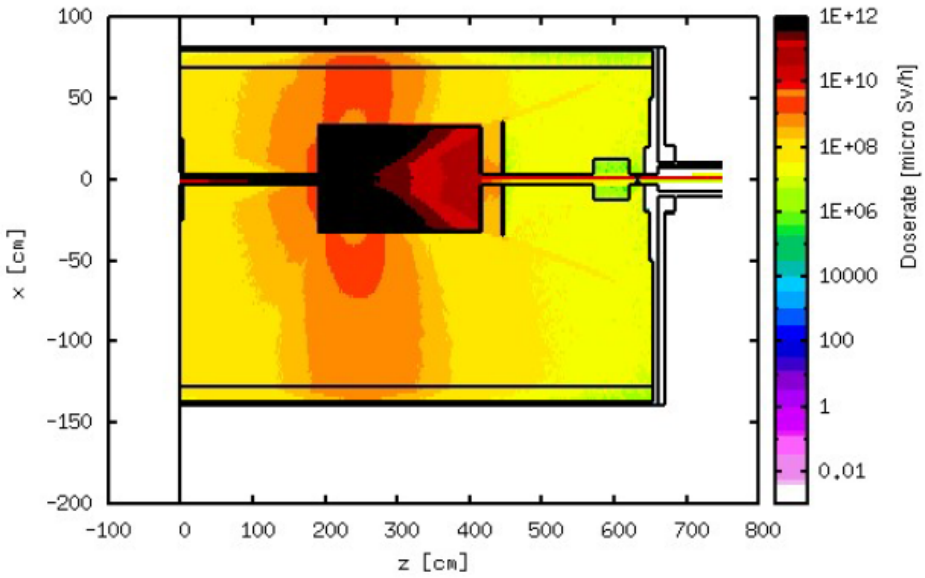

Figure 16: Total dose rate map (in µSv/h) around OH from ID source photons with BEATS geometry and shielding.

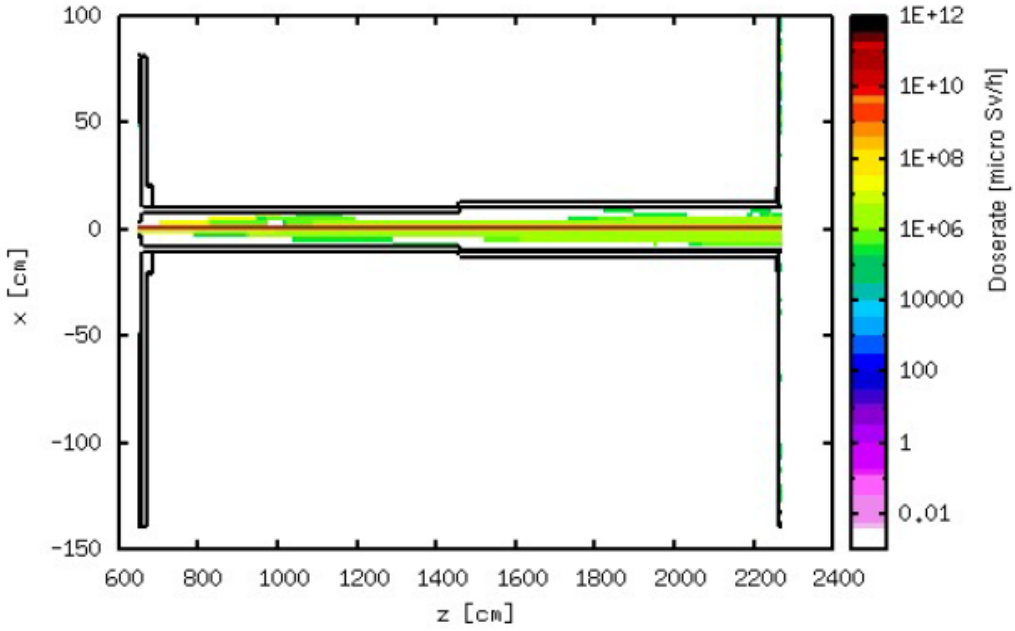

Figure 17: Total dose rate map (in µSv/h) around TL from ID source photons with BEATS geometry and shielding.

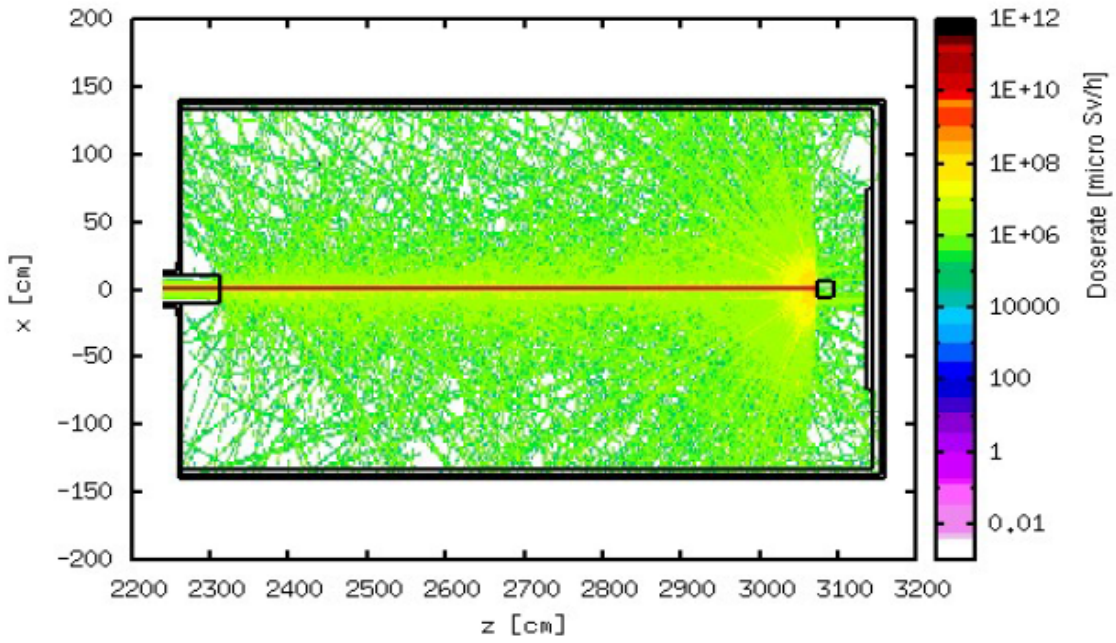

Figure 18: Total dose rate map (in µSv/h) around EH from ID source photons with BEATS geometry and shielding.

4 Conclusion

FLUKA simulations have been done, in order to evaluate the radiation dose at the BEATS beamline. The Gas-Bremsstrahlung can be blocked by shielding elements, and the dose rate outside the hutches are below 0.5µSv/h within our guidelines.

5 Acknowledgment

BEATS Beamline is funded by the European Union's Horizon 2020 research and innovation programme. The project is coordinated by the ESRF. The radiation calculations were done under the supervision of ALBA CELLS (Spain). All the RUN processes were done at ALBA cluster, by Radiation Protection Officer (María-José García-Fusté), she was the person responsible for the deliverable of the work package (04) report [3], many thanks for her.

References

[1]- "The FLUKA code: Description and benchmarking" G. Battistoni, S. Muraro, P.R. Sala, F. Cerutti, A. Ferrari, S. Roesler, A. Fasso`, J. Ranft, Proceedings of the Hadronic Shower Simulation Workshop 2006, Fermilab 6--8 September 2006, M. Albrow, R. Raja eds., AIP Conference Proceeding 896, 31-49, (2007).

[2]- "FLUKA: a multi-particle transport code" A. Ferrari, P.R. Sala, A. Fasso`, and J. Ranft, CERN-2005-10 (2005), INFN/TC_05/11, SLAC-R-773.

[3]- Work package 04 report, work package title: Beamline Technical design and instrumentation procurement, García-Fusté M.J, Zahran I.Y and Hamad A.M (2020).

Assessment of shielding for Diamond-II beamlines

Doull R.E., Faruk S.

Diamond Light Source Ltd, Diamond House, Harwell Science and Innovation Campus, Didcot, Oxfordshire, OX11 0DE, United Kingdom

Abstract

In common with many synchrotron light sources around the world which are carrying out or planning upgrades, the Diamond machine upgrade involves replacing the current Double Bend Achromat lattice structure with a Multi-Bend Achromat in order to reduce the emittance of the electron beam and so increase the brightness and coherence of the emitted synchrotron light [1], the energy will also be increased from 3 GeV to 3.5 GeV, the current will remain at 300 mA. In addition to the upgrades to the accelerators, some beamlines will upgrade insertion devices (ID) and optics; other beamlines will move from bending magnet sources to insertion device sources on the new mid-straights created by the multi-bend lattice structure. This requires that the shielding requirements of all existing beamlines be reassessed. Using STAC8, we calculated the dose rates outside of the shielding using a constraint of 0.5 µSv/h (1mSv/y for 2000 hrs working year). Diamond was shielded to operate at 500 mA; therefore, in most cases, the existing shielding is sufficient for the increased radiation output of Diamond-II. STAC8 calculated that increased shielding is required for some beamlines. Due to the expense and technical difficulties of increasing entire walls or sections, we are using FLUKA models to confirm if additional shielding is needed and identify precisely where additional shielding is required.

1 Initial assessment of shielding

1.1 Assessment using STAC8

As Diamond-II will include many changes, the existing shielding needed assessing to ensure that radiation exposure to staff visitors and users is kept as low as reasonable practicable.

As the deadline for the initial assessment was challenging STAC8 was used to assess the shielding of all existing beamlines. We input the specifications of the new machine and where applicable new ID parameters. The existing shielding was used as a starting point and the dose rates outside the shielding calculated. Where the dose rate was greater than 0.5 µSv/h the shielding thickness was increased until the calculated dose rate was below 0.5 µSv/h.

Table 1 shows the beamlines where the shielding thickness needed to be increased as calculated by STAC 8.

Beamline	Area 1	Additional Pb	Area 2	Additional Pb	Other areas
I02	EH 2 beamstop	2mm			
B07	Currently soft x-ray, new OH in design phase				
K11	Transport pipe	3mm			
I12	See sec 2.1				
I13	OH1 lat wall, Roof	1mm lat wall, 1mm roof, Restrict access to roof	OH2 end wall	2mm centred on beampipe 575mm diameter	
I14	OH1 lat wall, Roof	4mm lat wall, Restrict access to roof	OH3 upstream wall	1mm centred on beampipe 430mm diameter	3mm Pb beamstop 100mmx100mm EH2, Pb Skirting OH1
B16	OH1 end wall	17+13 ($1m^2$ centre)	OH1 Lateral wall	2	
B18	OH1 end wall	17+13 ($1m^2$ centre)	OH1 Lateral wall	2	
I20	OH1 roof	2mm roof, Restrict access			
B21	OH1 end wall	17+13 ($1m^2$ centre)	OH1 Lateral wall	2	
I24	OH1&2 roof	1mm roof, Restrict access	Transport pipe	3	

Table 1: Additional Beamline shielding calculated using STAC8

For some of the beamlines the additional shielding is trivial, easy to install and relatively inexpensive. Where increases to the roof have been calculated it has been decided that access to the roof will be restricted and an assessment will be made during operation to see if this will be made permanent. Table 1 shows that some beamlines require a significant amount of shielding, from a financial and technical perspective it was clear that this may not be feasible, and a more accurate analysis was required.

2 FLUKA Analysis

2.1 Beamline I12 STAC8 FLUKA comparison

I12 is a 4.2 T Wiggler beamline capable of taking white beam, STAC8 calculated a number of shielding increases:

OH2

Side wall (inboard): additional 3mm Pb in some areas. (Fig 1).
Side wall (outboard) additional 6mm Pb in some areas. (Fig 2)

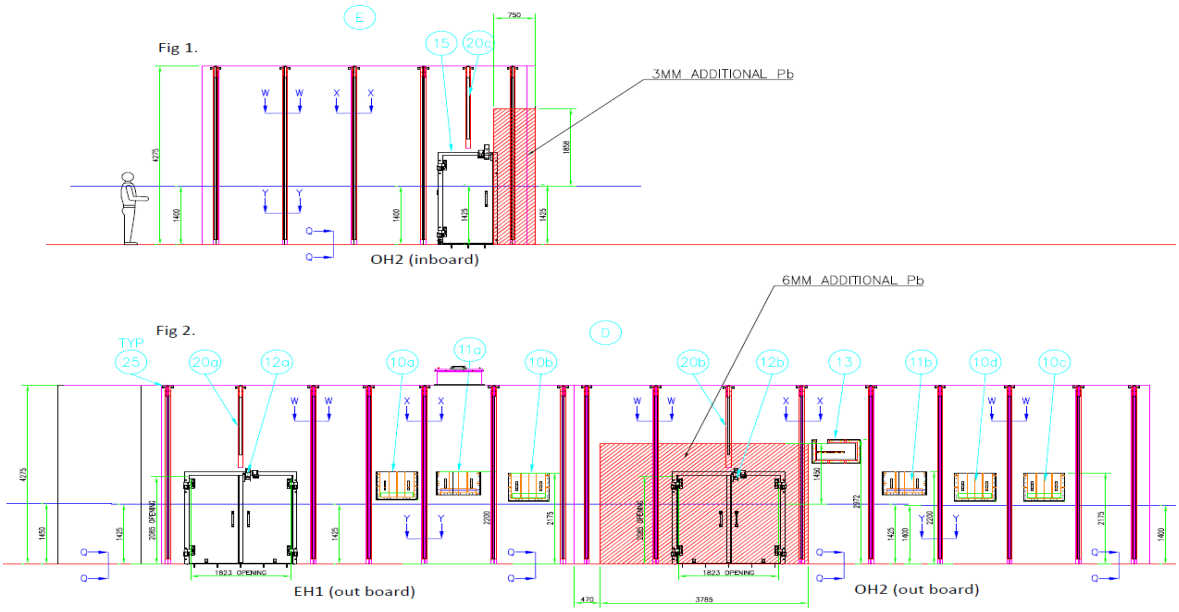

Figures 1 & 2: I12 OH2 Side walls

OH1, SS1, OH2 and EH1 roof 400mm (OH1, SS1, OH2) 391mm (EH1) wide strip from Downstream end wall along entire length of hutch roofs additional 3mm Pb. (Fig 3)

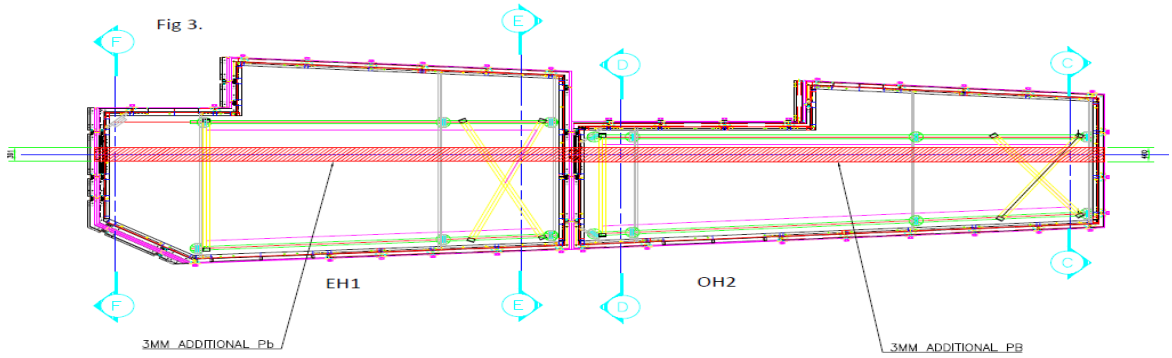

Figure 3: I12 Roof

EH1

Side wall (inboard with search door) additional 9mm Pb over most of the wall. (Fig 4)

Side wall 2 (inboard wall): 6mm Pb extra, all along. (Fig 5)

Side wall 3 (outboard wall): 5mm extra all along. (Fig 6)

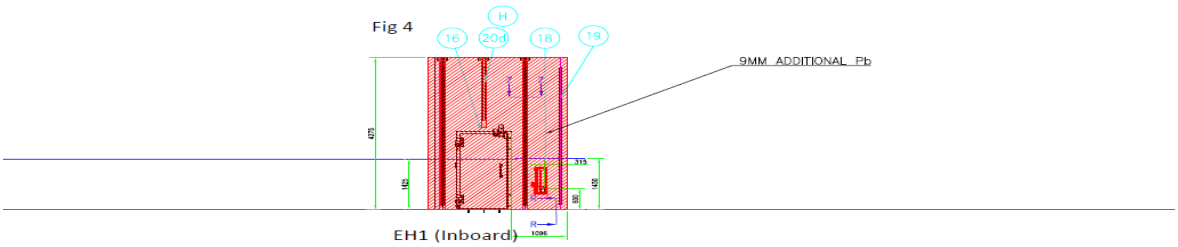

Figure 4: I12 EH1 search door.

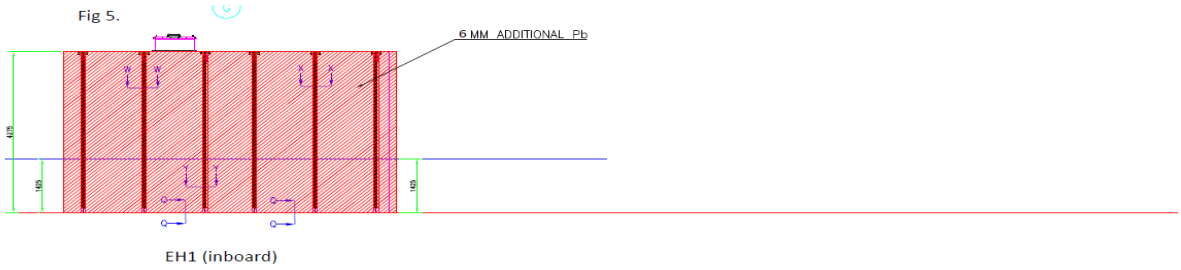

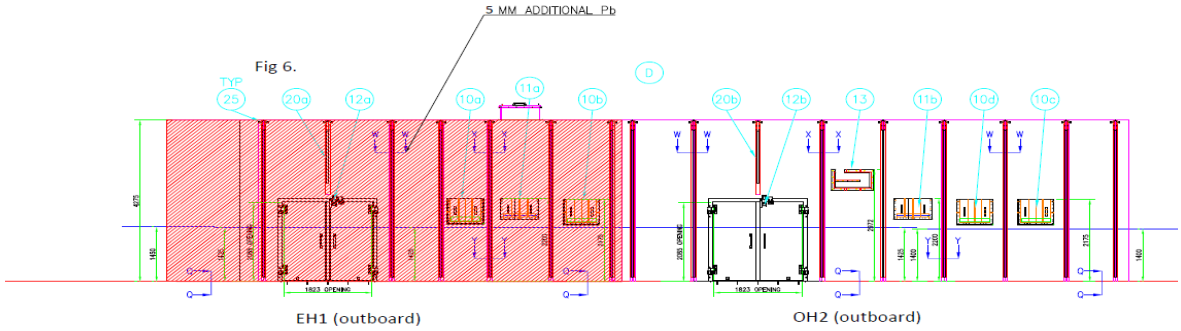

Figures 5 & 6: I12 EH1 Side walls.

As shown above the roof, a number of doors and surrounding areas were calculated as needing more shielding this presents a particular challenge for I12 as the beamline takes white beam into the Experiments hutch and the doors are already extremely thick and therefore heavy.

Using FLUKA a full model of I12 was bult and the following scenarios were considered.

- White Beam, terminated at shutter in OH2 and sample target and shutter EH1
- Mono Beam, terminated at shutter in OH2 and sample target and shutter EH1
- GB, terminated at shutter in OH2 and sample target and shutter EH1

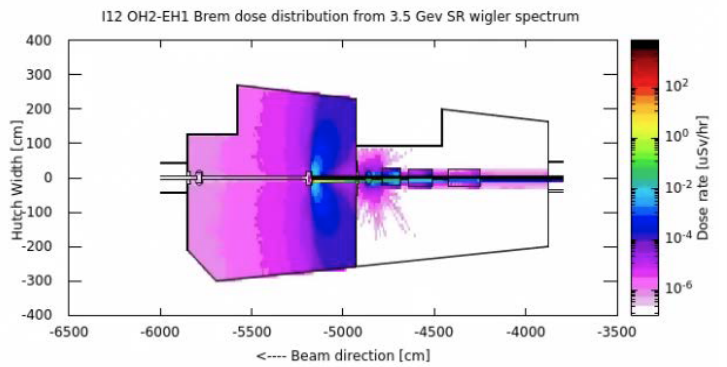

Figure 7: Sidewall dose distribution for GB Beam on Cu target in EH1.

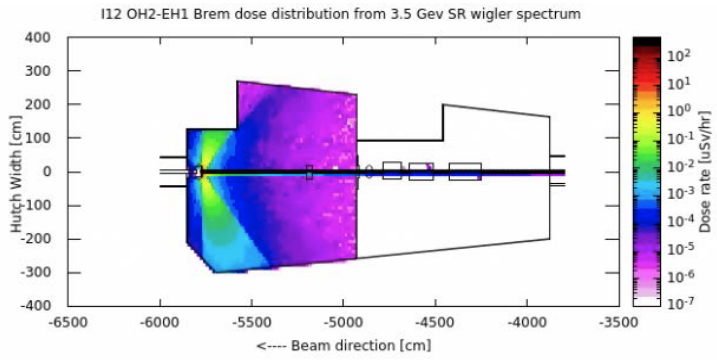

Figure 8: Sidewall dose distribution for GB Beam on EH1 W shutter.

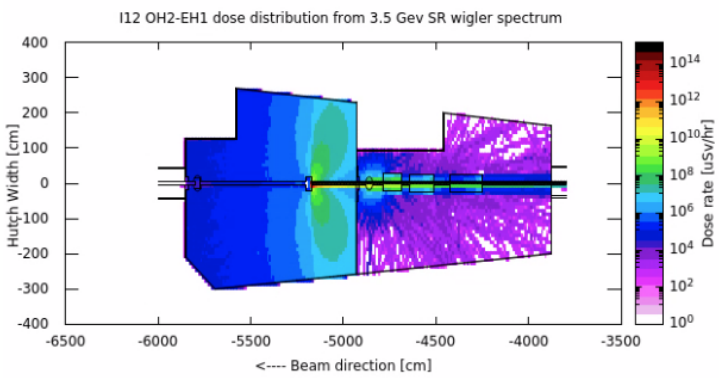

Figure 9: Sidewall dose distribution for Whitebeam on Cu target in EH1.

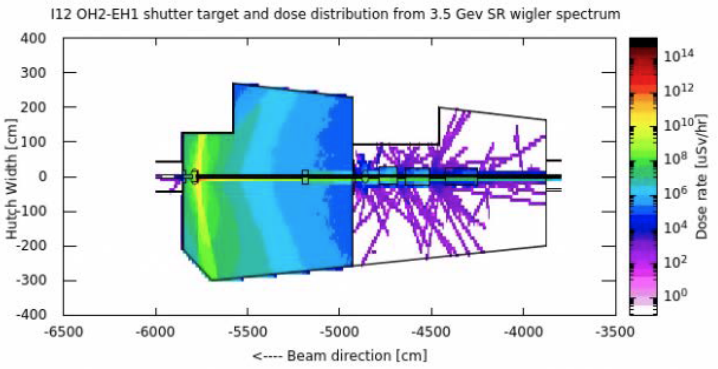

Figure 10: Sidewall dose distribution for Whitebeam on EH1 W shutter

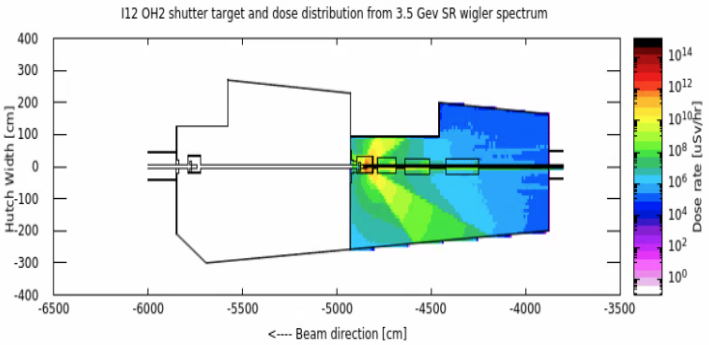

Figure 11: Sidewalls dose distribution for whitebeam on OH2 W shutter.

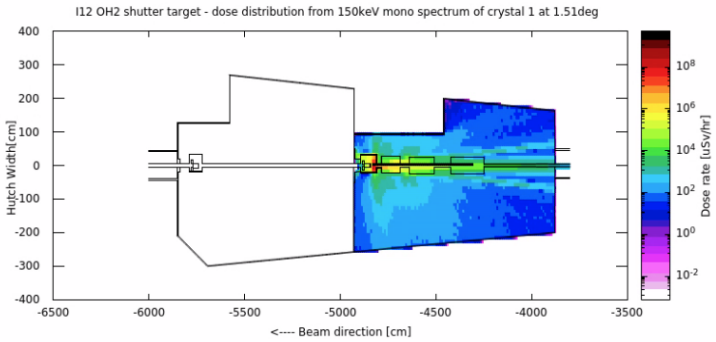

Figure 12: Sidewalls dose distribution for Mono beam from Crystal 1 to Crystal 2

For all the scenarios above the dose rate outside the shielding is less than 0.5 µSv/h, however if the beam was missteered by a mono crystal there could be a leak though the closed shutter (30µSv/h see figure 13). Engineers are looking at a redesign of the shutter.

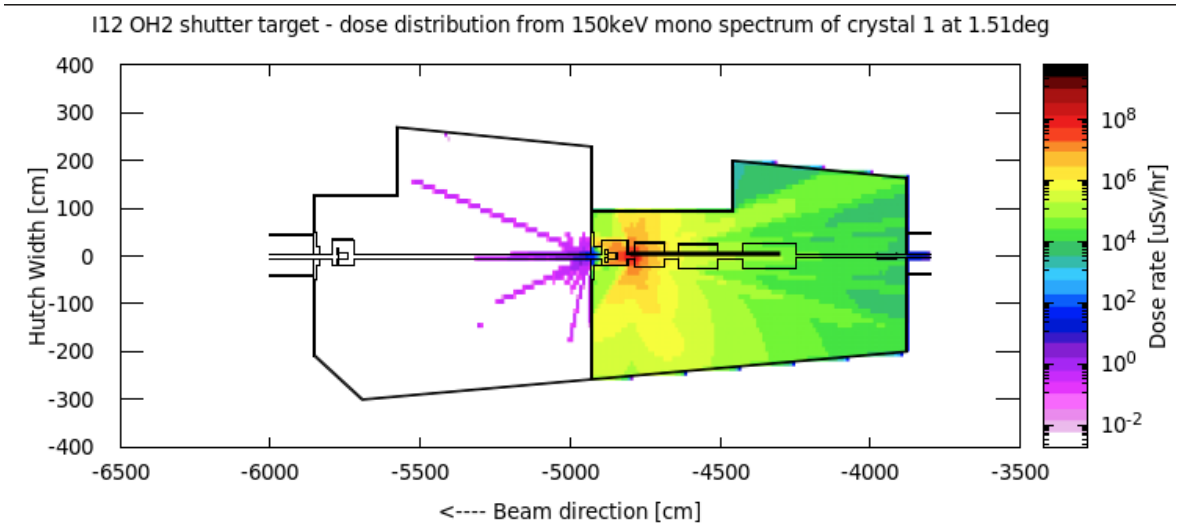

Figure 13: Leak from mono beam missteer (Side view)

2.2 Beamlines I13 and I14 STAC8 FLUKA comparison

Figure 14 shows a plan view of I13 and I14's optics hutch (same layout for each) the upstream side wall highlighted red was calculated to need 1mm additional lead for I13 and

4mm additional lead for I14. Adding this lead to the whole area of the existing wall would have been difficult as there are pipes and other services that would need to be removed.

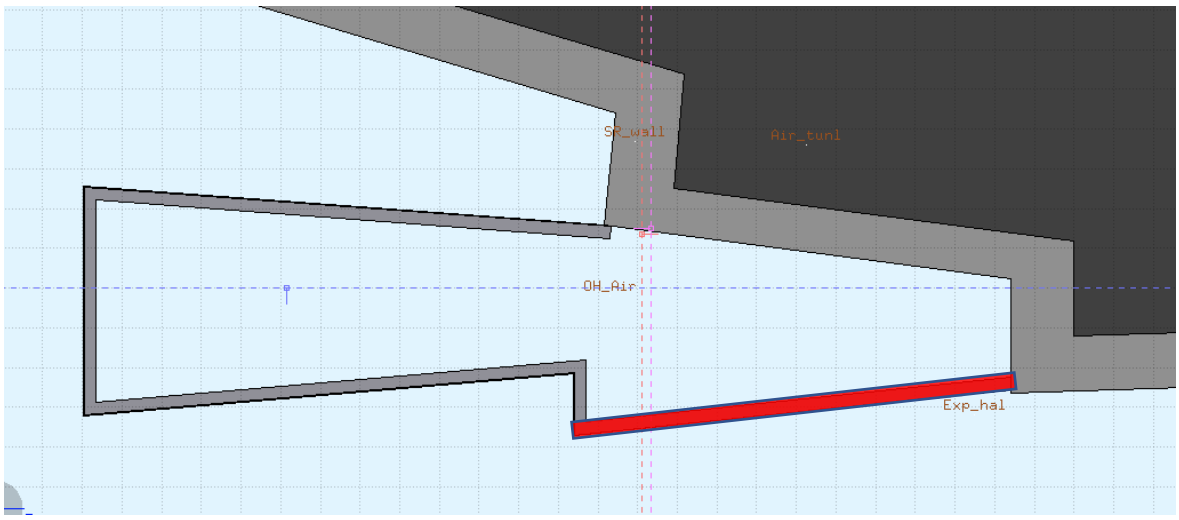

Figure 14: Dose rate outside I13 OH1 (Planview).

Initially we used FLUKA simulations to possibly narrow down where additional lead was needed, however the results show that dose rates outside the shielding are less than 0.5µSv/h.

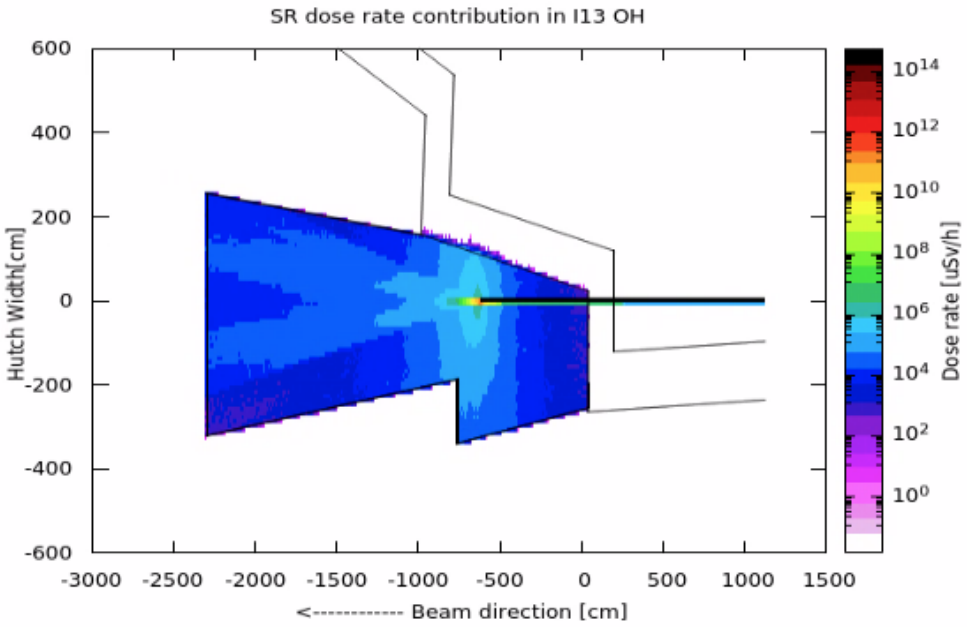

Figure 15: Dose rate outside I13 OH1 (Planview).

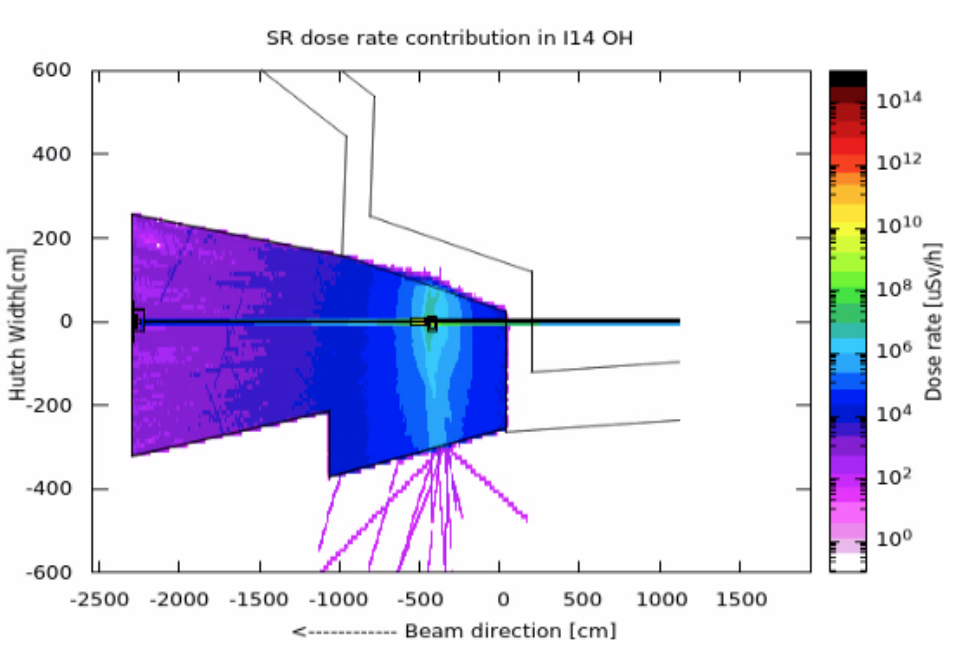

Figure 16: Dose rate outside I13 OH1 (Planview).

Figure 16 shows some radiation leaking through the sidewall, when we analysed the results we found this was groundshine, as there is no lead 'skirt' along this section of the wall. This will be installed before the end of the dark period.

2.3 Bending magnet beamlines

Figure 17 shows the change from double bend to a six bend achromat. This change allows beamlines formerly receiving light from bending magnets to now have insertion devices on the new 'mid-straights'.

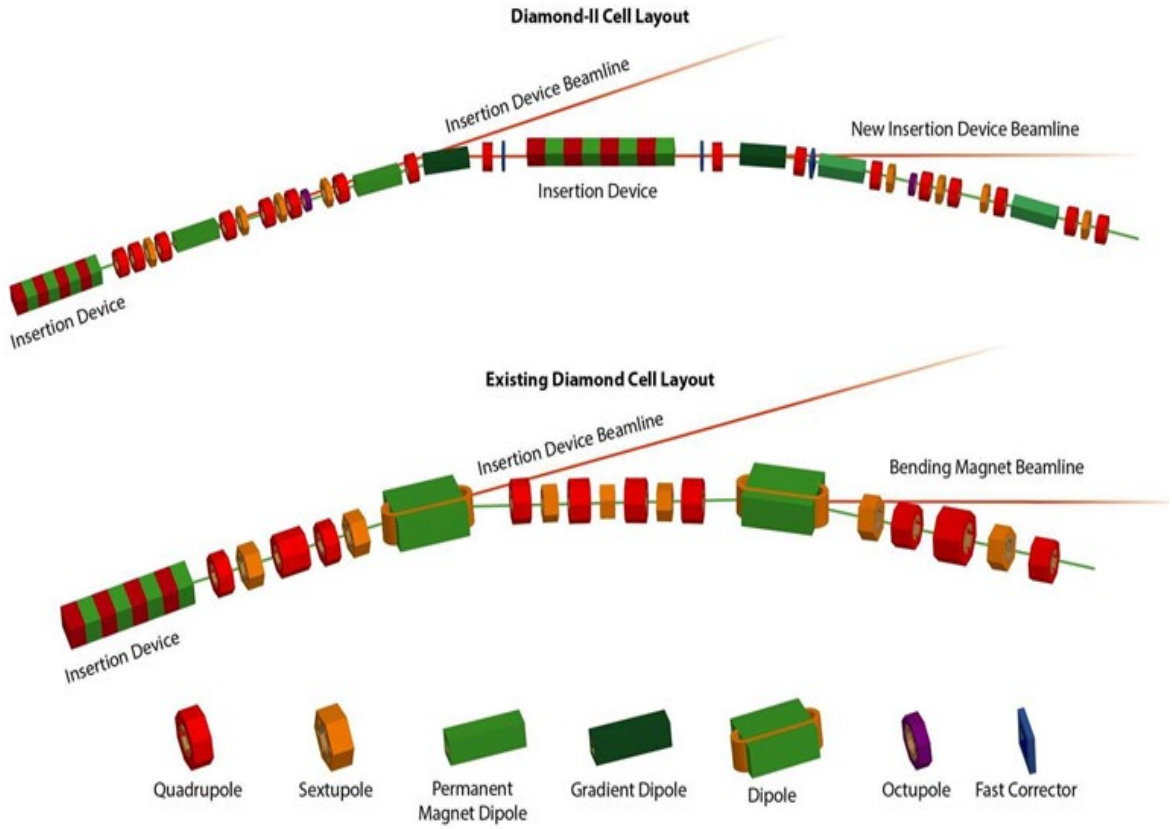

Figure 17: Comparison of Diamond-II and Diamond lattice.

Bending magnet beamlines were built with thinner shielding than the ID beamlines, however this new straight generates more gas bremsstrahlung, replacing or retrofitting all shielding is not financially viable so we are using FLUKA to assess where current shielding is sufficient and where additional shielding is needed.

B21, High-throughput SAXS Beamline currently has the following optic hutch shielding:

End wall, Side Wall and roof all 8mm Pb
Additional 25mm Pb on end wall, 1m^2 centred on beampipe
Experiments shutter 12 mm Tungsten Alloy

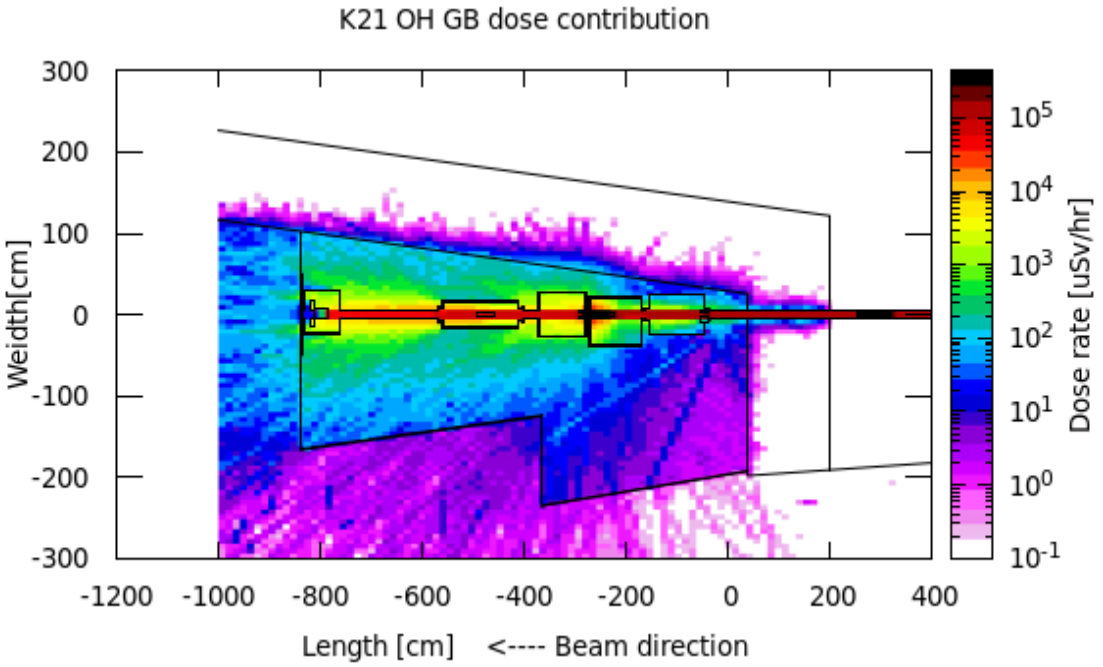

Figure 18: Dose rates outside current K21 optics hutch using D-II machine parameters.

As can be seen in Figure 18 the current shielding is not sufficient for the increased gas bremsstrahlung. The following changes are required:

- Front end: 3 custom apertures
- End wall: 50mm Pb, $2m^2$ centred on beampipe, 40 mm Pb $1m^2$ centred on beampipe
- Outboard perpendicular wall 25mm Pb full width 2m high from floor
- Experiments shutter increase to 65 mm Tungsten Alloy

Figure 19 includes the shielding listed above.

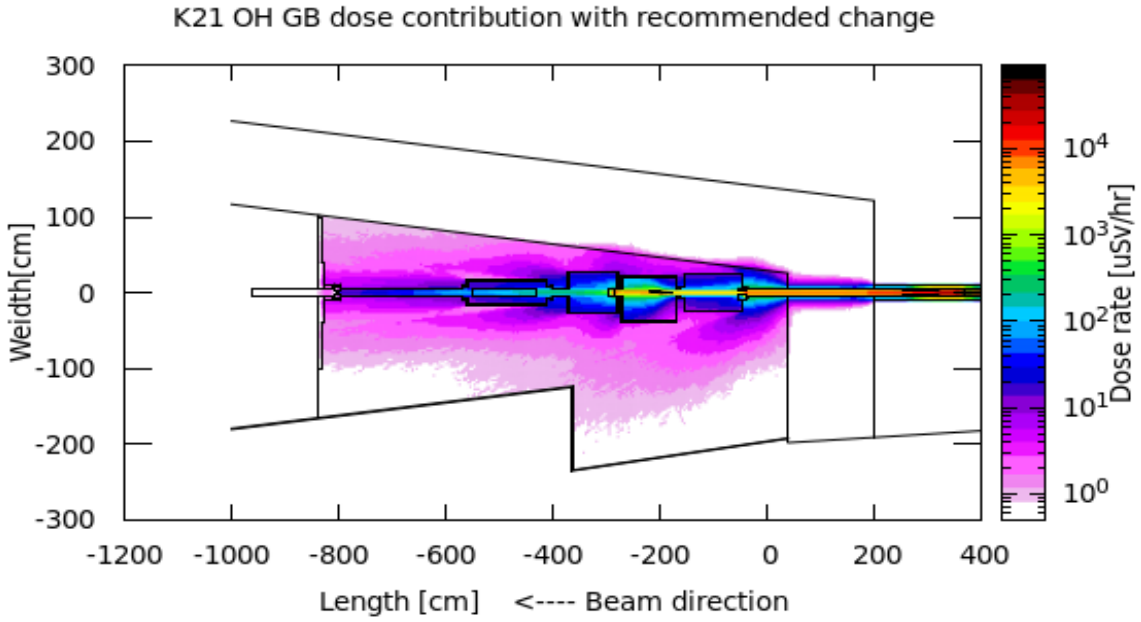

Figure 19: Dose rates outside K21 optics hutch with additional shielding using D-II machine parameters.

Beamlines K16 and K18 will also be moving from bending magnets to insertion devices these are currently being worked on and we are expecting similar results to K21.

3 Conclusion

The Diamond-II beamline shielding assessment has shown that although STAC8 calculates thicker shielding requirements than FLUKA it is still very useful when assessing many beamlines in a short amount of time, we assessed 33 beamlines and identified only 11 that needed additional shielding, FLUKA was then able to be targeted at those beamlines to narrow down further, creating FLUKA models for all 33 beamlines would not have been possible in the time available, also many plans change as they progress, in STAC8 these changes can be checked in minutes where as FLUKA can take hours or even days to re-run a simulation. In conclusion STAC8 and FLUKA can be used in conjunction on the large projects to save time and money.

References

[1] – R. P. Walker et al Diamond-II: Technical Design Report, (2022)

A beam containment scheme to protect radiation protection components for the world's most powerful x-ray laser beam

Ansari Z. [*], Boyd E.[*], Sinn H. [*], Zander S. [1], Leuschner A. [1], Gerdt S-L.[1], Liang T[1], Clement W.[1]

*European X-ray Free-Electron Laser Facility GmbH, Holzkoppel 4, D22869 Schenefeld. Germany

[1] Deutsches Elektronen Synchrotron DESY, Notkestr. 85, D22607 Hamburg. Germany

The European X-ray Free-Electron Laser Facility GmbH (European XFEL) is the world's most powerful x-ray laser machine. The design parameters are listed in table 1 [1], [2]. For radiation protection such parameters pose a challenge on how to stop or block such a powerful beam to protect human life.

Beam lines at XFEL are separated from the accelerator with beam shutters that contain ceramics, metal and an active detector. The beam shutters are connected to the radiation interlock system and protect life by switching off the XFEL beam if these are drilled through. Material testing performed on metals, ceramics, rock, concrete and water has shown that a focussed XFEL beam can drill through several centimetres of material within seconds, or less. The question is how to protect radiation protection components that protect life to ensure smooth facility operation.

This talk focusses on a beam containment interlock scheme called the safety equipment protection system (SEPS interlock) that relies on the position of focussing optics (mirrors or compound refractive lenses) and the state of the beam shutters (open/close) to switch off photon pulses to the beam lines if the optics focus the x-ray beam on to the beam shutter.

	Photon energy range (keV)	Pulse Energy (mJ)	Average Power (Watts)
SASE1 & 2	4.7 - 30	3.3	89
SASE3	0.25 – 3	10.7	290
The pulse duration is 8 – 20 femtoseconds.			

Table 1: Design parameters of photon pulses produced by the European XFEL accelerator

References

[1] - R. Abela et al: " The European X-ray Free-Electron Laser Technical Design Report", ISBN 978-3-935702-17-1.

[2] - E.A. Schneidmiller and M.V. Yukarov: " Photon beam properties at the European XFEL Saturation Tables (December 2018 revision)", unpublished.

[3] - Decking and Scholz: " Lasing performance of the European XFEL", unpublished.

Radiation Protection at SLAC's Future MEC-U Laser Facility

Bauer, J.[1], Rosenstrom, A.[1,2], Connolly, P.[1,2], Liu, J.[1], Rokni, S.[1]

[1]Radiation Protection Department, SLAC National Accelerator Laboratory,
2575 Sand Hill Road, Menlo Park, CA 94025, USA

[2]Department of Nuclear and Radiological Engineering,
Georgia Institute of Technology, North Ave NW, Atlanta, GA 30332, USA

Abstract

The Matter in Extreme Conditions Upgrade (MEC-U) is a flagship laser facility for plasma physics and fusion science that will combine high energy kilojoule (kJ) and high rep rate (10 Hz) lasers with the Linac Coherent Light Source (LCLS) at the SLAC National Accelerator Laboratory. The project is currently in the design phase with first operation estimated as early as end of 2027.

With MEC-U's high-intensity optical laser systems, laser-target interactions will accelerate electrons and protons that will become a source of prompt dose from ionizing radiation. These electrons and protons will also be able to activate material inside the target chamber, in the hutch, and in the environment.

The talk introduces the MEC-U project, presents the electron and proton source terms used in the FLUKA-based radiation protection analyses, discusses the estimated number and type of laser shots, and shows how personnel and environment will be protected from prompt and residual radiation. Shield walls will protect the personnel from prompt radiation while laser and utility pipes cross the walls. The expected residual radiation in devices in and around the target chamber, in the target chamber itself and in support structures is being studied, and the radiation doses to staff and users who will be working in and around the hutch are being estimated. Potential impact on the environment (groundwater and air) are also being studied.

1 Introduction to MEC-U Project

1.1 Upgrade to MEC-U

At SLAC's Linac Coherent Light Source (LCLS), the Matters in Extreme Conditions (MEC) instrument in Hutch 6 already combines the LCLS Hard X-ray Free Electron Laser (FEL) light with tightly focused optical laser light for its experiments. Its optical laser, with 1 J per pulse, 5 Hz, 40 fs time length, and a power of 25 TW, creates due to its focusing an ionizing radiation hazard when interacting with matter [1].

The new MEC-U "Upgrade" project will replace the MEC experiment [2]. Its experimental program includes studies of conditions inside planets and stars, studies of ion acceleration (creating short pulses of multi-MeV ions), studies related to relativistic plasma physics (*e.g.*, cosmic ray acceleration), and studies of ions stopping in plasmas (relevant to fusion science and astrophysics).

All plans and results of studies described in this paper are preliminary since the Preliminary Design Review will take place only in 2024.

1.2 MEC-U Layout

MEC-U will be located in a newly dug out underground cavern separated by several meters of soil from the most downbeam LCLS hutch (Figure 1).

Figure 1: Location of the proposed MEC-U Cavern with respect to LCLS Near and Far Experimental Halls (NEH and FEH), as well as location of proposed MEC-U Support Building

This 80 m long cavern will be split into three areas (Figure 2): The TAX hutch ("Target Area X-ray") for experiments making use of both the optical laser light and the LCLS FEL X-rays, the TAO hutch ("Target Area Optical") for experiments with only the optical laser light, and the Laser Hall for laser equipment. Shielding walls protect personnel against prompt radiation, while access mazes and penetrations for laser pipes, HVAC, cables, *etc.* still allow connections between the hutches. A support building will be on the south side, connected to the cavern through an access tunnel.

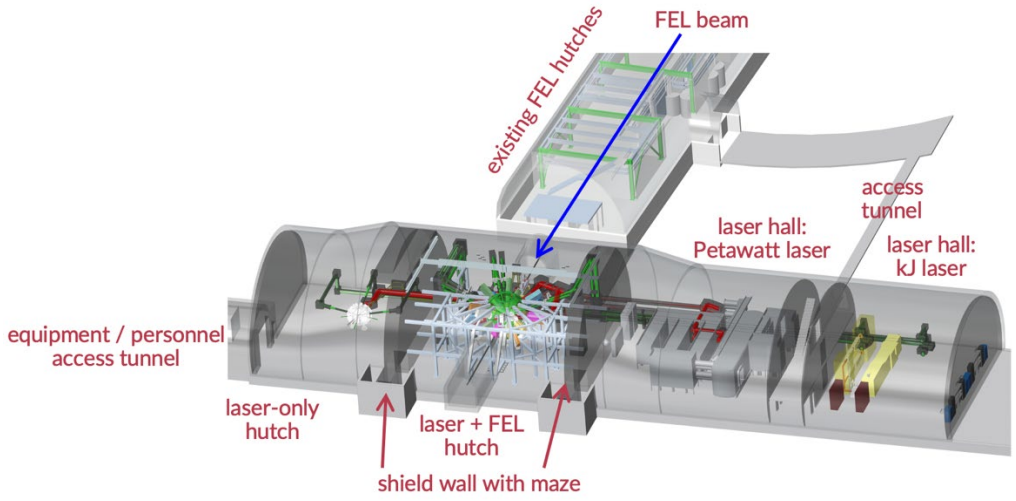

Figure 2: Drawing of the proposed MEC-U Cavern. In this drawing, the FEL X-ray beam comes from the top.

Figure 3 shows the currently proposed setup inside the two experimental hutches with the transport lines of the short-pulse laser in red and long-pulse laser in green.

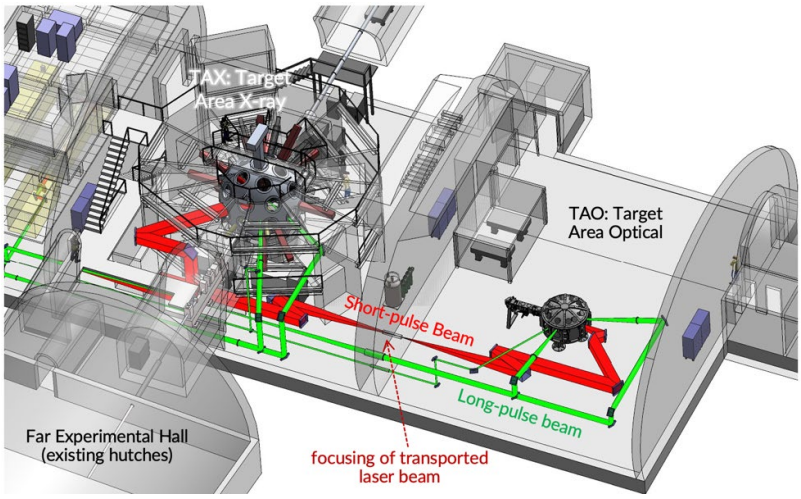

Figure 3: Drawing of the proposed TAX and TAO hutches. The FEL X-ray Beam enters the TAX hutch here on the bottom left side.

Further details of the TAX chamber are shown in Figure 4. In the current proposal, the vacuum chamber has a diameter of 4.5 m and a wall thickness of 10 cm aluminum. Several so-called SLIMs (SLAC Insertion Modules) attached to penetrations in the target chamber allow moving devices in and out without breaking vacuum. In the future, access by personnel to the inside of the target chamber should be needed only a few times a year.

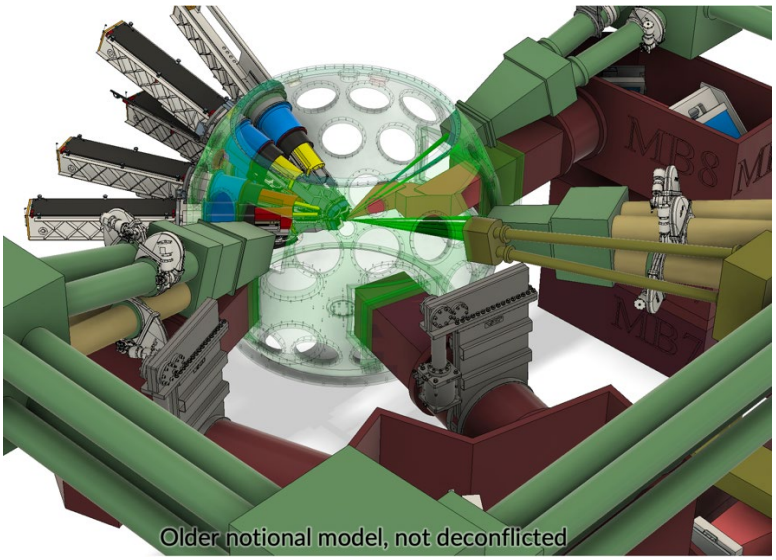

Figure 4: Drawing of the spherical target chamber in TAX with several SLIM (SLAC Insertion Modules) attached to penetrations. The model has since changed slightly.

1.3 MEC-U Plans for Laser Operation

The facility will operate two lasers, the High Energy Long Pulse (HE-LP) laser at 1 kJ per shot, 20 ns duration and 2 shots/hour, and the Rep-Rated Laser, which itself can be run in the long pulse mode with 200 J per pulse, 20 ns duration at 10 Hz, and in the short pulse mode with 150 J per pulse, 150 fs duration at 10 Hz. In that latter mode (RR-SP), the light will be focused to about 1 μ diameter, which gives a maximum irradiance of 3×10^{21} W/cm^2. It is the radiation hazard created in this mode that requires the attention of Radiation Protection.

The facility is expected to operate continuously with about 27 experiments each year. About 2/3 of these experiments will make use of the RR-SP laser.

2 Radiation Hazards and Source Terms

2.1 Laser-Target Interactions

Whenever laser light is both compressed in time and focused into a small area, the high electromagnetic fields create a plasma during an interaction with matter and accelerate both electrons and ions. Figure 5 is an informative sketch to illustrate the complex interactions going on during such laser-target interactions. Various models exist to describe the behavior for different subsets of input parameters.

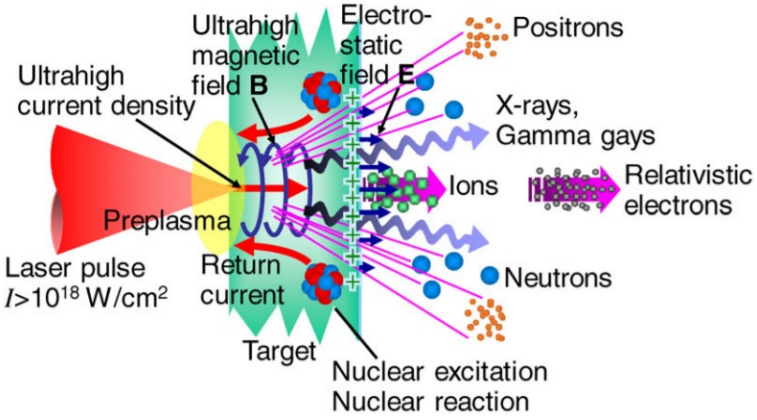

Figure 5: Sketch of the laser and plasma with its constituents during a laser-target interaction, indicating the complex interplay during that time. Drawing taken from Ref. [3].

The radiation of concern are hot electrons as well as protons. While metal targets lead mainly to acceleration of electrons, hydrocarbons lead more to acceleration of protons and ions. Liquid/frozen (also called cryogenic) targets are, for example, liquid hydrogen or liquid argon. Interactions by the laser with these targets will lead to acceleration of these types of particles. Those cryogenic targets are also able to create high integrated doses since their targets are easily replenished.

2.2 Source Term for Hot Electrons

To estimate the radiation dose to personnel from hot electrons, SLAC undertook a study starting from Particle in Cell (PIC) code, specifically the EPOCH code [4]. From these simulations, a hot electron spectrum was obtained which, in turn, served as the source term in FLUKA simulations [5]. The FLUKA results were compared to radiation measurements at both MEC and the TITAN laser facility at LLNL [6] and found to be in good agreement with each other.

Since this study gave results for a wide range of parameters, including those of future MEC-U operation, its parameterization was used as source term to the MEC-U FLUKA studies. Specifically, for the highest possible parameters achievable at MEC-U, Ref. [6] tells us that a hot electron temperature of 23 MeV is to be used, that 60% of the laser energy is converted into hot electrons, that the ratio between the amount of radiation going forward versus backward is 27:1, and that the radiation is distributed around the forward and backward directions in a cone with a Gaussian distribution at a sigma of $\sigma = \pm 45°$.

The FLUKA simulation uses a conservative 1 mm thick copper plate as solid target, and 300 μ thick He as liquid target.

2.3 Source Term for Protons

As proton source term, the result of a PIC simulation for the LMJ-PETAL facility at CEA/Cesta in France was used [7]. This spectrum was also considered by MEC-U scientists to be typical and both reasonable and conservative. The spectrum, with a cut-off at 115 MeV, is shown in Figure 6 with both the PETAL simulation result and the actual spectrum used in the FLUKA simulation. The average energy of the protons is 23 MeV, and only 5% of the laser energy is converted into accelerated protons. The opening angle of the radiation around the forward and backward directions is tighter with a sigma of just $\sigma = \pm 20°$ for the Gaussian distribution. Unlike for hot electrons, the same amount of radiation goes both forward and backward. The same radiation may also be expected for both solid and liquid targets. And since the spectrum of Figure 6 is the one of the radiation emitted by the target, no target needs to be simulated in FLUKA.

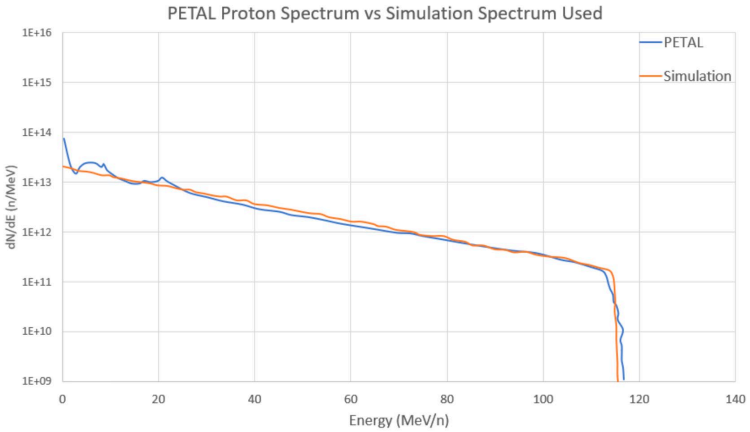

Figure 6: The proton spectrum used in the simulation is based on the PETAL simulation results from Ref. [7]. The figure shows that these two curves agree well with each other.

2.4 Number of Shots in One Year and One Hour

Finally, the simulation needs to know the number of shots per hour. This number was obtained in discussion with the MEC-U scientists as a reasonable upper limit. The numbers are conservative in that they assume all shots at the highest energy and highest irradiance. In reality, most shots might not be perfect, and quite some time may be spent on setup. However, the ultimate goal is to operate continuously with frequent shots, and once the shield walls for the experimental hutches are built, adding additional shielding to the wall is cost-prohibitive.

For the radiation analysis of the shielding wall, we therefore assume 4,000,000 shots in one year on solid (high-Z) targets, and 24,000 of those in one hour. For liquid (low-Z) targets, 50,000,000 shots are assumed in one year, and 36,000 of those in one hour. Note that this adds up to a continuous radiation of about 60 W throughout the year. For activation calculations, where controls may be added during the course of the operation, we assume only $1/10^{th}$ of these number of shots.

3 Prompt Radiation and Its Mitigation

3.1 Bulk Shield Walls

As mentioned above, these shield walls, one between the TAX and TAO hutch, another between the TAX and Laser Hall, are big investments that cannot be easily upgraded. The shielding criteria are maximal 1 mSv in 1 year, 50 µSv in 1 hour to a person, with the assumption that the above-mentioned shots are spread equally over 6,000 hours with each person spending up to 1,000 hours at the wall. This translates to maximal 6 mSv for all the above-mentioned shots in one year. To be conservative (and since the project does not want to limit the direction that the laser is allowed to point to) all shots are assumed to go straight into the wall.

Figure 7 displays the results for the three source terms, each time with the laser shooting left into the wall. The round area on the right is the target chamber. The square box around it is only a non-physical artifact from the FLUKA geometry. The area to the left (in the area on the other side of the shield wall) has the highest radiation for the proton source term, while the hot electron source term is dominant inside the hutch. The results are shown for a shield wall of 1.6 m thick heavy concrete (with a density of 4.0 g/cm^3), which is the thickness at which the required limit is met.

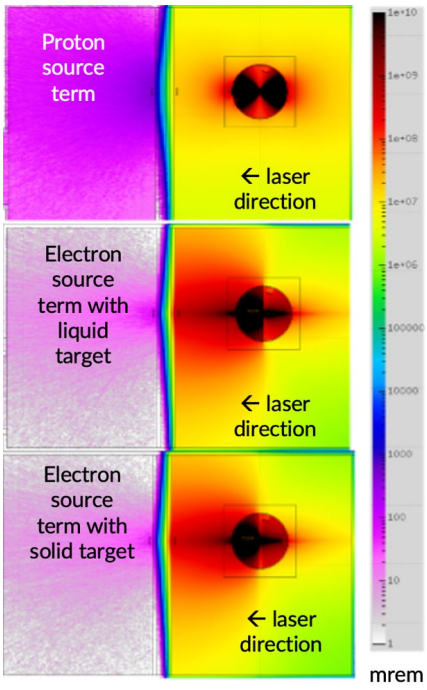

Figure 7: FLUKA simulation results from laser-target interactions at the center of the target chamber (sphere on the right). The radiation drops strongly when passing through the shield wall. The results show how the proton source term dominates on the other side of the shield wall. Results are for 1 year of shots straight into the shield wall. Plane view at target height. The square box around the target chamber is an artifact of the FLUKA geometry.

3.2 Entrance Mazes at Shield Walls

Personnel entrance to the TAX hutch will be through mazes at the east end of each shield wall as shown in Figure 8. The depth of these mazes was chosen to meet the requirement of not more than 6 mSv in 1 year (Figure 9).

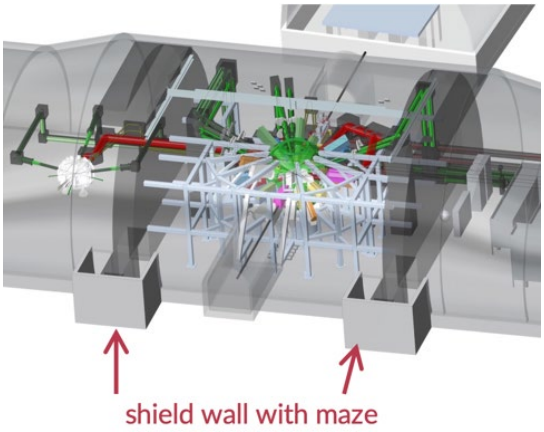

Figure 8: Drawing of the proposed TAX hutch with maze at the east end of each shield wall for personnel access.

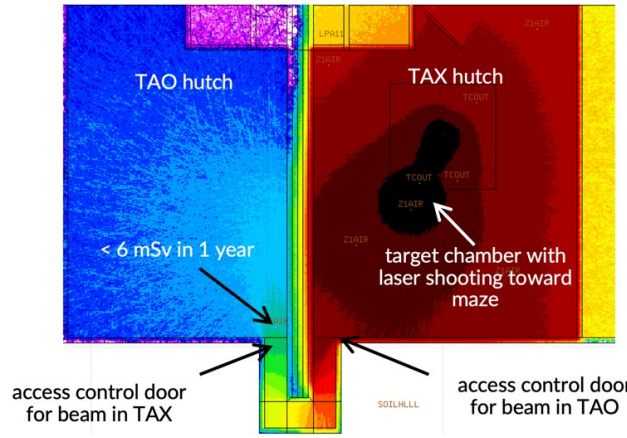

Figure 9: FLUKA simulation result of shots towards maze shows that the limit of <6 mSv in 1 year can be met outside the maze. Plane view at the height of the maze. Again, the square box in the hutch on the right side is a FLUKA geometry artifact.

3.3 HVAC *etc.* Penetrations through Shield Walls

The project plans to run HVAC pipes, exhaust pipes and other utilities through the shield walls at the very top of the cavern. Iterating with the civil engineers, a maze-style shielding was designed for these large penetrations that is suitable to the engineers while still meeting the above-mentioned requirement of maximal 6 mSv outside the hutch from 1 year worth of shots (Figure 10).

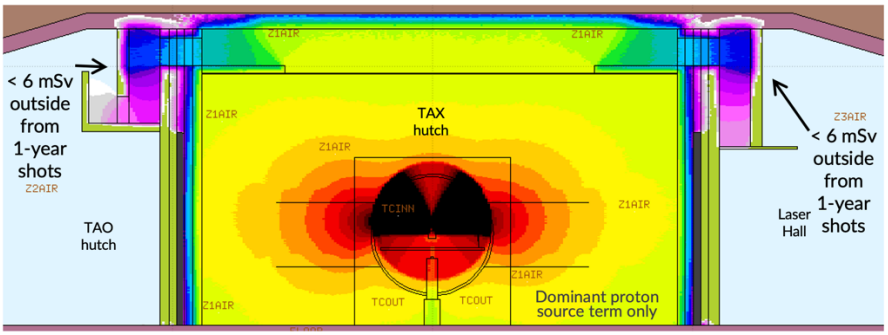

Figure 10: FLUKA simulation results for the penetrations on the top of shield walls. The limit of maximal 6 mSv in one year outside the hutch can be met. Elevation view across the shield wall penetrations. Again, the square box in the hutch on the right side is a FLUKA geometry artifact.

3.4 Laser Penetrations through Shield Wall

A maze-style penetration shielding is, however, not possible for the penetrations that bring the laser beam through the shield walls since mazes would require large deflections of the laser beam that would degrade the laser light quality. Luckily, physics reasons led the laser engineers to plan for focusing the laser during the transport. By placing the focal spot in the middle of the penetration through the shield wall, that penetration can now be limited to a smaller diameter of 44 cm. Figure 11 shows the current diameter and location of these penetrations together with a stick figure for scale.

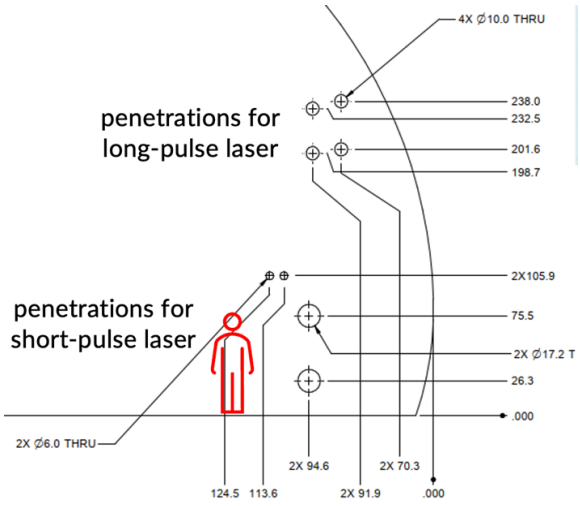

Figure 11: Drawing indicating the locations and dimensions of the laser penetrations through the shield wall. The stick figure gives an indication of the scale. The curved line indicates the edge of the cavern.

Some radiation may still go straight through the laser penetration and continue along the vacuum chamber, but access by personnel to this area can be prohibited until an optics element intercepts that radiation and scatters the radiation sufficiently. This can be seen in Figure 12 left and right.

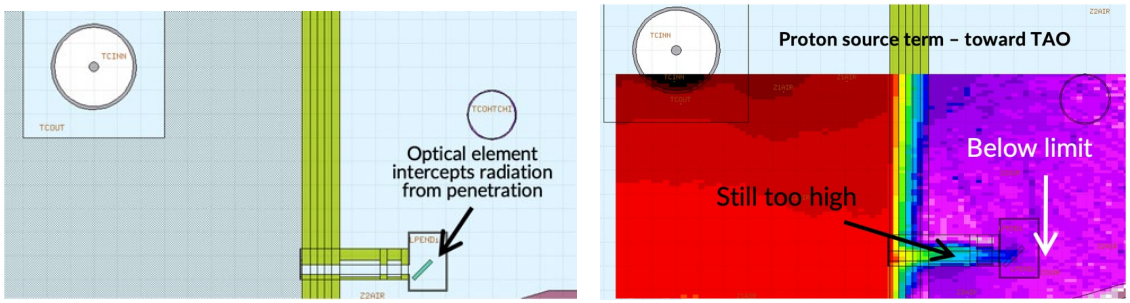

Figure 12: Proposed shielding at a penetration for the short-pulse laser. The left side gives a plane view of the geometry, the right side gives the FLUKA simulation result. Behind the first optical element past the penetration, the dose rate is sufficiently low, but between the penetration and the optical element the dose rate is still too high, and personnel must be excluded from this area.

3.5 South Entrance Tunnel

Laser-only experiments in TAO are at this moment in the deferred scope. Some basic studies were nevertheless performed. The project wants to keep the south entrance tunnel open for equipment access. This requirement precludes a maze inside the tunnel to shield against radiation from the TAO chamber. With the currently foreseen size, length, and bend of the tunnel it will be sufficient to use distance to protect personnel. Placing the access gate inside the tunnel far enough from the TAO hutch will protect personnel from radiation even without added shielding.

4 Activation and Its Mitigation

4.1 Activation Hazard

As mentioned above, full operation of the RR-SP laser at the maximal rate is equivalent to a 60 W beam inside the target chamber. For activation analysis, we assume only 10% of the shots, *i.e.*, assume an equivalent 6 W beam. Even this beam will create significant activation. Other accelerators at SLAC experience similar beam losses at various spots, but MEC-U is unique due to its need to frequently access the area of the beam loss and due to the challenges to implement suitable shielding against the residual radiation.

To understand how the hazard may impact operation and to guide the engineers for possible mitigations, the activation levels were studied. In addition to assuming 10% of the maximal number of shots (5,400,000 shots in one year), we also assume 200,000 shots on liquid targets in three days (equivalent to one experiment), and 36,000 shots on liquid targets in one hour (the best performance that can be expected in one hour). A sketch (not to scale) is given in Figure 13.

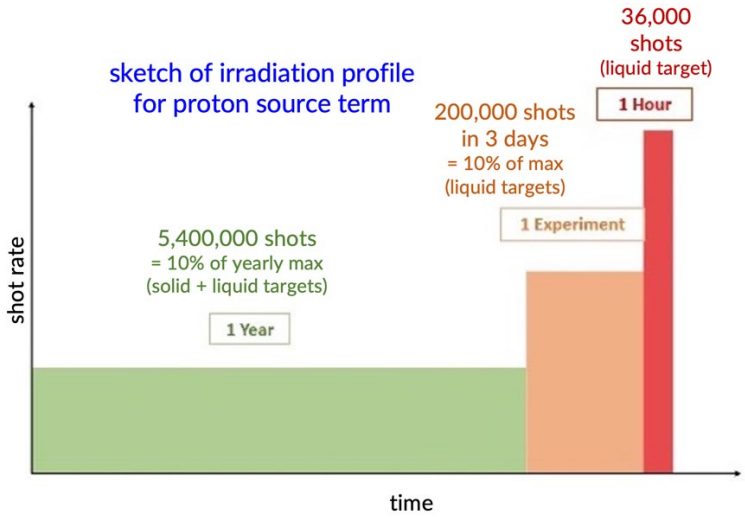

Figure 13: Sketch of the irradiation profile used for most activation analyses, here for the proton source term. The profile combines shots over 1 year followed by shots in 3 days, followed by shots in 1 hour.

4.2 Platform around Target Chamber

One study was prompted by a question from engineers about the use of steel vs. aluminum as material for the platform that allows personnel to access the area around the target chamber. While steel activates more than aluminum (as expected), the dose from the platform is dwarfed by the dose from the aluminum target chamber itself (Figure 14). The usage of steel instead of aluminum is therefore acceptable.

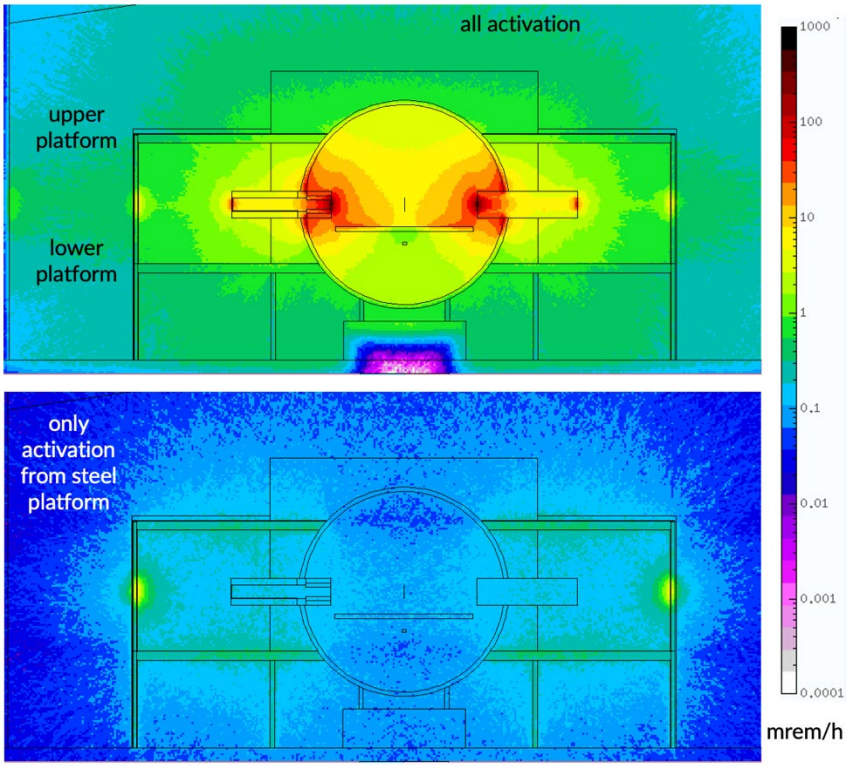

Figure 14: Dose rates from activation according to FLUKA simulations. The geometry consists of the target chamber (sphere in the centre) and the platform outside the target chamber. The top plot gives the dose rate from all material in this area; the bottom plot gives the dose rate from only the platform. Again, the square with the thin line is an artefact of the FLUKA geometry.

4.3 Aluminium Alloy

A similar question from the engineers was whether a specific alloy of aluminum would be preferred or required, and whether the amount of cobalt in the aluminum alloy is of concern. The studies showed that both the 5000- and 6000-series aluminum alloys give comparable activation, while the 7000-series aluminum creates about twice the radiation, though that difference disappears after about a 1-day cool-down. Since the project does not plan to use any 7000-series aluminum, the recommendation was that both 5000- and 6000-series aluminum is acceptable. Studies also showed that up to 0.15% cobalt by weight does not change the dose significantly.

4.4 Dose to Personnel

The main question for radiation protection regarding activation is how much dose personnel will receive cumulatively within one year from all sources. This cannot be answered by a simple simulation but must be combined with estimates of the operation of the laser throughout the year and which personnel will be when at the various locations. In spite of large uncertainties, the result will still be valuable as estimate of what to expect.

For this analysis, FLUKA simulations were performed to obtain the dose rates at various points at the hutch (Figure 15). The dose rates from various times after beam shutoff were then interpolated to be able to determine the dose rate at any time and to permit integration of the dose for any time period (Figure 16).

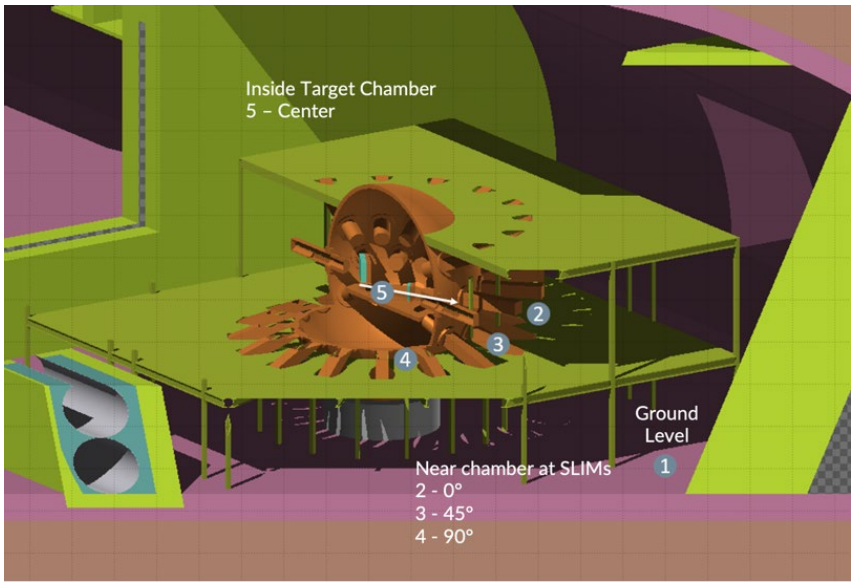

Figure 15: FLUKA geometry plot with indication of the various locations for which residual dose rates were obtained.

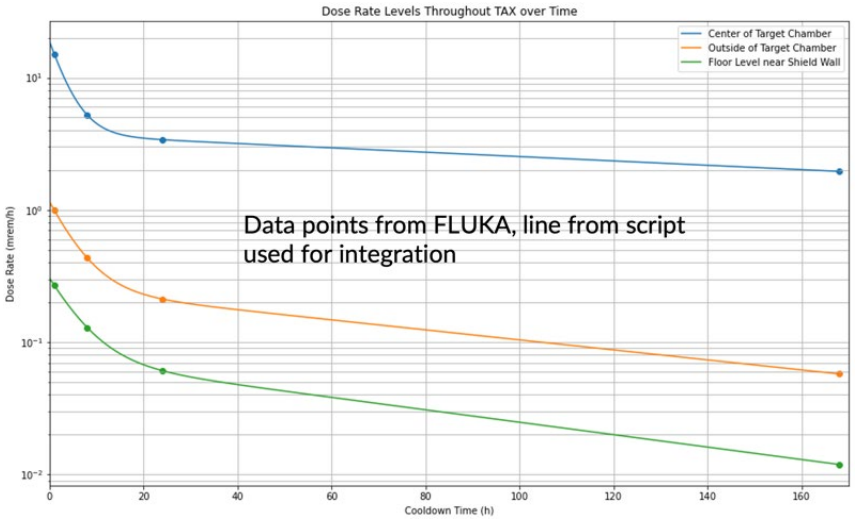

Figure 16: Residual dose rates at various times with interpolation between them. The three locations correlate to locations 5, 3, and 1 of Figure 15.

In consultation with the scientists, estimates were obtained about the shot pattern for the experiments: Typically the beam will be off for five days to tear down the old experiment setup and install the new experiment setup. The next two days would see shots without FEL X-rays, while during the last seven days the laser would operate during the assigned shift with the FEL X-rays to take data for the experiment.

In addition, estimates were made how many hours after the beam turned off (including a 1-hour cool-down period) personnel will enter the hutch and how long they will stay at the various locations. Figure 17 gives a visual representation of that pattern. Note that the vertical axis does not indicate a physical quantity, but only indicates (as an integer) whether beam is on, beam is off without access, and where a person is located.

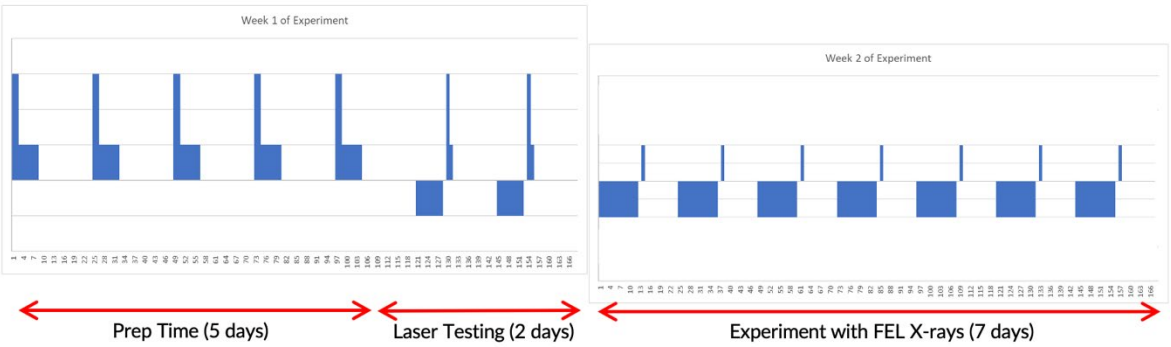

Figure 17: Sketch to indicate possible beam operation during an experiment, time off before entry, and location of an instrument scientist inside the hutch during access. In this scenario, the laser operates only during laser testing time and the experimental time, with short access to the hutch in between. More access is foreseen during the prep time.

All this information is then combined to obtain the estimated dose in one year to a scientist, a user, or an instrument technician. At the time of the workshop, the analysis was still being performed.

As mentioned earlier, these estimates are associated with large uncertainties. Although based on experience with MEC, both the pattern how experiments are executed and where which person will be for how long are rough estimates. The assumption of 10% of the maximum number of shots is also an estimate. Initially the number of shots will sure be lower, but after some years of operation, the number of shots might exceed this 10% estimate. Additional dose comes from work on activated detectors, activated optics and activated targets and target holders, as well as from time spent inside the target chamber itself.

5 Other Considerations

5.1 HVAC / Exhaust / Ground Water

Studies assuming full operation found the activity in air to be low enough that after a 1 hour cool-down period the Derived Air Concentration will be below 1. Similarly, the dose to the public will also be below the limits. With a dose < 0.1 mrem/year for the maximum exposed individual there will even be no need for continuous air monitoring.

Dust of activated target material may possibly be pumped out through the exhaust system. The exhaust system will therefore need to be set up with HEPA filters.

Activation of ground water in both the soil and the wall's concrete was also studied. While the concentration of tritium will be below the limits, the Na-22 concentration requires a more detailed analysis.

5.2 Access Control, Laser Control, Radiation Monitors

Design for the Access Control System has not yet started in earnest, but, of course, hutch access will be allowed only with both the X-ray FEL beam stopped and the ionizing radiation laser hazards mitigated. To permit laser light in the hutch for alignment purposes, the ionizing radiation hazards must be mitigated. Possible solutions may be attenuating the laser light during access (similarly to the implementation at MEC), turning off amplification stages during access, or using a separate low-power laser for alignment.

Radiation Monitors will also be required with some installed outside the hutches and interlocked to the prompt radiation generation, others installed inside the hutches for residual radiation and interlocked to the access state.

6 Schedule and Outlook

Numerous decisions will still need to be made by the project, including the exact shape of the cavern. The Final Design Review is planned for Fall 2024, start of construction for 2025, First Light for the end of 2027.

Additional changes to the design are already anticipated: Operation in the TAO hutch is currently deferred but may be put back into scope. Discussions are on-going on possibly adding a multi-kJ long-pulse laser, as well as a second Short-pulse Laser with the same irradiance as the currently planned RR-SP laser, but with operation only for a few experiments.

The authors are thanking the scientists and engineers of MEC-U for the numerous discussions of the various aspects of the project. This work was supported by Department of Energy contract DE-AC02-76SF00515.

References

[1] - *Ionizing Radiation from Optical Laser Light Interacting with Matter: Simulations with Particle in Cell Code and FLUKA*, J. Bauer, T. Liang, J. Liu, and S. Rokni, p.112-120, in *Proceedings of Ninth International Workshop on Radiation Safety at Synchrotron Radiation Sources*, Hsinchu, Taiwan, April 19-21, 2017
[2] - *Matter in Extreme Conditions Upgrade Conceptual Design Report*, MECU-DR-0003, March 9, 2021
[3] - H. Daido *et al.*, Rep. Prog. Phys. **75**, 056401 (2001)
[4] - T.D. Arber *et al.*, *Contemporary particle-in-cell approach to laser-plasma modelling*, Plasma Phys. Control. Fusion **57**, 113001 (2015)
[5] - A. Ferrari, P.R. Sala, A. Fassò and J. Ranft, *FLUKA: A Multi-particle Transport Code*, CERN- 2005-10, INFN/TC_05/11, SLAC-R-773 (2005)
[6] - T. Liang, J.M. Bauer, J.C. Liu, and S.H. Rokni, *Bremsstrahlung Dose Yield for High-Intensity Short-Pulse Laser-Solid Experiments*, Rad. Prot. Dosimetry, 1-9, doi:10.1093/rpd/ncw325, SLAC-PUB- 16783 (2016)
[7] - B. Martinez *et al.*, *Numerical investigation of spallation neutrons generated from petawatt-scale laser-driven proton beams*, doi:10.48550/arXiv.2105.11094 (2021); later published as doi:10.1063/5.0060582 Matter Radiat. Extremes **7**, 02440 (2022)

ELI Beamlines facility: Heading towards operations

Olšovcová V., Cimmino A., Horváth D., Lefebvre B., Šesták M., Truneček R., Versaci R.

ELI Beamlines, ELI ERIC, Za Radnicí 835, Dolní Břežany, Czech Republic

Abstract

In 2021, The Extreme Light Infrastructure European Research Infrastructure Consortium, ELI ERIC, was established. The consortium is an international European project aiming at building and operating the next generation of high power lasers for fundamental research and industrial applications in Europe. The ELI Beamlines laboratory in the Czech Republic became an integral part of the Consortium on 1.1.2023.

ELI Beamlines aims at the development of ultra-short high brilliance X-rays sources and acceleration of electron and proton beams. After the RadSynch19 conference, and despite the delay caused by the worldwide Covid pandemic, a large amount of work has been carried out in the laboratory. Different beamlines and workstations have been commissioned, a new workstation has been built, and several experiments have been performed. This contribution provides an update, summarizing the work done in the past years, and lessons learnt.

1 Introduction

1.1 The Extreme Light Infrastructure ERIC

In 2021, decade-long joint effort of the European laser research community was in consummated/crowned by the establishment of The Extreme Light Infrastructure European Research Infrastructure Consortium (ELI ERIC) by the European Commission [1, 2]. ELI ERIC is the largest international civil laser-based facility, whose founding members are the Czech Republic, Hungary, Italy, and Lithuania, while Bulgaria and Germany are founding observers. Romania is expected to become another founding observer in 2024. Further, several other countries (including Poland, Portugal, Spain, and Switzerland) are considering joining the Consortium in the near future.

ELI ERIC offers a large collection of high-power and ultra-fast lasers to users coming from the physical, chemical, material, and medical research scientific communities. The ELI ERIC facilities are located in Hungary, Romania, and the Czech Republic. The “ELI Attosecond Light Pulse Sources” facility, ALPS, sited in Hungary exploits pulses of attosecond length [3], while the Romanian “ELI Nuclear Physics” facility, NP, focuses on photonuclear physics, bringing together high power lasers and nuclear physics [4]. ELI Beamlines in the Czech Republic performs research in high-field high-density physics, high-brightness sources of X-rays, as well as secondary proton, electron, and ion beams [5].

1.2 ELI Beamlines

ELI Beamlines, located on the outskirts of Prague, Czech Republic, became an integral part of ELI ERIC on January 1, 2023. The research activities include the development and testing of novel technologies for multi-PW laser systems, plasma physics, high field physics experiments, production of femtosecond secondary sources of ionizing radiation (extreme ultraviolet radiation, X-rays, gammas, electrons, and protons) to be used in interdisciplinary applications in physics, biology, medicine, and material sciences [4].

ELI Beamlines houses four major laser systems of femtosecond pulse length, up to 10 PW power, and up to 1 kHz repetition rate, see Table 1. As of 2023, laser L2 is still under construction, while lasers L1, L3, and L4 are in operation for user experiments, even though laser L4 only in the long pulse (nanosecond) regime. The laser beams are distributed to twelve experimental stations (or beamlines), with a possibility of adding more in the future. Ionizing radiation is produced in nine of these stations, each pursuing a unique research program. The licences to operate the stations producing ionizing radiation were secured from the Czech State Office for Nuclear Safety gradually, between 2018 and 2023.

In house experiments started in the first half of 2018. The first user call was launched already the following year 2019, followed by the first user experiments successfully performed later that same year.

Laser	Peak energy [J]		Peak power [TW]		Max. rep. rate [Hz]	
	Target	Current	Target	Current	Target	Current
L1 - Allegra	0.1	0.03	5	1.5	1000	1000
L2 – DUHA	2	-	100	-	50	-
L3 – HAPLS	30	30	1000	333	10	3.3
L4 - ATON	1500	500	10 000		1/min	1/min

Table 1. Main laser systems at ELI Beamlines and their current and targeted parameters

2 Experimental stations

2.3 Current status of the technology implementation

Nine of the existing experimental stations are presently expected to generate ionizing radiation. At seven of them, the interaction of the laser-generated high-energy ionizing radiation beam with the surrounding equipment and materials is capable of producing secondary high energy mixed radiation fields. These beamlines aim at the acceleration of electrons up to tens of GeV or protons up to a few hundreds of MeV. Over the last several years some stations came into regular operation (HHG, PXS), other started the second phase of commissioning (ALFA, ELIMAIA, P3), while other began their commissioning only recently (LUIS, ELBA). As of 2023, the works on the testing station TERESA were halted after several experimental campaigns. One station, Gammatron, is still under installation and the start of its commissioning is planned for 2024. The overview of the experimental stations, together with their goal, status of commissioning and so far achieved parameters is presented in Table 2.

Station	Main goal	Commissioning Started	Commissioning Status	Primary particle	Energy [MeV] Target	Energy [MeV] Current
HHG	Ultrashort tunable coherent extreme ultraviolet soft X-ray	2018	operation	X-ray	(0.5-25) 10^{-5}	(0.5-25) 10^{-5}
PXS	High-brightness X-ray beams	2019	operation	X-ray	0.003-0.077	0.003-0.077
Gamma-tron	Ultrafast and bright hard X-ray	2024	installation	Electron	2000	--
LUIS	Generation of spontaneous and subsequently, coherent	2022	1st phase	Electron	1000	--

	photons					
ELBA	Electron acceleration	2023	1st phase	Electron	50 000	600
ALFA	Electron acceleration	2021	2nd phase	Electron	300	150
TERESA	Testbed for proton and electron acceleration	2019	frozen	Proton Electron	15 150	
ELIMAIA	Proton acceleration	2020	2nd phase	Proton	250	30
P3	High field plasma interaction, high energy density physics	2020	2nd phase	mixed source	1000	--

Table 2. Overview of experimental stations at ELI Beamlines producing ionizing radiation.

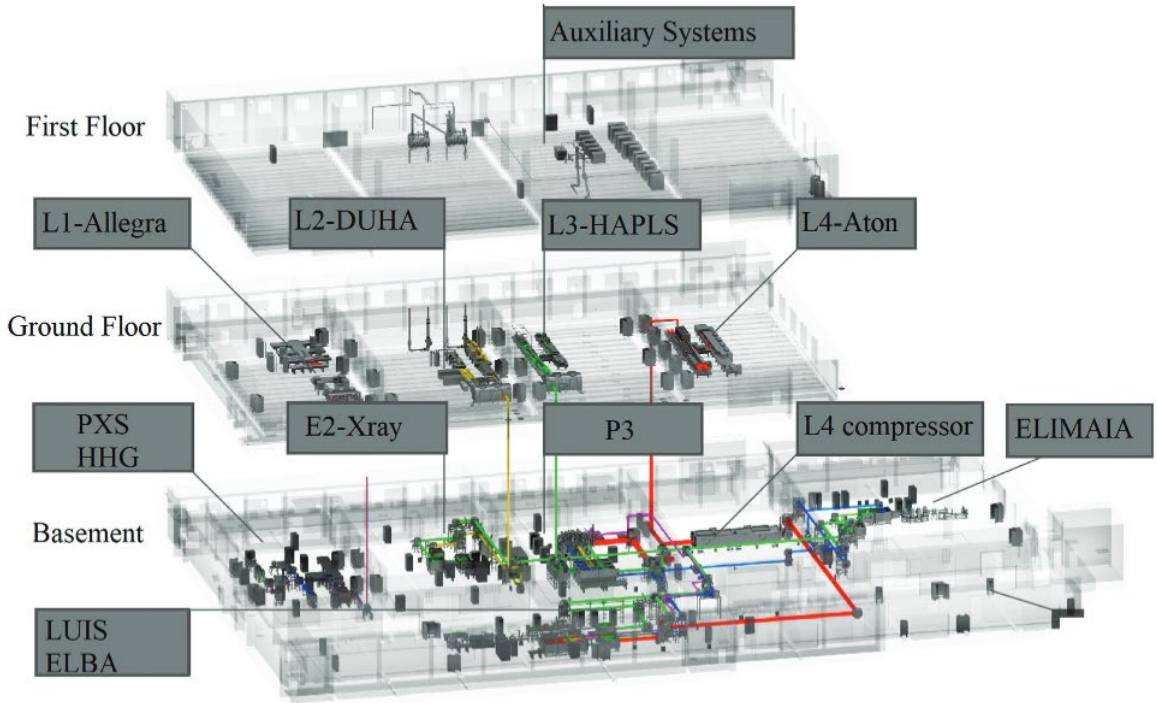

Figure 1: Diagram of the experimental building, indicating the locations of the main technological units.

2.4 Source term

Ionizing radiation generated within laser-target interactions has some unique characteristics. First of all, it is the time structure of the generated radiation field, which follows the structure of the original laser beam, having pulse length in the order of femtoseconds (or even shorter in the case of ELI ALPS). Further, high power lasers typically operate in a low repetition rate (single shots to tens of Hz), even though some systems of lower parameters (such as L1-Allegra) can achieve kHz repetition rate.

Additionally, the radiation field comprises of various types of particles (e.g. photons, electrons, protons, neutrons, muons) spanning over a very large energy range (from tens of GeV down to eV).

Last, but not least, the laser-target interaction (and therefore the description of the generated radiation) is a subject of research in itself. Furthermore, since the whole process

is rather sensitive to many parameters, the resulting radiation field suffers from limited experimental reproducibility.

3 Radioprotection measures

3.1 Some of the RP challenges

The specific time structure of the field causes unreliability of the response of the active detection systems that may interpret the spuriously occurring signal (e.g. one fs pulse every 100 ms) as noise and display zero dose [7], or suffer from saturation, due to extreme dose rates in a single pulse. Any real-time detection is further complicated by the inherent presence of a strong magnetic field (coming from laser-target interaction), that can reach 10^2 kV/m.

As mentioned in section 2.2., the understanding of the shot-to-shot source terms is limited. However, radioprotection considerations and modelling (typically based on the Monte Carlo method) rely on the description of the source term and therefore face mathematical and computational challenges. The used source term is either extrapolated from previous experiments or estimated by particle-in-cell simulations [8]. This implies the source term suffers from intrinsic uncertainties much larger than those affecting source terms used in conventional accelerators. Therefore, a conservative worst-case scenario approach is adopted at ELI Beamlines.

3.2 Monte Carlo simulations

During the preparatory and installation phase of the ELI Beamlines implementation, radioprotection assessment was mostly driven by Monte Carlo simulations. The Radioprotection group at ELI Beamlines uses mainly the general-purpose code FLUKA [10, 11]. The team exploits Monte Carlo simulations for several kinds of studies. First of all, the code is used for developing radiation field maps to assess the risks for humans (ambient dose equivalent) and machines (dose deposited, high energy hadron fluence and Si-1 MeV neutron equivalent fluence). Further, the MC simulations are used for the design of local radiation shielding and radiation beam dumps. Additionally, the code is used to estimate possible induced radioactivity of materials exposed to the radiation field.

3.3 Personal Safety Interlock

The fundamental active layer of protection that has been implemented at ELI Beamlines over the last several years, is the Personal Safety Interlock (PSI), whose aim is to recognize presence of hazards to people, initiate automatic protective measures, trigger alarms, and eliminate the hazard automatically, if possible. The covered hazards include, but are not limited to, laser and ionizing radiation, vacuum, and high voltage. The system is designed as an all-inclusive, redundant, fail-safe, independent electron system compliant with an international standard for Functional Safety of Electronic Safety Systems [9]. The PSI system is interfaced with, i.a. laser control systems and radiation and gas monitoring systems.

The first section of PSI has been in operation since 2020, the last one is expected to be fully operational by the end of 2023. To enable the safe operation of all relevant experimental stations even before the full employment of PSI, the Temporary personal safety system was installed. This system covers only laser and ionizing radiation hazards and when complemented by administrative measures allows operation with defined limitations.

3.4 Monitoring system

In terms of surveillance of the current radiological situation, the PSI system relies on an online monitoring information system (MIS). The system was implemented during the years 2019 to 2022. The MIS combines gas detectors (to monitor the concentration of technical gases) and passive and active detector technologies to monitor prompt radiation levels, activation, and contamination in relevant areas. The detection systems were chosen to meet measurement objectives, ranging from complex information needed in the high occupancy areas (control rooms) to simple indicators providing early warnings in low-occupancy areas (plant rooms).

4 Lessons learnt

4.1 Do not blindly trust your measurements

One of the first commissioning experiments, driven by the L3-HAPLS laser, demonstrated that it is vital to keep in mind that the interpretation of detector readings in these unique laser-generated fields requires critical thinking.

In an experiment designed to test various target systems, X-rays and low energy electrons were expected to be produced. Since the setup was enclosed in a vacuum chamber of 5 cm thickness aluminium wall, no radiation was expected to leak outside. However, within the first day of the campaign, a dose rate of about 3uSv/h of neutrons having energy above 20 MeV was detected. To understand the situation, several other detection systems were added, both passive and active, for the remainder of the campaign. Further investigation of the internal evaluation logic of the original detector and comparison of readings of the additional systems revealed that indeed, no high energy neutrons were generated. Apparently, the detector software misinterpreted large energy deposition of strong gamma flashes for a contribution of a high energy neutron. On the other hand, there is a high probability that neutrons in the energy range of 200 keV-15 MeV region were present. Still, their origin remains unclear, the probable cause being the laser prepulse. More details can be found in [12].

4.2 Tiny changes can lead to radically different radiation fields

An irradiation experiment at a station dedicated to electron acceleration driven by the L1-Allegra laser revealed the sensitivity of the radiation field to even small changes in the geometry setup.

The experiment was designed to test the response of passive luminescence chips and map the radiation field. The maximum energy of the electron beam was 50 MeV, the repetition rate was 550 Hz. The area mapped by the chips was 5 x 20 cm^2 vertically centered on the beam, the irradiation was done in air, immediately behind the window of the chamber. The added Gafchromic film nicely reproduced the enhanced shielding of the screws holding the window flange, but the chips' readings were difficult to interpret. To gain better understanding, we tried to reproduce the experiment by Monte Carlo means. The study revealed a strong dependence of the quality of the beam emerging from the interaction chamber both on the precise positioning of the magnet inside the chamber and the real beam divergence (which can differ shot-to-shot), see Fig. 2. This experiment has shown that even a simple geometry setup has its pitfalls. In fact, the chip readings are likely to be a superposition of a number of effectively different radiation fields. More details can be found in [13].

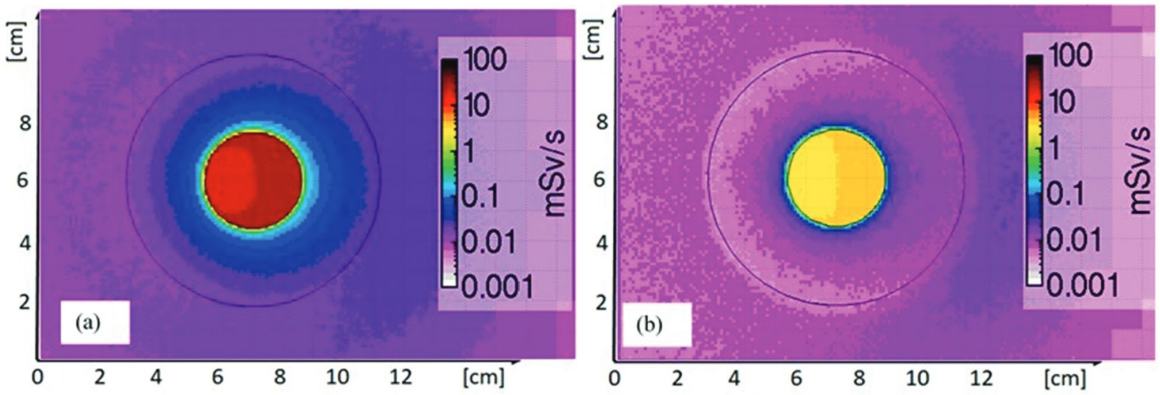

Figure 2: Monte Carlo ambient dose equivalent rate outside the exit window of the interaction chamber assuming an electron beam with 3.5 MeV average energy and 2.5 full width at half maximum. The beam divergence was set to (a) 12 mrad and (b) 100 mrad.

4.3 No source term is weak enough to be neglected

The high uncertainty on the expected source term and the sensitivity of the laser-target interaction to many various parameters imply the necessity to be always cautious.
An experiment was designed as a preparatory test for the main experimental setup. It was performed in a small interaction chamber (1 cm thick steel wall), driven by a commercial class 4 laser (1 kHz repetition rate, water jet target). Since the expected source term was an exponentially decreasing spectrum of protons, with maximum energy of 1 MeV, no detectable radiation outside the chamber was expected, which was also confirmed by the Monte Carlo simulation. However, a measurement by a single electronic personal dosimeter showed a dose rate of 12 uSv/h in the close chamber vicinity. Since the known doubtful reliability of EPDs measurement in the prompt laser-generated field, passive luminescence chips were installed, which detected up to 200 uSv over 12h operation. This confirmed the need to be cautious in all the laser-target experiments aiming at particle acceleration, including those seemingly insignificant.

5 Conclusions

The newly established research consortium, The Extreme Light Infrastructure ERIC, was introduced. The presentation focused on ELI Beamlines seated in the Czech Republic, the current status of commissioning, and the technology available to the user community. The experimental stations are currently in various stages of commissioning, with some of them already in routine operation.

Radiation fields generated by laser driven accelerators have unique features that represent a challenge for ensuring radiation protection. Therefore, a conservative approach has been adopted during the preparatory studies and the design of the introduced safety measures, in compliance with the ALARA principle. These are in more detail described in [14].

It can be concluded, that during the so far performed commissioning and user experiments, the implemented safety measures proved to work correctly, keeping the ambient dose levels in the populated areas on background levels. These experiments also emphasised the necessity to be cautious, since any Monte Carlo simulation can be only as solid as the input, which in the case of laser-driven facilities suffers from higher uncertainty and higher safety factor than in conventional facilities is thus needed. Unfortunately, due to too many unknown parameters and shot to shot differences, it is still impossible to reproduce campaigns by means of simulations. Last, but not least, given the peculiarities of the field, the interpretation of detector readings requires critical thinking.

In the future, a dedicated campaign with as many fixed laser parameters as possible is planned, in an attempt to gain a better understanding and to characterize the radiation field.

References

[1] – European Research Infrastructure Consortium (ERIC): https://ec.europa.eu/info/research-and-innovation/strategy/strategy-2020-2024/our-digital-future/european-research-infrastructures/eric_en
[2] - ELI Whitebook. Eds. G. A. Mourou, G. Korn, W. Sandner, J. L. Collier. THOSS Media GmbH, 2011. https://eli-laser.eu/media/1019/eli-whitebook.pdf
[3] – S. Kühn, M. Dumergue, S. Kahaly et al. J. Phys. B: At. Mol. Opt. Phys, **50**, 13, 132002 (2017).
[4] – The White Book of ELI Nuclear Physics Bucharest-Magurele. Eds. Chambaret, J.P., Dabu, R., Ursescu, D. Romania (2010). http://www.eli-np.ro/whitebook.php
[5] – B. Rus, F. Batysta, J. Čáp et al. Proc. SPIE 808010 (2011)
[6] – "ELI, The Extreme Light Infrastructure ERIC", ELI Beamlines Research Programs; https://www.eli-beams.eu/about/projects/completed-projects/eli/research-programs/ (current as Sep. 24, 2023)
[7] – F. Borne, D. Delacroix, J. M. Gelé et al. Radiat. Prot. Dosimetry **102** (1), 61-67 (2002).
[8] – P. L. Pritchett, Space Plasma Simulations. Lecture Notes in Physics, **615** (2003).
[9] – IEC 61580:2010. Functional Safety of Electrical/Electronic/Programmable Electronic Safety-related Systems, International Electrotechnical Commission (2010).
[10] – C. Ahdida, D. Bozzato, D. Calzolari et al. Frontiers in Physics 9, 788253 (2022).
[11] – G. Battistoni, T. Boehlen, F. Cerutti et al. Annals of Nuclear Energy 82, 10-18 (2015).
[12] – V. Olšovcová, I. Ambrožová, A. Cimmino et al. Rad. Prot. Dosimetry. In press.
[13] – A. Cimmino. Rad. Measur. Submitted.
[14] – A. Cimmino, V. Olšovcová, R. Versaci et al. Nuclear Science and Engineering, (2023)

Top-up Operation Safety Features at the Canadian Light Source

Cubbon, G*, Street, D.*, Bewer, B.*
*Canadian Light Source
44 Innovation Boulevard
Saskatoon, SK, Canada S7N2V3

Abstract

The Canadian Light Source, located in the prairie province of Saskatchewan, is a third-generation synchrotron facility operating with a 2.9 GeV electron beam. User operation began in 2005, and was limited to decay mode where beam was injected once every 12 hours to refill the storage ring. In decay mode the front-end safety shutters were kept closed to protect personnel on the experimental floor from potential radiation produced during the injection process. Making the transition to beam injection with safety shutters open required a defence in depth approach to ensure the risk of radiation exposure to personnel during beam injection was mitigated. The safety features were designed and implemented, including safety interlocks to inhibit top-up operation when safety conditions were not met, will be discussed. The CLSI Top-Up mode of operation was reviewed and approved by the Canadian federal regulator in 2018, and CLS first operated in Top-Up in 2019.

1 Introduction

The beginnings of the Canadian Light Source (CLS) date back to 1962 with the start of the Saskatchewan Accelerator Laboratory (SAL). The facility, located on the University of Saskatchewan campus, was developed for research in high energy physics, and included the addition of EROS 'Pulse Stretcher Ring' in 1984, a forerunner to Canada's first synchrotron.

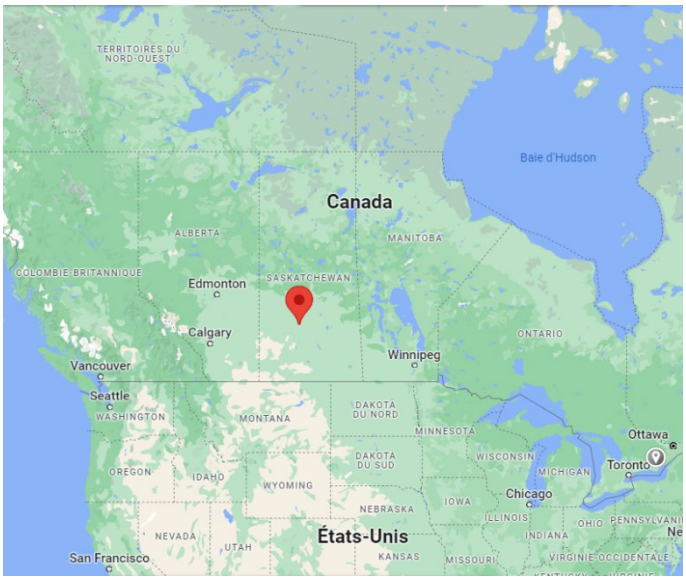

Figure 1: Canadian Light Source Location

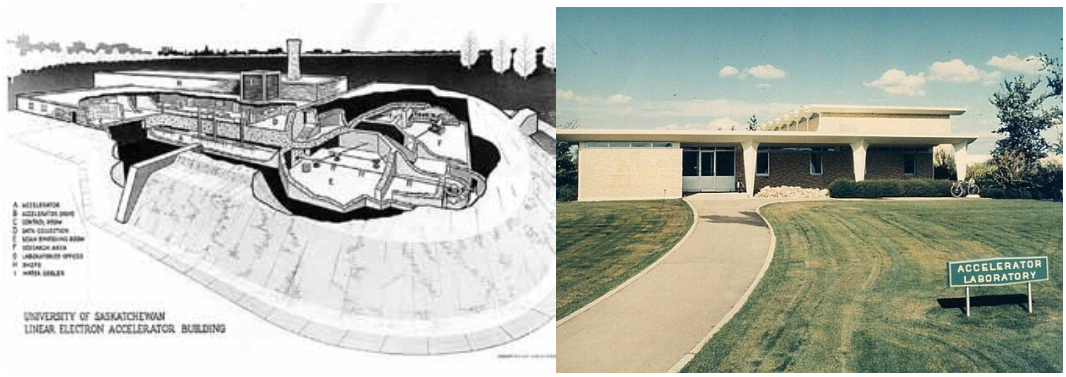

Figure 2: Saskatchewan Accelerator Laboratory

In 1999, the SAL 300 MeV linear accelerator was modified to serve as the 250 MeV injector for the new 3rd generation synchrotron facility addition. The ~ 12,000 m^3 building addition incorporated the existing SAL linac located two stories underground, a transfer line to connect the linac to the new booster ring, a 2.9 GeV storage ring, and the beamline experimental and ancillary facilities. The 170.88 m circumference storage ring is comprised of 12 repeating cells with each cell containing two dipole bending magnets, focussing magnets, and a 4.8 m straight section, which provide the synchrotron light to 22 commissioned beamlines. The facility was designed for 500 mA stored beam operation, however normal operations at the facility have been restricted to 250 mA as the maximum operating current. In 2005, the Canadian Light Source began normal operation as a synchrotron facility with 6 beamlines.

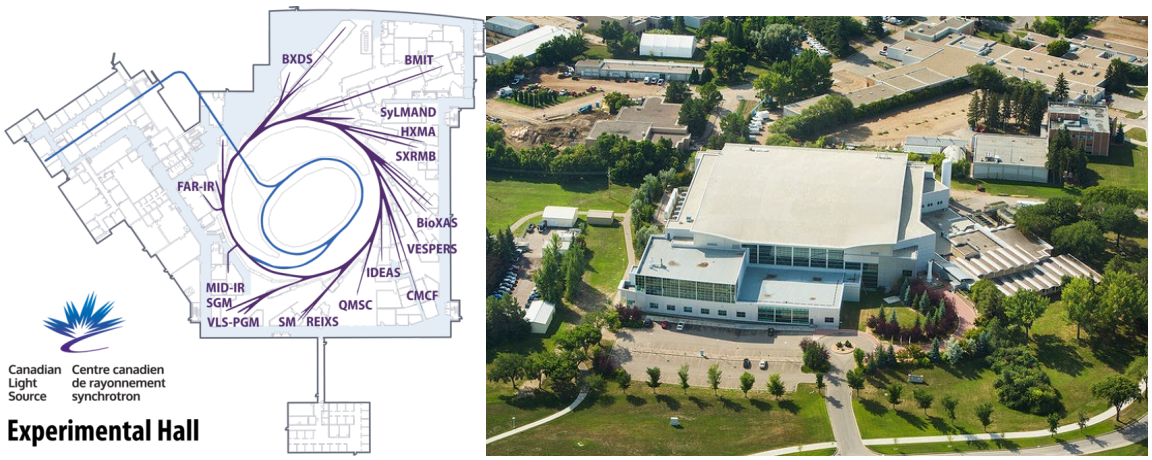

Figure 3: Canadian Light Source

Initial operation of the CLS facility was in the 'decay mode' of operation, where the storage ring was refilled every eight or twelve hours depending on operational needs. Decay mode included closing of the beamline front end safety shutters to ensure personnel safety during the injection process. Decay mode injection results in a loss of productive beam time for research not only due to there being no synchrotron light during the five to ten minute injection process, but also because the removal of the synchrotron light results in time lost due to thermal re-stabilisation of beamline optics. The top-up mode of operation, where a pulse of electrons is injected periodically (usually every few minutes) to maintain the maximum storage ring current, greatly improves beamline availability by eliminating the thermal changes to beamline optics caused by closing the beamline front end safety shutters during injection.

2 Top-Up Mode Hazard Assessment

In the top-up mode of operation, beam injection with the beamline safety shutters open is permitted. The change in operations required that radiation levels be maintained well below regulatory requirements, design criteria, and maintained As Low As Reasonably Achievable (ALARA).

Regulatory Limit	Design Limit
20 mSv/Year (NEW)	10 mSv/Year (NEW)
1 mSv/Year (Public)	1 mSv (Accident Scenario)
50 µS/y (Outside Facility)	< 5 µSv/h (Accellerator)
	<2 µSv/h (Beamline)

Figure 4: CLS Radiation Limits

An evaluation of the potential consequences identified four primary risks to personnel safety from top-up operation:

- Injected electrons travel down beamline
- Beamline Shielding Inadequate
- Storage Ring – Injector Energy Mismatch
- Poor injection efficiency

An internal failure mode analysis using DIMAD was completed [1]. The analysis considered kicker magnet failure, injection orbit misalignment, off-energy particles, and dipole short circuit. The investigation determined the probability of an electron escaping the storage ring vacuum and travelling down a beamline was 'extremely unlikely' when a circulating electron beam was stored.

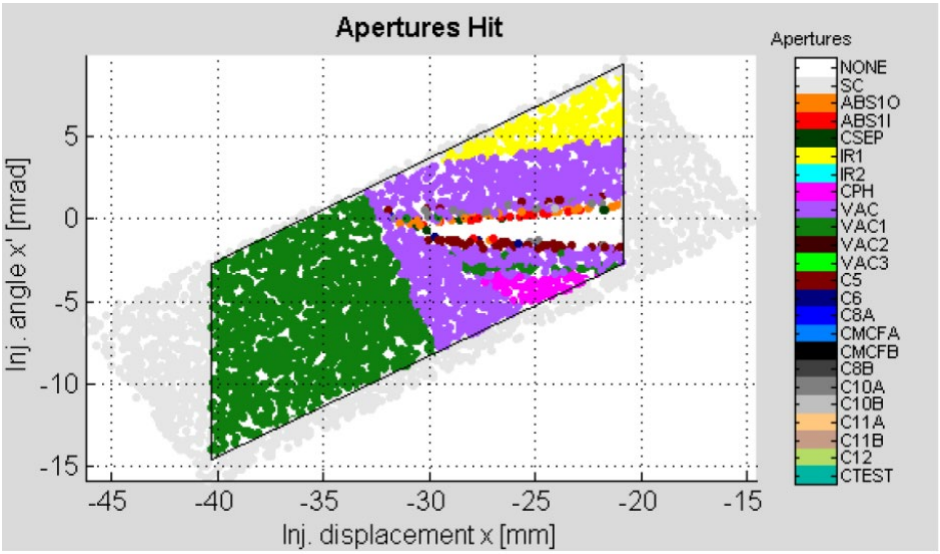

Figure 5: Example of DIMAD plot showing at which aperture the injected beam is lost for particles launched by the shotgun injection. Plot is for no errors in the storage ring.

In addition, accident scenarios were investigated. A theoretical analysis showed the expected worst-case radiation resulting from for a 1 nC pulse of electrons transported down beamline front-end to be 402 µSv [2]. Worst case or accident scenario testing was also completed that included:

- Normal injection
    - Radiation levels outside beamline enclosures were unchanged whether front end safety shutters were open or closed
- Energy Mismatch
    - Energy mismatches of 1, 2, and 4% between injected and stored beam were tested with all results being < 100 μSv/h outside beamline enclosures
- Vacuum Valve Closed
    - Vacuum valve for each straight section closed and tested one at a time
    - Injection pulse lost at valve
    - Maximum radiation of 1.4 mSv/h outside a beamline enclosure

The theoretical and measurement results indicated operation of top-up mode could be achieved within all regulatory and design limits.

3 Top-Up Mode Safety Features – Defence in Depth

An important safety feature of the top-up mode of operation is to insure the injection process can only occur into an approved storage ring configuration that supports a circulating electron beam with minimal losses. A simple and effective way to achieve the requirement is to ensure the injection process cannot occur unless stored beam is circulating. Operating in top-up mode requires a special interlock key that is part of the safety system to be enabled in the control room to indicate top-up mode is active. Enabling the key permits top-up mode provided all safety conditions are met. Top-up mode (or any injection with safety shutters open) cannot be enabled without the key switched correctly. A redundant and independent storage ring beam current monitoring system is integrated into the top-up mode of operation safety chain to ensure injection is only permitted when the stored beam current is at an acceptable level.

The presence of stored beam in the storage ring is monitored for this safety system in two ways. Firstly, a redundant monitoring system measuring the difference between the forward and reverse power in the superconducting cavity was implemented. Absence of a sufficiently large power difference indicates beam is not present in the storage ring, and prevents injection.

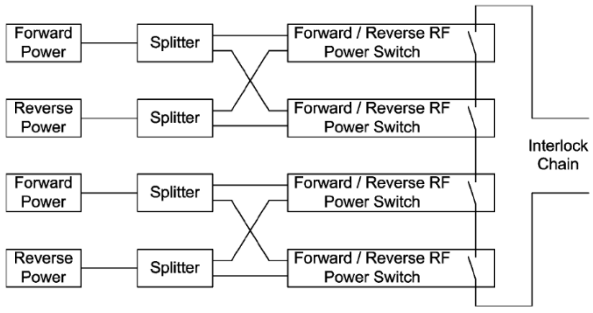

Figure 6: Block Diagram of the Forward-Reverse Power Switch

Secondly, four (4) beam current switches independently monitor the storage ring Beam Position Monitor (BPM). Each of the switches is hardwired into the safety interlock chain, and all 4 switches must indicate that the level of stored beam has exceeded the threshold for which top-up operation is permitted.

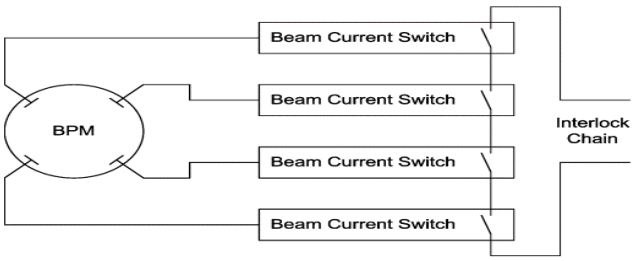

Figure 7: Block Diagram of the Beam Current Switch

Several machine protection systems are in place that also mitigate the risk of excess radiation levels due to injection non-conformities. Although these machine protection systems are not safety rated, they provide a level of redundancy to support the safe operation of top-up and include:

- Dipole Energy Interlocks
  - Transfer line to storage ring dipole power supply (0.5%)
- Bad orbit protection
  - Beam dumped when bad orbit detected
- Injection Efficiency
  - > 90% or injection stopped
- Transfer Line Collimator
  - Shielded collimator in storage ring tunnel removes off-orbit injected electrons
- Cumulative Injection Charge Limit
  - An upper limit to total charge injected in one hour is limited to reduce the impact of an accident scenario

The defence-in-depth approach also includes an array of real time radiation monitors strategically located throughout the facility. The monitors are designed to integrate the radiation produced by all modes of the accelerator operations and provide a cumulative hourly combined gamma and neutron dose. During normal operation, should the limit of 2.5 µSv cumulative hourly dose be reached, the injection process is interlocked until the cumulative hourly dose resets at the beginning of the next hour.

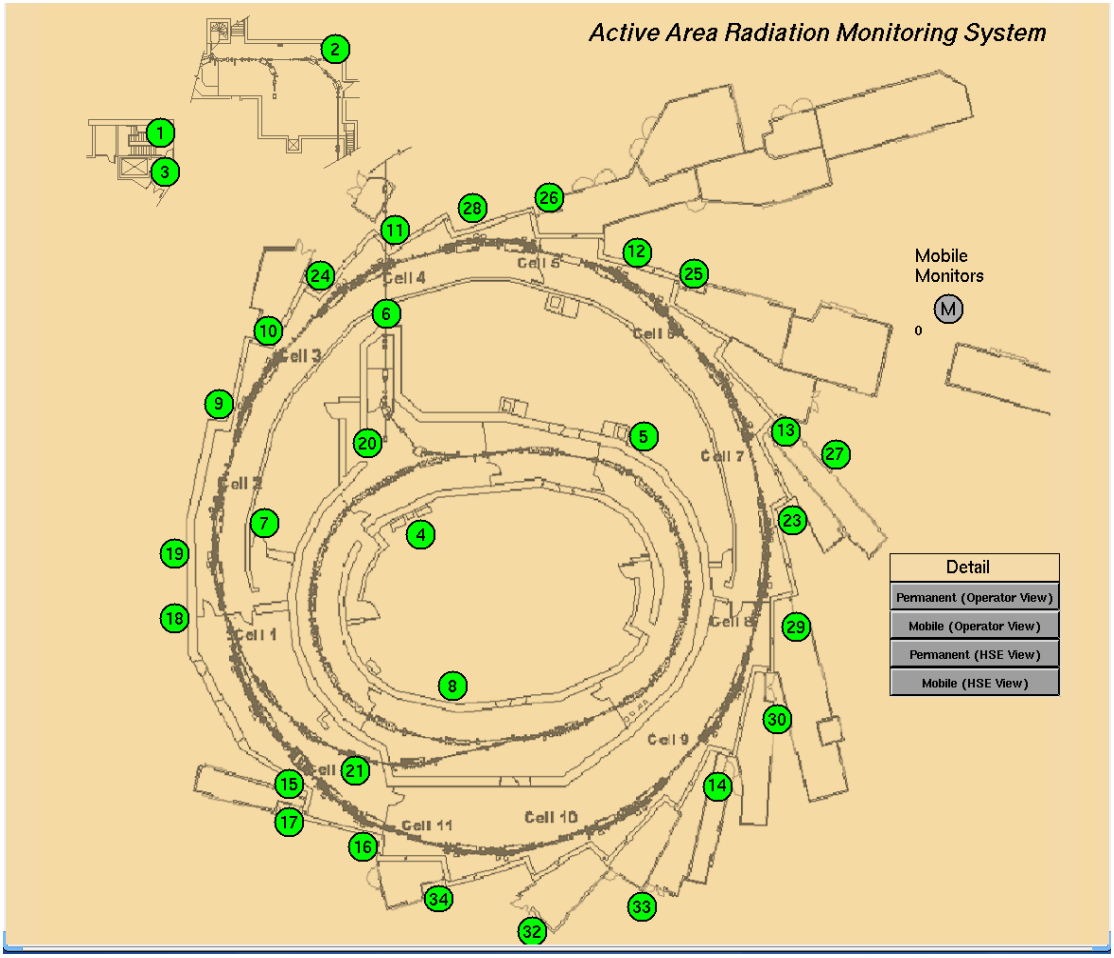

Figure 8: Active Area Radiation Monitoring System (AARMS) Locations

A strong radiation protection program also plays an important role in the defense-in-depth approach. Process and procedures for shielding design and configuration control, accelerator and beamline area lockup, commissioning and routine radiation surveys, passive area monitoring using area dosimeters, and strong controlled work processes contribute to the overall safe operation of the facility.

4 Approval

Initiation of the regulatory approval process for top-up mode required the design, implementation, and testing for the process to be completed and thoroughly documented. Once the changes were designed and implemented, testing was completed during specially designated periods not used for synchrotron research. During much of the testing, the experimental hall was evacuated and facility access restricted as a precaution.

On May 3, 2017, documentation supporting the safety case for top-up mode operation was forwarded to the Canadian Nuclear Safety Commission (CNSC). The documentation included a hazard assessment of the change to top-up mode, detailed analysis and design documents considering the mitigation of the hazards identified, as well as the test results. On October 17, 2017, CNSC staff indicated they were satisfied with the safety case for the top-up mode of operation and forwarded the request for an amendment to the operating license for final approval.

On February 20, 2018, after a public commission hearing was held to consider the licensing amendment request, CLS was granted a license amendment to permit top-up mode operation during routine operation.

The detailed planning, implementation, and testing resulted in a robust approach to the safety of top-up operation. Top-up mode is now fully implemented and used almost exclusively during normal operation, with no radiation exposure related concerns arising.

References

[1] L. Dallin, IPAC2012
[2] P. Chowdhury and G. Cubbon, RADSYNCH 2015

Radiation Protection on Sirius, the new Brazilian synchrotron

Moura F.N. [1], Lima L.P[1], Vieira A.L.C[1], Neto F.A.B[1]

[1]Brazilian Center for Research in Energy and Materials (High Technology Polo II - R. Giuseppe Máximo Scolfaro, 10000 - Bosque das Palmeiras, Campinas - Brazil)

The Brazilian Synchrotron Light Laboratory (LNLS) accommodates the new Brazilian synchrotron Sirius. In 2018, the linear accelerator was installed and commissioned, acquired from TPS, with a final energy of 150 MeV; in 2019, the booster reaches the final energy of 3 GeV, and the storage ring was validated with the first image in the beamline. Currently, Sirius operates in decay mode, with three injections per day to maintain 100 mA. In May 2023, the machine will work in top-up mode and, in 2024, the goal is to reach the final current of 350 mA with the installation of the superconducting cavity.

All accessible areas of Sirius respect the annual dose of 1 mSv. However, inside the tunnel, there is a change in the classification of the area, from a controlled area to a free area after waiting 06h for the controlled loss of the beam, known as the cooling time due to localized activations. The Sirius shield was elaborated using a Monte Carlo simulation [1] and was built in a unique way, with ten openings for the passage of equipment on the roof and people through eleven chicanes. Radiometric surveys are made at each increase in current or change in operating mode. There are no records of irregularities regarding shielding, doses above the limits allowed in the operation or radiological emergencies at the facility.

Currently, the installation has a monitoring system with 18 pairs of detectors (gamma radiation and neutrons) around the accelerators and 17 in the installation phase on the beamlines; 435 dosimeters (thermoluminescent, LiF, and optically stimulated, CaSO4 dosimeter pairs) spread around the shielding and external area of the installation. Inside the accelerators, there are 100 scintillator detectors for Bremsstrhalung gas developed in-house and high-dose dosimeters (alanine).

Due to the lack of radioprotection standard for synchrotrons, the safety assumptions and procedures adopted at Sirius are based on experience, acquired with UVX, and other synchrotrons around the world. The radiation protection group seeks to consolidate shared experience and theoretical knowledge in periodic machine studies. Mainly, the activation of components inside the tunnel and the integral dose value at that location are evaluated. So far, it has been possible to trace beam loss points, which are confirmed with external detectors.

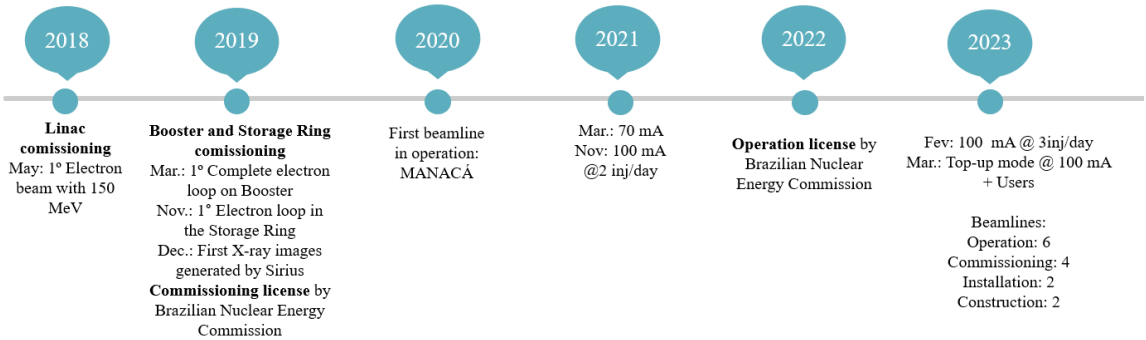

Figure 1: Timeline with Sirius milestones.

References

[1] Netto, F.A.B. Radiation Protection Status of Sirius Project. 10th International Workshop on Radiation Safety at Synchrotron Radiation Sources. Sweden, 2019.

Radiation Protection and Personal Safety System at SOLARIS National Synchrotron Radiation Centre

Magdalena B. Jaglarz , Dagmara Michoń, Barbara Zdrodowska- Pawluś, Krzysztof Wawrzyniak , Mateusz Augustyn, Adriana I. Wawrzyniak

National Synchrotron Radiation Centre SOLARIS Jagiellonian University,
Czerwone Maki 98, 30 -392 Kraków

Abstract

All the activities undertaken at National Synchrotron Radiation Centre SOLARIS concerning radiation protection comply with requirements described in Atomic Law. In accordance with applicable law the National Atomic Energy Agency (PAA) oversees SOLARIS operations in this area. At SOLARIS, the radiation measurements using radiation monitor stations (RMS), thermoluminescence dosimeters (TLDs) and portable radiometers have been carried out since 2015 [1]. Furthermore, radiological safety of employees exposure is controlled through individual thermoluminescent dosimeters (TLDs) and, if necessary, also electronic dosimeters [2].

Moreover, SOLARIS research infrastructure was equipped with Personal Safety System (PSS) to protect facility personnel and users from ionization radiation by controlling access to designated areas and stopping synchrotron operations in the event of the hazardous situation. PSS is based on programmable logic controllers (PLCs) which are reliable, fail-safe, redundant and diverse (especially the most critical parts). RMS are measuring radiation level at the facility 24/7 and in some cases provide beam stopping when preset dose rate or accumulated dose threshold is exceeded.

The first users started doing their experiments on the SOLARIS beamlines in 2018 [3]. Since then, the synchrotron has been under continuous development and several improvements to the radiation shielding have been implemented that enabled it to fulfill the ALARA principle.

Solaris research infrastructure will be presented through the prism of radiological protection in particular with the effective use of the PSS system.

1 Overview at Solaris Centre

1.1 Location

Our facility is located in Krakow, Poland. The Synchrotron SOLARIS is situated approximately 12 km from the centre of Krakow. Overview presented in Figure 1 is somewhat outdated because SOLARIS is currently in the midst of a substantial expansion of the facility, specifically the experimental hall.

Figure 1: Overview at SOLARIS

Performing operations during the construction and operation of heavy machinery presents a challenge. However, we are now closer to our goal than we were previously. The consolidation of the buildings occurred in July during the summer shutdown.

1.2 Storage ring parameters

The basic operational parameters for SOLARIS are gathered in Table 1.

The SOLARIS storage ring main parameters

PARAMETER	VALUE
Energy	1.5 GeV
Max. current	500 mA
Circumference	96 m
Main RF frequency	99,93 MHz
Max. number of circulating bunches	32
Horizontal emittance (without insertion devices)	6 nm rad
Coupling	1%
Tune Q_x, Q_y	11.22; 3.15
Natural chromaticity ξ_x, ξ_y	-22.96, -17.14
Corrected chromaticity ξ_x, ξ_y	+1, +1
Electron beam size (straight section centre) σ_x, σ_y	184 µm, 13 µm
Electron beam size (dipole centre) σ_x, σ_y	44 µm, 30 µm
Max. number of insertion devices	10
Momentum compaction	3.055×10^{-3}
Total lifetime of electrons	13 h

Table 1: The SOLARIS storage ring main parameters

1.3 Operation

In 2018, the first group of researchers began conducting experiments on the SOLARIS beamlines. In the ongoing progression, SOLARIS continually expand, new experimental lines are being installed, and as a result, there is an increasing number of new users.

Figure 2 provides an overview of the number of beamlines currently in operation, under construction, and in the conceptual phase.

As a standard operating procedure, SOLARIS runs continuously for 24 hours a day, six days a week.

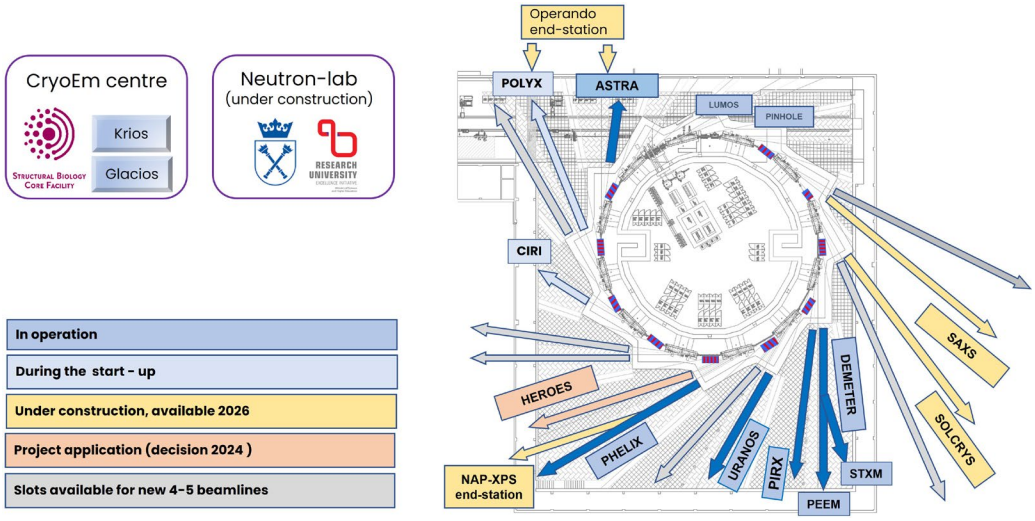

Figure 2: Overview of the SOLARIS research infrastructure

As previously mentioned, the facility is expanding due to the limited space for additional beamlines, as indicated on the right- hand side on the figure 2.

2 Radiation Safety at SOLARIS

2.1 Legal acts regulating the activity of SOLARIS

The authority that supervises SOLARIS' operations is the National Atomic Energy Agency (abbreviated as PAA). All SOLARIS activities concerning radiation protection are in compliance with the requirements described in the formal regulations, known as the Atomic Law.

In general, the Director of SOLARIS, acting, on behalf of the Rector of the Jagiellonian University, is responsible for ensuring compliance with radiation protection requirements, among other tasks. The head of the organizational unit is likewise accountable for ensuring that external employees receive radiological protection equal to that afforded to internally employed staff within the same facility.

Furthermore, the Radiation Safety Officer, among other responsibilities, internally oversees compliance with radiation protection requirements.

The Table 2 contains the annual limits for the effective dose to the whole body, area classification information, and description of individuals eligible to work in those areas.

Category	Dose limits	Who?	Area classification
Radiation workers category A	20 mSv/year	No workers at Solaris	Controlled area
Radiation workers category B	6 mSv/year	Technical team of Solaris, Radiation Protection Officer	Supervised area
Public	1 mSv/year	Administrative and external workers, users, visitors	Unclassified area

Table 2: Workers categories at SOLARIS Centre

Employees may work under exposure conditions only after obtaining a certificate from qualified medical doctor, confirming their fitness for such employment. If the annual dose limit is exceeded, the employee must undergo a medical examination. Continued work under exposure conditions requires approval from a licensed physician.

A pregnant woman cannot be employed in a position where an unborn child could receive a dose greater than 1 mSv. It is essential to promptly inform the radiological safety officer of pregnancy to determine suitable working conditions.

In reference to the table above, in Figure 3, the classification of areas in terms of radiation exposure is displayed. The SOLARIS synchrotron zone is designated as an accelerator laboratory. Unclassified areas (up to 1 mSv per year) are open to the general population, users, administrative workers, guests, this covers experimental hall and laboratories. Supervised areas (up to 6 mSv per year) are accessible to SOLARIS employees of categories B. These include the Klystron Tunnel, Service Gallery, fenced and signposted regions. Access to controlled areas (more than 6 mSv per year) is prohibited during the operation of the machine. These areas include the Linac Tunnel and the Ring Tunnel.

With regard to our employees, SOLARIS Team is continuously growing. Currently, the total number of employees stands at 112, with 93 of them qualified for category B.

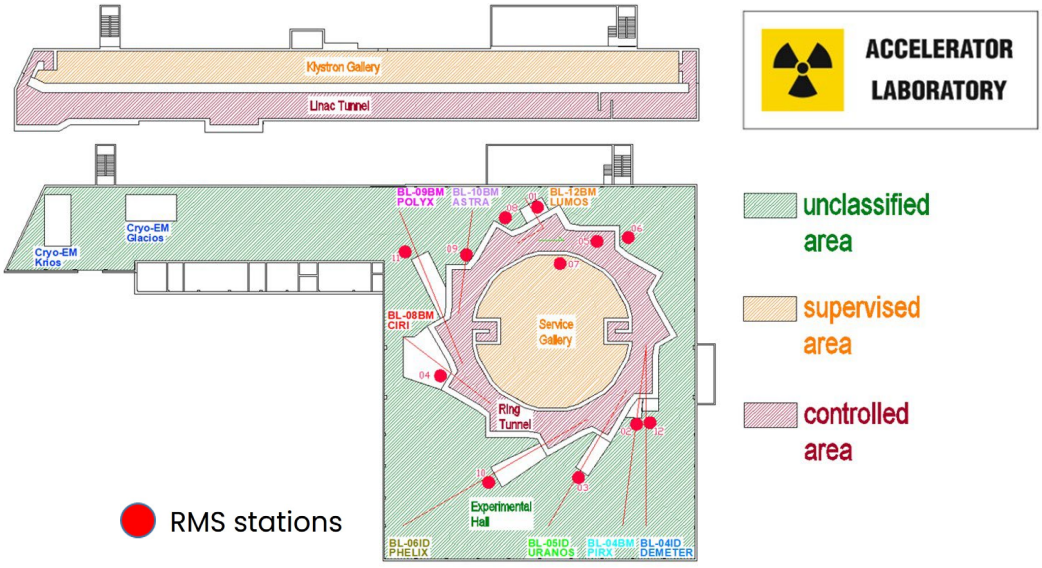

Figure 3: Classification of areas in SOLARIS

2.1.1 How is the radiation monitored at SOLARIS?

Environmental dosimetry at the SOLARIS Synchrotron is conducted using thermoluminescence dosimetry (TLD) as well as with ionizing radiation monitoring stations (RMS). Environmental thermoluminescence dosimetry (TLD) is used for continuous measurement of accumulated doses at selected points throughout the facility to assess radiation exposure. Dosimeters are distributed in 45 points within the unit. To monitor the doses received by SOLARIS employees, Personal TLD dosimeters are used, which are read in accredited laboratories every 3 months.

The facility has 12 ionizing radiation station from two different companies (figure 4), two of which include not only ionization chamber but also neutron detectors. They are located in various places in the experimental hall, as marked in Figure 3.

Dose rates and accumulated doses are continuously monitored locally and in the control room using a dedicated application based on the Tango control system. Furthermore, defined signals are continuously archived, allowing us to easily reconstruct the history of events. At the RMS stations, alarm thresholds are configured to include warning light and audible signals. Exceeding the alarm threshold at selected stations results in the shutdown of the synchrotron or a specific experimental beamline. Each beamline has its dedicated ionization chamber.

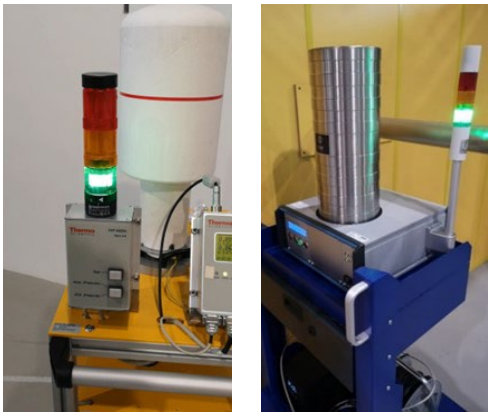

Figure 4: Radiation Station Monitors in SOLARIS

The unit is also equipped with portable radiometers, including Geiger – Müller counters, proportional counters and ionization chambers. Electronic personal dosimeters are used by employees when accessing supervised or controlled areas, and they are available in the Control Room.

3 Personal Safety System

Personal Safety System (PSS) role is to protect individuals, including personnel and users, from ionizing radiation at SOLARIS. It achieves this by controlling access to restricted areas and halting machine operation when unsafe situations occur. The PSS is based on programmable logic controllers (PLC) and its various components are designed to be reliable, fail- safe, redundant and diversified, with particular emphasis on the most critical parts. Radiation monitoring stations measure radiation during machine operation and ensure the beam's stop if thresholds of a dose rate are exceeded.

The machine area is divided into three zones, each one with different access definition. Zone 1 includes the first part of the Linac Tunnel, Zone 2 covers the second part of it, and the Zone 3 corresponds to the Ring Tunnel. The main entrances to the zones are equipped with elements, which guarantee no entry inside the tunnels, when the access is forbidden, and allow performing the controlled access procedure and the search procedure when it is required. Every tunnel has also an emergency exit (E2 and E3 marked in Figure 5). The Z1 and Z3 doors can be opened from the inside by pressing the " Unlock door" green light push button on the internal PSS panel (during controlled exit procedures) or by pressing a green button located directly next to the doors (during the Linac shutdown state and in emergency situations). During controlled entry procedures, the doors Z1 and Z3 are unlocked by an operator in the control room by pressing a button in the Control Access panel (Figure 7). The door Z2 is opened directly by the entering/ exiting person by pressing "Unlock door" buttons placed on both sides of the door. Emergency doors are closed in a way that they cannot be opened from the outside during accelerator operation, but they can be opened by pushing the green button next to the door from inside in emergency situations.

In case of an emergency, it is always possible to use red mushroom emergency button positioned next to the door. This action disconnects the door electromagnet, unlocking the door and stopping the beam. In the event of a PSS and/or BMS (Building Management System) failure, it is still possible to open all the doors through green emergency boxes, located next to the doors. Access is allowed when a synchrotron part is completely switched off, and is granted to different groups under varying conditions. The door leading to the zone is unlocked by PSS, granting unlimited access inside the tunnel to authorized personnel (this access is managed through the BMS system).

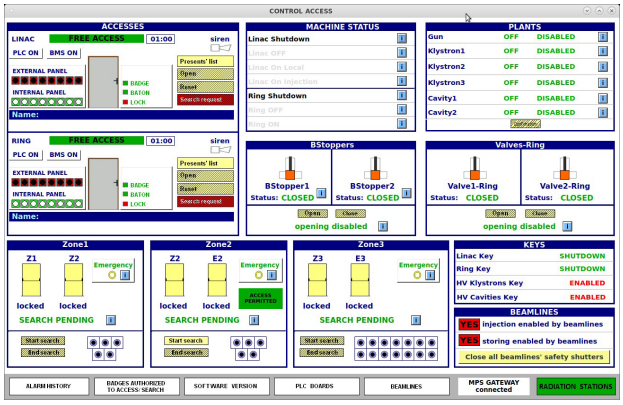

Figure 5: Control Access Panel

3.2 Synchrotron PSS

Personal Safety System is divided to Synchrotron and Beamlines PSS. The Synchrotron's PSS applies to the accelerator's tunnels and their proximity. It includes a search procedure that ensures there are no people inside the tunnels and prevents the machine from being turned on. When our employees are trained on this topic, they are asked to check carefully if there is on one in the tunnels. In the tunnels, especially in the ring there are new components- front ends therefore its crucial to check all areas. In order to break the search routine during the tests - mystery operators (human- sized mascots) appear in the tunnels and hope for transportation back to the Control Room. It sharpens the senses and perceptiveness a lot.

Additionally, it can switch off the machine in case of an emergency due to pressing an emergency button, exceeding a radiation alarm threshold (two RMS stations are connected to the Synchrotron PSS), and forcing the doors that lead to the tunnels.

3.3 Beamline PSS

Beamline PSS, applies to the lead hutch, and includes a search procedure that guarantees the absence of individuals inside the hutch during the beamline operation. Each beamline also has an RMS station connected to the PSS. The main hutch key is designed to ensure that only authorized individuals conduct experiments. Without turning it to the correct position, there is no possibility to open the so- called safety shutters. To initiate an experiment, the key must be in "enabled" position and a hutch search must be performed. If there are no other obstacles related to machine operation, it is then allowed to begin measurements.

The Beamline PSS terminate the experiment, i.e., by closing the safety shutters, in the following situations: exceeding a radiation alarm threshold, pressing the emergency button, or forcing the door leading to the hutch.

As for the emergency buttons, they are positioned in the synchrotron tunnels, at the entrance doors to the tunnels, in the middle of the lead hutches, as well as at their entrance doors. To ensure the appropriate location of emergency buttons, we have a panel (Figure 7). When one presses a button, it is easy to verify its location.

4 Storage ring light signals

Information element has been introduced so that individuals in the experimental hall can be aware of the synchrotron's status. This light column (Figure6) is connected to the machine status, with each colour corresponding to a specific status, as is described.

Figure 6: Storage Ring Light Signals

5 Conclusions

Measurements of radiation levels and assessments of dose levels are conducted continuously at the SOLARIS Synchrotron in order to ensure safe working conditions for everyone. Radiological trainings and building awareness among employees will be carried out.

Additionally, Personal Safety System undergoes a comprehensive annual inspection related to the operation of this system, which aims to eliminate any irregularities. However, conducting, for example, the search procedure also provides ongoing testing of the system.

Due to the construction of new beamlines, modifications to the PSS are necessary. These changes must not disrupt the operation of the entire system, so after such intervention, a series of tests must always be conducted. These actions involve various sections such as automation and control systems to make comprehensive changes.

References

[1] – J. Wikłacz, Magdalena Jaglarz, Adriana Wawrzyniak „Radiation levels around SOLARIS 1.5 GeV storage ring after the machine commissioning" Radsynch19, 10th International Workshop, MAX IV Laboratory, Sweden May 2019

[2] – Magdalena B. Jaglarz, Justyna Wikłacz, Adriana I. Wawrzyniak, "Radiation safety at Solaris 1.5 GeV storage ring" IPAC2019, Melbourne, Australia, JACoW Publishing doi:10.18429/JACoW-IPAC2019-THPRB059

[3] – A.I. Wawrzyniak, P. Andryszczak, G.Cioś, K.Guła, G.W.Kowalski, A.M. Marendziak, A. Maximenko, R. Panaś, T. Sobol, M. Szczepaniak, J. Wiechecki, M. Wiśniowski, M. Zając, A. Curcio "Recent developments at SOLARIS National Synchrotron Radiation Centre" IPAC2022, Bangkok, Thailand JACoW Publishing doi:10.18429/JACoW-IPAC2022-TUPOPT024d

Measurements of Bremsstrahlung by Field Emission from the BESSY HOM Cavities

Huck H., Bergmann Y., Bundels A., Pichl L.

Helmholtz-Zentrum Berlin für Materialien und Energie
Hahn-Meitner-Platz 1
14109 Berlin, Germany

Abstract

Since 2015, the BESSY II storage ring runs on four HOM damped normal conducting single cell BESSY type cavities, which are also in operation at several other European synchrotron light sources. While the usual input power per cavity is 40 kW, it is possible to operate them with up to 80 kW. Recently, the corresponding cavity test stand has been upgraded with an 80 kW solid-state amplifier (SSA) as well, enabling easy measurements of ambient radiation dose rates due to field emission at highest power without electron beam. We present first results of these measurements, indicating a sharp exponential rise of Bremsstrahlung after a certain power threshold, up to values of 1 mSv/h at 1 m distance.

1 Introduction

At modern synchrotron light sources, the main contributions of ionizing radiation are synchrotron radiation, bremsstrahlung and neutrons, originating from deflection, scattering or loss of the actual high-energy electron beam. However, there are usually a number of further X-ray sources nearby, which can be dedicated ones like X-ray tubes, or parasitic (unwanted) sources like the dark current from RF cavities.

At a running storage ring, outside exclusion areas the dose rates due to field emission from RF cavities should be negligible, but it can become the major source of ionizing radiation when the cavity is operated in a dedicated test stand or during maintenance periods, when access to the storage ring tunnel is granted.

In the vicinity of local impurities like dirt or scratches in the cavity walls, electrons can escape these walls due to local spikes in the field strength. The free electrons are subsequently accelerated in the RF field, and eventually lost at other locations inside the vacuum chamber, giving rise to bremsstrahlung. The trajectories can get quite complicated and varying depending on starting phase and actual positions of the local emitters, but the main contributors to the dose rate outside are usually the electrons passing near the axis of the cavity and hitting the opposite wall, having gained maximum energy at optimum starting phase. This energy corresponds to the effective accelerating voltage

$$U_{eff} = \sqrt{2 \cdot R_{eff} \cdot P}$$

with the shunt impedance R_{eff} and the intra-cavity power P. The actual amount of field emission or dark current is hard to predict, as it depends on many factors, not all of which are theoretically fully understood. For super-conducting cavities, the effects are much worse and usually limit the general performance, especially the achievable gradient, of the individual devices. The highest dose rate ever measured at HZB was 5 Sv/h from a TESLA 9-cell cavity. From the SRF case, we expect an exponential rise of field emission with cavity power, but for normal conducting cavities the experimental data and literature are scarce.

2 BESSY HOM Cavity

In the early days of BESSY II, the storage ring ran on four single cell DORIS type cavities, recycled from DESY. These were replaced about ten years ago by strong HOM damped single cell normal conducting cavities, which had been developed by a collaboration headed by BESSY [1]. The cavity type was first tested at the MLS [2] and at DELTA [3], and later also installed at ALBA [4] and DIAMOND.

With a shunt impedance of 3.4 MΩ the cavities can be powered up to 80 kW, corresponding to an U_{eff} of 740 kV, though the usual input power at BESSY II is around 40 kW (520 kV). Shortly after installation of these cavities in the tunnel, ambient dosimetry recorded a dose rate of 5 µSv/h at 3 m transverse distance from an unconditioned cavity operating at 40 kW (without beam). On axis, the dose rate can be two to three orders of magnitude higher.

A dedicated test stand was established in 2015 in order to condition spare cavities, but also to test and tune a new LLRF system. Recently the corresponding transmitter (SSA) was upgraded from 40 kW to 80 kW, enabling easy measurements of ambient radiation dose rates due to field emission at highest power without electron beam.

3 Setup

The test stand comprises a separately fenced-in exclusion area on the roof of the storage ring tunnel and several mobile lead walls (Fig. 1). This shielding design was based on FLUKA [5, 6] simulations and the previously mentioned early measurements in the tunnel. The main idea was to attenuate the bremsstrahlung as close as possible to the source while still providing easy access to the cavity, waveguides and cooling water. For the 80 kW upgrade, we installed additional lead and heavy concrete shielding based on new simulations.

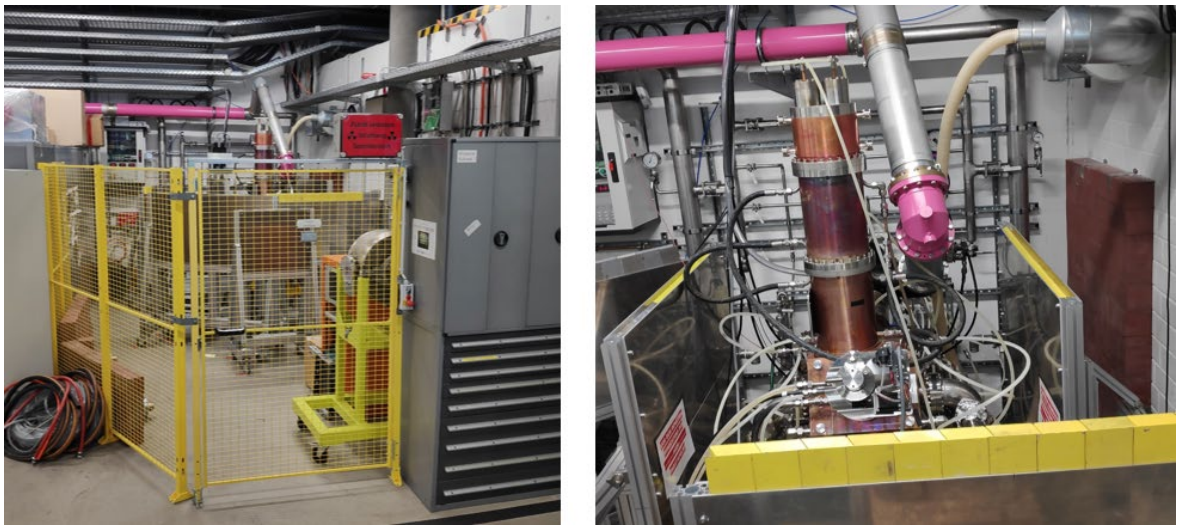

Figure 1: Test stand for spare storage ring cavities (BESSY HOM cavities)

4 Measurements

Shortly after upgrading the test stand, we reached up to 71 kW (cw) in the cavity (695 kV), limited by coupling and cooling. At this power, we measured up to 9 µSv/h at the borders of the fenced-off exclusion area, and up to 900 µSv/h directly below the cavity at 125 cm distance to the cavity axis. The latter measurements were taken by the mobile ionization

chamber automess 6150 AD [7], calibrated for the energy range of 60 keV to 1.3 MeV. After an initial slight drop in dose rate, no significant further conditioning effect could be observed.

Later tests were mostly done pulsed (250 ms per second), to improve the cooling and reduce the radiation. Several times the power was ramped slowly up to 71 kW and down again, while recording the readings of the automess device. The resulting dose rates as function of power and scaled by the duty cycle are plotted in Fig. 2.

A roughly exponential rise with power can be seen, starting at a threshold power of approx. 30 kW, and reaching up to approx. 500 µSv/h at 71 kW.

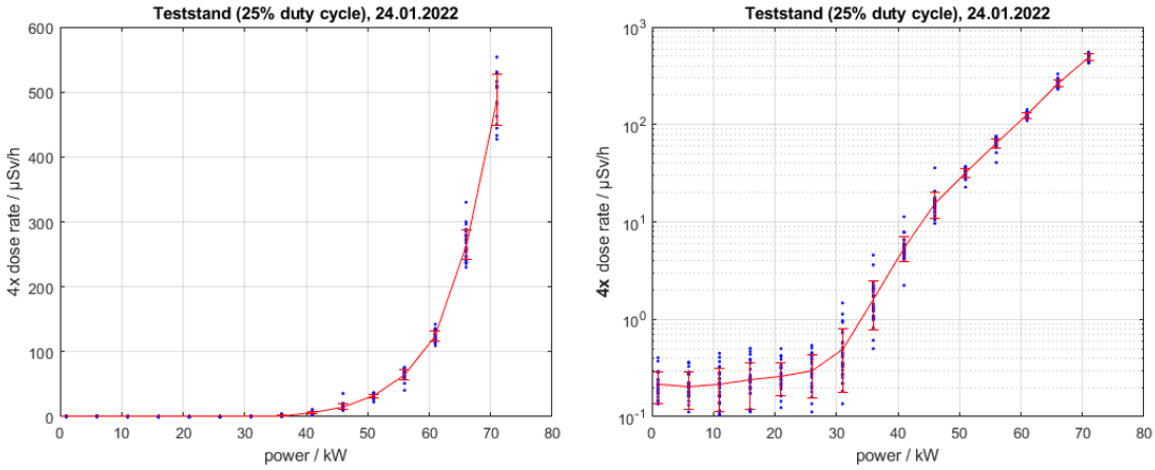

Figure 2: Dose rate below the cavity vs. cavity power, linear (left) and logarithmic plot (right) (same data). The measured values have been multiplied by 4 to take into account the duty cycle of 25%.

We also performed limited measurements on the storage ring cavities installed in the tunnel, to crosscheck these rather unexpectedly high dose rates. During a few hours of temporary access to the storage ring, each of the four cavities was separately ramped up and down, and the automess device was repositioned to approx. 1 m transverse distance to the respective cavity. Due to time constraints, these measurements had to be done very fast, resulting in rather noisy data (Fig. 3). Still, the exponential behaviour was reproduced, with maximum dose rates between 100 and 650 µSv/h depending on the cavity. Three of the four cavities behaved very similarly to each other, reaching 100-200 µSv/h at 70 kW, but the fourth one ("PAHR2") could only be powered up to 58 kW, limited by vacuum events. It should be mentioned that all four cavities had not yet been fully conditioned to full power, and are only occasionally operated above 40 kW.

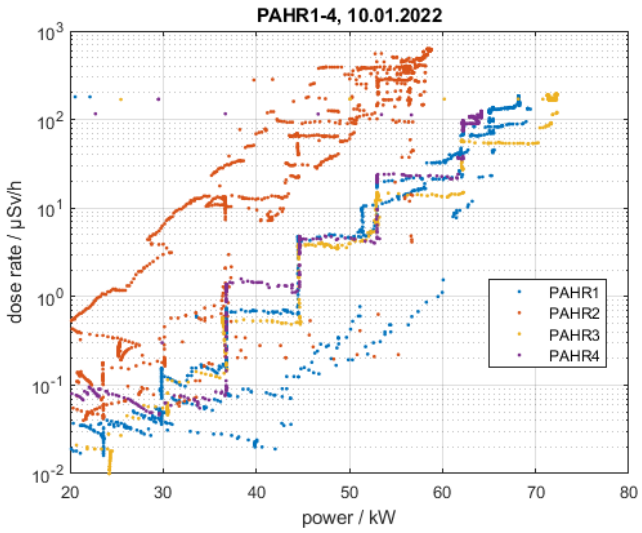

Figure 3: Field emission of the installed storage ring cavities in the tunnel without beam. Each of the four cavities was powered up individually; the dose rate was measured transversely at approx. 1 m distance.

5 Conclusions

We measured X-ray dose rates from field emission close to 1 mSv/h at 1 m transverse distance from a normal conducting cavity (500 MHz, 71 kW, 700 kV). An exponential rise of field emission with power was observed, starting at a certain threshold. Although the individual cavity was not in an optimum condition regarding surface quality and cooling, preliminary tests with other cavities show a similar behaviour with moderately varying threshold power. In the case of well-conditioned BESSY HOM cavities, the radiation surpasses background level at approx. 30 kW, and rises above 1 µSv/h at approx. 40 kW.

6 Outlook

Once the ongoing LLRF tests at low to medium power will be completed, we plan to do further high-power measurements on two other spare cavities in the test stand. For this, some cooling issues need to be resolved, the coupling has to be optimized, and additional local shielding will be installed to bring down radiation levels in the accessible areas nearby the test stand.

References

[1] - W. Anders et al., Proc. IPAC2017, Copenhagen, Denmark, THPIK013.
[2] - F. Marhauser, E. Weihreter, Proc. EPAC2004, Lucerne, Switzerland, pp. 979-981, 2004.
[3] - T. Weis et al., Proc. RuPAC2006, Novosibirsk, Russia, pp. 138-140, 2006.
[4] - F. Perez, B. Bravo, P. Sanchez, A. Salom, Proc. IPAC2011, San Sebastian, Spain, pp.178-180, 2011.
[5] - G. Battistoni, S. Muraro, P.R. Sala, F. Cerutti, A. Ferrari, S. Roesler, A. Fassò, J. Ranft, "The FLUKA Code: Description and Benchmarking", Proc. of Hadronic Shower Simulation Workshop 2006, Fermilab 6-8 September 2006, M. Albrow, R. Raja eds., AIP conference Proceeding 896, 31-49 (2007).
[6] - A. Fassò, A. Ferrari, J. Ranft, P.R. Sala, "FLUKA: A Multi-Particle Transport Code", CERN-2005-10 (2005), INFN/TC_05/11, SLAC-R-773.
[7] - www.automess.de

Induced radioactivity in the Elettra storage ring

Alikaniotis K.[1], Casarin K.[1], Scian G. [1], Tromba G. [1], Ferrari A.[2]

[1]Elettra-Sincrotrone Trieste S.C.p.A.
S.S. 14 - km 163,5 in Area Science Park, 34149 Basovizza, Trieste, Italy
[2]Institute of Experimental Particle Physics, Karlsruhe Institute of Technology, Germany

Abstract

The Elettra storage ring will be upgraded to a new generation machine in the near future. The installation of the new storage ring in the existing tunnel will require the dismantling of almost all components of the present accelerator. As a consequence, an accurate prediction of induced radioactivity is essential for the decommissioning. Simulations by means of FLUKA Monte Carlo code have been performed to evaluate possible activation points after 30 years of machine operation. Preliminary results show that, in general, most of the elements inside the Elettra storage ring will be below to the release levels, but further investigations are necessary, especially in the most critical parts of the machine.

1 Introduction

Elettra, based in Trieste, Italy, is a third-generation synchrotron source in operation since October 1993. After more than 30 years of operativities, it will be upgraded to a fourth-generation machine in 2026 [1].

Recent changes in the Italian radiation protection legal framework (D.Lgs. 101/2020) [2], following the implementation of the European directive 2013/59/Euratom, have some consequences for Elettra. One particular aspect concerns the management and the release of radioactive materials and waste: Article 54 regulates the release of radioactive materials, in which the release levels follow the radiological non-relevance criterion (the 10 μSv-concept).

The planned decommissioning of the Elettra storage ring will produce a large quantity of accelerators components with no further use in the new machine: 284 magnets (approximately 8.5 tons of steel and copper), 84 magnet supports or “girders” (approximately 11 tons of concrete), 260 meters of vacuum vessel (approximately 1 ton of stainless-steel), a large number of cable trays and several kilometres of cables.

As a consequence, an accurate prediction of the induce radioactivity is crucial for the decommissioning process. Detailed calculations, by means of the FLUKA Monte Carlo simulation code of the induced radioactivity inside the storage ring tunnel, have been so started to prepare the release of materials from the regulatory control.

The following process knowledge is fundamental to allow the correct evaluation of induced radioactivity in a particle accelerator:

- The machine operational information, such as operational cycles, beam lifetime, *etc*. (details in section 1.1 and 1.2);
- The storage ring characteristics, such as the general layout and the detailed knowledge of the different accelerator components (material composition, geometry, *etc.*) (section 2.1);
- The physical processes involved in the production of radioisotopes and knowledge of the radioactive decay of the produced radioisotopes (section 2.2).

1.1 The Elettra parameters

In this section useful machine operational information are given.

Elettra is made up by 12 achromat, each containing a long straight section and a short section. The facility routinely operates at two different energies: at 2.0 *GeV* for the 75% of user time and 2.4 *GeV* for the remaining user time.

The facility operates during five cycles per year, whit an average period of eight weeks per cycle, for a total of about 5000 operative hours per year. After a start-up period of four days, the facility runs continuously for beamline operation, interrupted almost every week or 10 days by one or two days of operation dedicated to accelerator physics researches.

The Elettra filling pattern correspond to a maximum stored current of 300 *mA* (at 2.0 *GeV*) and 140 *mA* (at 2.4 *GeV*), with a beam lifetime of about 100 hours in last years.

1.2 Beam loss scenarios

In collaboration with machine physicists, beam loss scenarios occurred during the 30 years of machine activity has been investigated.

Three types of beam losses occur: losses during injection, losses during stored beam decay (for RF cavities or magnets stopping), and losses (wanted or unwanted) during beam dumps.

In Elettra, losses during beam injection are the most relevant one. For this reason, simulations have been performed in this scenario.

In absence of the record of the electron losses track through the years, some conservative assumptions were adopted to increase the radiation levels calculated in simulations, such us the incident beam profile and the target geometry. Details are given below, in section 2.2. Moreover, in addition to simulations, experimental measurements by means of radiochromic films have been carried out inside the storage ring to locate the major machine hotspots, *i.e.* the highest points of losses (details in section 3.1).

2 Simulation studies

Simulations have been performed by means of the FLUKA Monte Carlo particle transport code [3].

2.3 The Elettra storage ring modelling

A FLUKA model of a standard achromat of the storage ring was built. The code includes a detailed (millimetre scale details) three-dimensional description of all accelerator components (magnets, girders, vacuum vessel, etc.) based on manufacturing drawings, detailed in geometry and elemental composition.

The model of some accelerator components and the standard achromat model is shown in Figure 1 and in Figure 2, respectively.

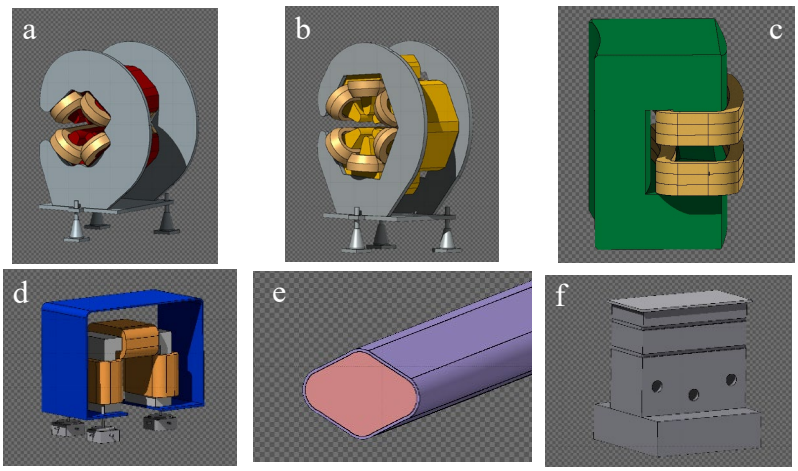

Figure 1. Fluka 3D description of some accelerator components. a) Quadrupole - QBC; b) Sextupole - SBC; c) Dipole (bending) - BAC; d) Corrector - CAC; e) Vacuum vessel; f) magnet support

Figure 2. Fluka 3D model of a standard achromat, section 3.

2.4 FLUKA calculations

Beside the precise geometry modelling, the most accurate models for activation studies were selected in FLUKA: the evaporation of fragments, coalescence effects in the emission of nucleons as well as the photo-neutron production. All hadrons were followed in energy until stopped or captured, including fast and thermal neutrons.

The selected beam energy was 2.0 GeV, and the beam spot was defined with a Gaussian distribution (σ_x = 0.5 *cm*; σ_y= 0.2 *cm*). The beam was assumed to dump on a single location, perpendicular to the surface, without any significant divergence to maximize the activation.

Activation maps have been calculated for all the different storage ring components, such as magnets, vacuum vessel, supports. Preliminary results show that, in general, most of the elements inside the Elettra storage ring will be below the release levels, but further investigations are necessary, especially in the most critical parts of the machine.

By way of example, Figure 3 shows the activation map expected for a quadrupole magnet in two extreme cases: in an ideal case of non-losses (3a), in which activation is only due to Bremsstrahlung photons, and in a very conservative beam losses case (3b), in which all electrons are lost at one point. The highest activation is located on the pole tips and coil in both cases, with about three order of magnitude of difference between them.

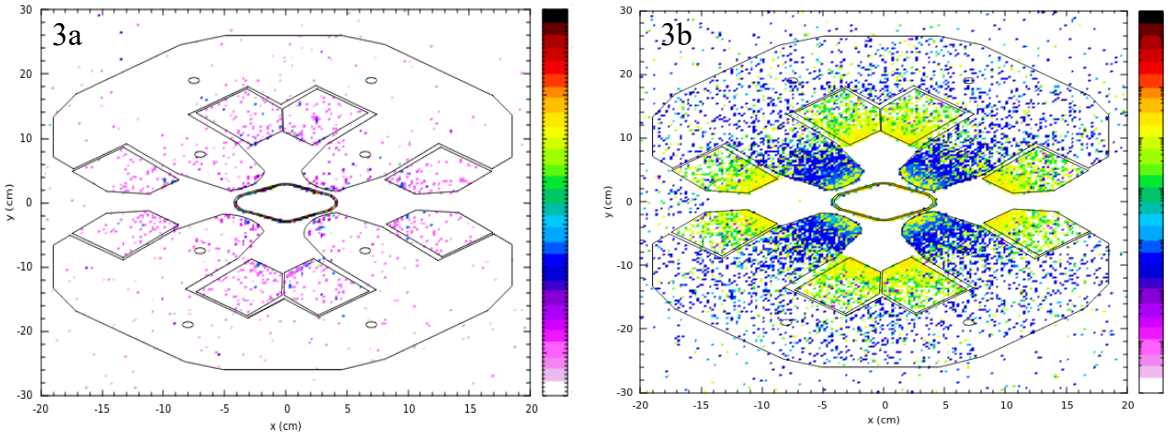

Figure 3. Activation maps for the quadrupole magnet Q3_S3.1.
Total activity (all isotopes) per unit volume integrated over all *z* axis. Cooling time *t = 0s*.
3a) Ideal case of no beam losses (Bremsstrahlung photons activation); 3b) Conservative beam losses case (all electrons lost at one point in injection losses for 30 years).

The determination of the radionuclides is the basis of the release process: A shorted list of nuclides which is expected to find in some accelerator components is reported in Table 1. The result comes from simulations, and the found radionuclides agree with similar studies present in literature for same materials and same primary particles [4], [5].

Magnet Coils (material: copper)	**Magnet Yoke** (material: AISI 1018)	**Vacuum Vessel** (material: AISI 316LN)
Ni-63	Co-56	Mo-99
Co-60	Fe-55	Mo-93
Co-58	Mn-54	Ni-63
Fe-55	Cr-51	Ni-59
	V-49	Co-58
	V-48	Co-57
		Co-56
		Fe-55
		Mn-54
		Cr-51
		V-49
		V-48

Table 1. Exemplary (shortened) nuclides list from activation studies by FLUKA Monte Carlo code.

3 Experimental studies

As mentioned above, experimental activities have been carried out in addition to simulations. The description in below subsections.

3.5 EBT3 radiochromic films measurements

Radiochromic films have been used to map the storage ring in order to locate the machine hotspots.

Radiochromic films are designed to be suitable for the measurement of absorbed doses of ionizing radiation, and their blackening, after the film calibration, is proportional to the absorbed dose.

The films used in this work are the GafChromic EBT3 films [6] (batch number 05122101), and they were handled according to the procedures described in the AAPM TG-55 report [7] and in the user guideline provided by the manufacturer together with the films.

The EBT3 is a self-developing film, it doesn't require post-exposure processing and it can be read with commercial flatbed RGB (Red Green Blue) color scanners.

The film is tissue equivalent and water resistant, its dose response ranges from 1 *cGy* to tens of *Gy*, and it has got a high spatial resolution (about 25 μm).

During 2022, hundred pieces films of dimensions of (4x4) cm^2 where placed along the storage ring, in measure for an average period of eight weeks per cycle: every end of machine cycle, the films were analysed and new ones were replaced before the start of next cycle. Figure 4 shows the machine hotspots' map, and Figure 5 shows the different blackening of the EBT3 films during a machine cycle.

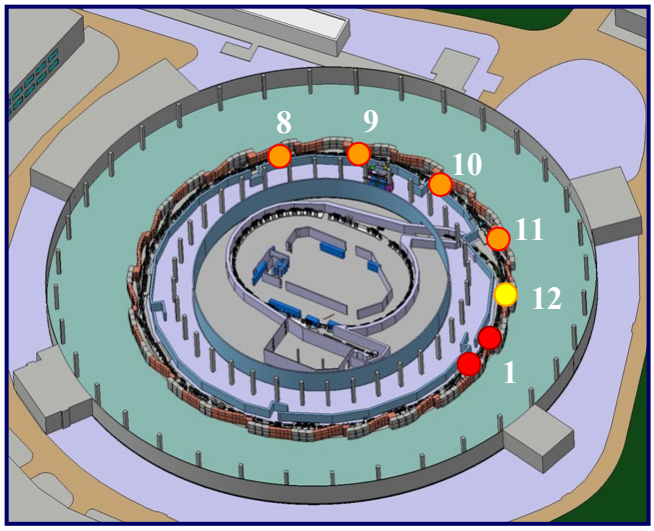

Figure 4. Machine hotspots' map. EBT3 films measurements.
The major beam losses are in section 1 (red dots), the first section after the injection, in which absorbed doses of about 150 *Gy* per cycle were recorded by the films. Films in section 8, section 9, section 10 and section 11 (orange dots) record doses of about 60 *Gy* per cycle, while films in section 12 record doses of about 5 *Gy* per cycle. In other sections non-significant doses were recorded by the films.

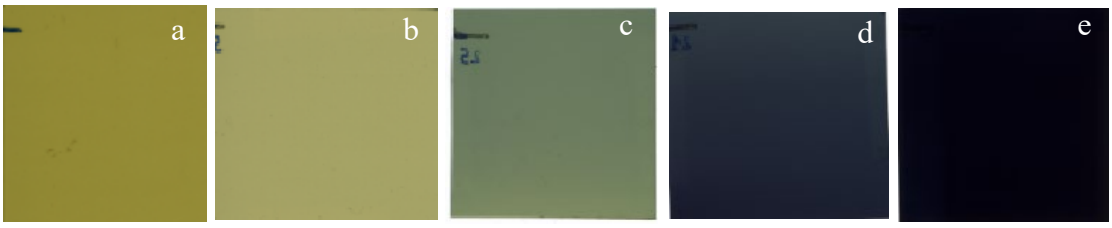

Figure 5. Examples of different blackening of the EBT3 films after one machine cycle.
a) Film non-irradiated; b) Film with non-significant absorbed dose; c) Film from section 12; d) Film from section 11; e) Film from section 1.

3.6 Gamma Spectrometry and Beta Analysis measurements

The GafChromic experimental activity was useful to locate the most critical magnet supports inside the storage ring. These supports need to be released immediately during the decommissioning: it is so necessary to locate the critical ones and make destructive analysis on them to study their activation.

The first support considered is the girder in section 12.1. According to the map in Figure 4 it is not the most critical one, but for these first measures it was in the best position to make coring without create any problem to the machine.

Comparing radiochromic films results and simulation activation results on the magnet support in section 12.1 (see Figure 6), two coring of 5 *cm* diameter have been made: one in the upper part of the support and the other one in the lower part, for a deep of 40 *cm*. These two coring were then divided in smaller samples (each of 3-4 *cm*) and analysed by gamma spectrometry and beta analysis. The gamma spectrometry analyses were made by the radiation protection team at Elettra, for an acquiring time of 7200 *s*, while the beta analyses were carried out by an external company. In both case no radionuclides from activation were found and/or it are under the minimum detectable activity.

Further investigations in other critical supports are planned during next machine shutdowns.

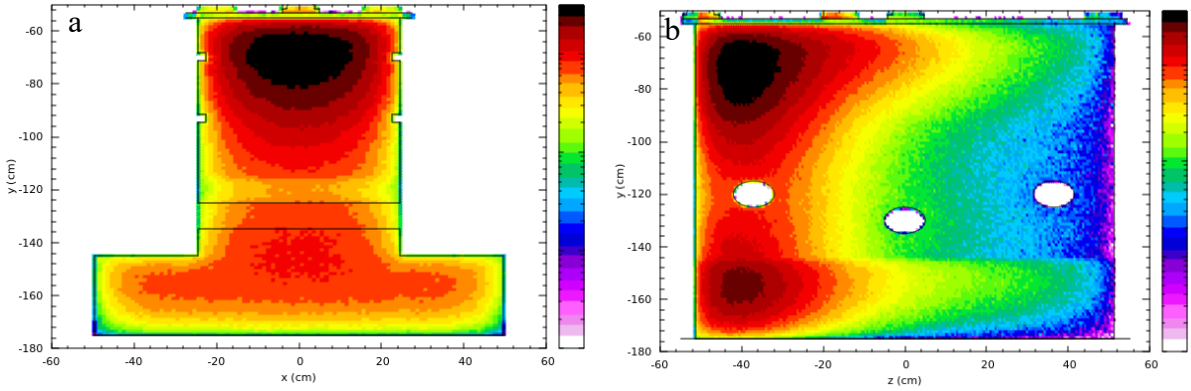

Figure 6. Total activity (all isotopes) integrated over all *z* axis for the first magnet support in section 12.1. FLUKA results. Beam energy 2.0 *GeV*. Cooling time $t = 24$ *h*. Conservative beam losses case.
a) Girder activation - front view; b) Girder activation - lateral view.

4 Conclusions

The present paper provides a preliminary study of the induced radioactivity in the Elettra storage ring. Calculations and measurements suggest that, in general, Elettra storage ring will be below the release levels, significant activation occurs only in few areas, essentially downstream of the injection zone. However, even in these areas, activation will be limited to components, vacuum vessels, close to the electron beam. Further experimental investigations and improvements in calculations are in progress.

References

[1] - E. Karantzoulis, et al., *The Elettra 2.0 Project*, Proc. IPAC2022 (2023)
[2] - Legislative Decree 31st of July 2020, n. 101. Implementation of council directive 2013/59/Euratom
[3] - A. Fassò et al., CERN-2005-**10**, INFN/TC_05/11, SLAC-R-**773** (2005)
[4] - M. Brugger, et al., PNST **4,** 363-366, (2014)
[5] - P. Berkvens, Radiat. Prot. Dosim. **115 (1-4)**, 475-480, (2005)
[6] - Ashland, http://www.gafchromic.com/gafchromic-film/radiotherapy-films/EBT/index.asp (2023)
[7] - AAPM TG-55, Rep. 63, Med. Phys. **25.11**, 2093-2115, (1998)

Decommissioning of UVX, the first Brazilian synchrotron

Moura F.N. [1], Lima L.P[1], Neto F.A.B[1], Szabo T.V[1], Moraes IC[1], Madacki R[1].

[1] Brazilian Center for Research in Energy and Materials (High Technology Polo II - R. Giuseppe Máximo Scolfaro, 10000 - Bosque das Palmeiras, Campinas - Brazil)

1 Introduction

In 1997, the Brazilian Synchrotron Light Laboratory (LNLS) started a second-generation synchrotron light source, called UVX, which operated with electron beams at an energy of 1.37 GeV and 250 mA. The injection system included a 120 MeV linear accelerator and a 500 MeV Booster. The machine operated in decay-mode, with two injections per day and most of the beamlines were based on dipole magnets. On August 2019, the UVX synchrotron light source ceased operation for user research activities.

2 Objective

In Brazil, the Brazilian Nuclear Energy Commission defines radiation protection standards for all radioactive installations. For the decommissioning of the UVX, the general recommendation was followed with the writing of the decommissioning plan, practical actions for monitoring the machine components and storage the individual dose history.

Simulations with FLUKA.CERN [1] were performed to evaluate possible activation points after 22 years of operation.

3 Methodology and results

In absence of the record of the electron losses tracks through the years, some conservative assumptions were adopted to increase the radiation levels calculated, such as the incident beam profile and the target geometry.

The analysis of electron beam losses considered the transfer lines between the linac, booster, and storage ring, as well as the normal beam lifetime. The study also included an evaluation of the activation due to high energy photons from Gas Bremsstrahlung. The beam incidences in simulation were concentrated on a single location, perpendicular to the surface, without any significant divergence to maximize the activation. However, during the operation, the beam losses occurred at a grazing incidence, distributed across the accelerator component. The scenarios with the highest activation potential found were due to losses in the linac transfer line and per lifetime in the storage ring. The worst-case material was steel.

in active monitoring Geiger muller (GM), ionization chamber and gamma spectrometer were used in active monitoring. The UVX magnetic lattice was monitored before being disassembly and only the final dipole of the linac to booster showed counts above 20 cps and 0.2 uSv/h. A detailed monitoring procedure was defined in parts with dose potential by literature [2] and simulation results. All points remained within the natural background radiation (0.1 uSv/h) whose result agrees with calculations.

4 Conclusion

The recommendations of the Brazilian radioprotection standards were followed and there were no complications during the disassembly of the machine, which took place two years after the end of its operation. Even with the enormous conservatism employed, due to the

absence of records with defined parameters, the results obtained in the simulations showed activation levels comfortably below the limits. As a lesson learned, it is recommended to draw up a decommissioning plan detailing frequent beam loss locations, recorded values, and machine parameters that can be used in analytical calculations or simulations for future generations.

References

[1] Cerutti, F., et al. “New Capabilities of the FLUKA Multi-Purpose Code", Frontiers in Physics 9, 788253 (2022).
[2] IAEA. Decommissioning of particle accelerators. International Atomic Energy Agency, 2020.

Combining Alanine Dosimeters and Monte Carlo Simulations: A method for demagnetization forecast by high dose exposure

Moura F.N. [1], Moraes I.C. [1], Estevão D.M.M.[1], Neto F.A.B[1], Rodrigues Jr. O.[2]

[1]Brazilian Center for Research in Energy and Materials (High Technology Polo II - R. Giuseppe Máximo Scolfaro, 10000 - Bosque das Palmeiras, Campinas - Brazil), [2]Nuclear and Energy Research Institute (Professor Lineu Prestes Avenue, 2242 University City São Paulo, São Paulo – Brazil)

1 Introduction

Sirius, the new Brazilian synchrotron, was designed to operate with 3 GeV, 350 mA in top-up mode and 0.25 nmrad of emittance, which represents a photon flux per second of the order of 6.5×10^{16} for bending device. According to the literature [1], high-dose deposition by photons and neutron generation represents a long-term risk of demagnetization of magnetic lattice components.

2 Objective

This work presents the results of experiments carried out with alanine/EPR [2] dosimeters and Monte Carlo simulations with the FLUKA.CERN [3] code to investigate photon and neutron dosimetry.

3 Materials and methodology

The use of high-dose dosimeters composed of alanine and read by Electron Paramagnetic Resonance (EPR) appears as a viable and robust dosimetry method for monitoring throughout the useful life of the machine. In this study, at each measurement point, three alanine pellets purchased from Bruker BioSpin Corporation were placed in a PLA holder.

In the first experiment, with 12 months of exposure, the dosimeters were positioned on central permanent magnetic dipoles, called BC, made of NdFeB during the machine commissioning phase. The current increased from 5 to 40 mA, and the main objective was to confirm which region of the BC (begin, middle or end) would present the highest dose.

4 Results and discussion

As a result, the middle region of BC (BC01) showed a maximum measured value of 386±10Gy. For the simulations, a segment of the ring was modelled, including a BC and the alanine dosimeters (Figure 1a). Due to the absence of the electron losses tracks, the dose maps around the dosimeter's region were evaluated for various beam losses profiles (Fig. 1b) for different types of particles, indicating a neutron contribution for dose lower than 1%.

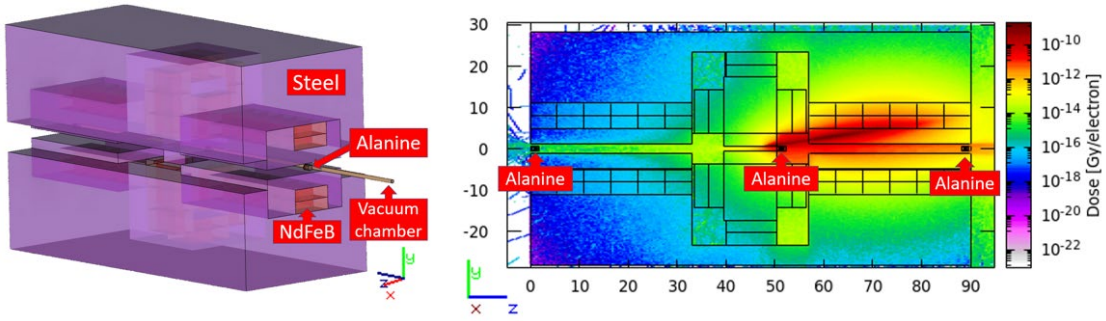

Figure 1: (a) Simplified BC geometry in FLUKA (b) Vertical dose distribution for an arbitrary beam loss.

5 Perspectives

The work represents a promising validation methodology between experimental dosimetry and simulation. Furthermore, new measurement points will be considered due to the installation of new beamlines, beam current increase, operation in top-up mode, and experimental evaluation of the contribution of neutrons.

References

[1] Samin, Adib J. "A review of radiation-induced demagnetization of permanent magnets." Journal of Nuclear Materials 503 (2018): 42-55.

[2] "Numerical analysis of the alanine response using Monte Carlo: Correlation with experimental results." Radiation Physics and Chemistry 190 (2022): 109824.

[3] Cerutti, F., et al. “New Capabilities of the FLUKA Multi-Purpose Code", Frontiers in Physics 9, 788253 (2022).

Estimation of long target effect using multi-points kernel method in synchrotron radiation shielding calculation

Asano Y.

Research centre for nuclear physics Osaka university
10-1 Mihogaoka Ibaraki Osaka, 567-0047 Japan
Radiation science centre High energy accelerator research organization KEK
1-1 Oho Tukuba Ibaragi, 305-0801 Japan

Abstract

Multi-points kernel method is improved to compare a point kernel method and Monte Carlo code to estimate the leakage dose distribution with and without considering buildup effect and photon polarization effect. As the results, Maximum leakage doses are almost same between the multi-point kernel method and a point kernel method, so that shielding design does not need revised, and the position of maximum leakage dose is improved by using the multi-points kernel method.

1 Introduction

Synchrotron radiation beams have huge intensity with low energy, and the photons are strong attenuation condition. In addition, the beamline components, its placement, and the beam directions are usually variable easily. The shielding design and the leakage dose estimation, therefore, must be carried out carefully and quickly for each beamline. And these must be conservative in the viewpoints of safety.

Generally, in order to satisfy such requirements, the point kernel with scattering method [1] is used for the shielding design of the synchrotron radiation beamlines. In addition, due to the development of computers and the improvement of the usability of general-purpose Monte Carlo codes, these codes such as FLUKA [2] and PHITS [3] are employed for detailed evaluation of the shielding conditions. Both tools are useful. However, each code has some important points to use to shielding design for synchrotron radiation beamline. For example, it is important to evaluate the buildup effect and target self-shielding for using point kernel method and how to apply the weighting factor for the photon energy distribution and photon energy step for Monte Carlo codes.

For the point kernel with scattering method is generally employed the fixed scattering point that is the photon injection point to the target and summing up the scattering photons due to the target with considering the self-shielding to obtain the rapid assessment of the shielding condition. In the case of the thin target in comparison with the distance of the estimation points and almost design cases of the hutch shielding can be applied, this method is effective to quick estimate the leakage doses with satisfied accuracy. However, there are some problems for the long target cases. To clear these problems, the multi-points kernel with scattering method (MPKM) are improved and compered to the standard point kernel method.

2 Multi-points kernel with scattering method

The sizes of synchrotron radiation beam are small and the target lengths within the optical elements are generally short in comparison with the distance from the injection points to the estimation points so that the point can be adopted to the injection area and the

scattering point for the leakage dose estimation as illustrated in Fig.1 including the relation between the scattering point and the leakage estimation points. In these cases, the scattering angel from the beam axis to the estimation point can be assumed to the fixed scattering angle and the total scattering photons including K-fluorescent photons with the same scattering angle can be integrated as shown in formulas as follows.

$$\Phi(E,\theta,\emptyset) = \frac{\Phi_{CS}(E,\theta,\emptyset)}{r^2} + \frac{\Phi_{IS}(E\rightarrow E',\theta,\emptyset)}{r^2} + \frac{\Phi_{FL}(\mathrm{E})}{4\pi r^2} \quad \text{-----(1)}$$

where Φ(E,θ,ø) is the energy, *E*, spectrum at the estimation point that is the distance, *r*, from the injection point with the scattering angle, θ, and azimuthal angle,ø. The first term of the right hand side formula is the total photon flux due to coherent scattering as indicated in formula (2).

$$\Phi_{CS}(E,\theta,\emptyset) = \int_0^L (\sum_{CS}(E,\theta,\emptyset) * \Phi_0(E) e^{-\mu(E)*l} * e^{-\mu(E)*m(\theta,\emptyset)}) dl \quad (2)$$

where $\Phi_{CS}(E,\theta,\emptyset)$ is the total photon fluence with the direction of θ and ø due to coherent scattering. L is the effective target length as shown in Fig.1 and $\sum_{CS}(E,\theta,\emptyset)$ is the cross section of the cohent scattering with considering photon polarization. $\Phi_0(E)$ is the synchrotron radiation source spectrum and $e^{-\mu(E)*l}$ is the photon attenuation by the target with the target thickness *l* and the attenuation coefficient of $-\mu(E)$. The last term, $e^{-\mu(E)*m(\theta,\emptyset)}$, is for the target self-shielding with the track length, $m(\theta,\emptyset)$, of the scattering photons within the target. The second term is the total flux with the direction of θ and ø due to incoherent scattering as follows,

$$\Phi_{IS}(E\rightarrow E',\theta,\emptyset) = \int_0^L (\sum_{IS}(E\rightarrow E',\theta,\emptyset) * \Phi_0(E) e^{-\mu(E)*l} * e^{-\mu(E')*m(\theta,\emptyset)}) dl \quad \text{---(3)}$$

where $\sum_{IS}(E\rightarrow E',\theta,\emptyset)$ is the incoherent scattering cross section. In this scattering process, the photon energy is changed from *E* to *E'* depending on scattering angle (θ, ϕ) so the specrum must be converted to sum up the total scattering spectrum. The third term is the flux due to the fluorecence photons as follows,

$$\Phi_{FL}(\mathrm{E}) = \int_0^L (\sum_{FL}(E,\theta,\emptyset) * \Phi_0(E) e^{-\mu*l} * e^{-\mu(E)*m(\theta,\emptyset)}) dl \quad (E=E_k) \quad \text{- (4)}$$

$$\Phi_{FL}(\mathrm{E}) = 0 \quad (\mathrm{E} \neq E_k) \quad \text{---(5)}$$

where $\sum_{FL}(E,\theta,\emptyset)$ is the K-fluorecence emission cross section and photon energy is E_k.

Then the leakage doses outside the shield wall can be calculated using the formula (6).

$$D_{(\theta,\emptyset)} = \int_0^{Emax} C(E) * B(E,T) * \Phi(E,\theta,\emptyset) * e^{-\mu_T(E)*T}\, dE \quad \text{---(6)}$$

where $D_{(\theta,\emptyset)}$ is the leakage outside the shield wall at the scattering angle θand azimuthal angle ø . $C(E)$ and $B(E,T)$ are the conversion factors from the photons with energy *E* to doses and the buildup factor of the shield wall with the thickness of *T*, respectively. The $\mu_T(E)$ is the attenuation coefficient of the shield wall.

For the shielding calculation of synchrotron radiation beamlines, the point kernel with scattering method is useful in almost cases to obtain the satisfactory results with quickly and conservatively. However, some different leakage distribution will be appeared for long targets in comparison with the distance from the injection point to the shield wall. To

compensate the disadvantage, the MPKM method is improved by using segmented targets as illustrated in Fig.2.

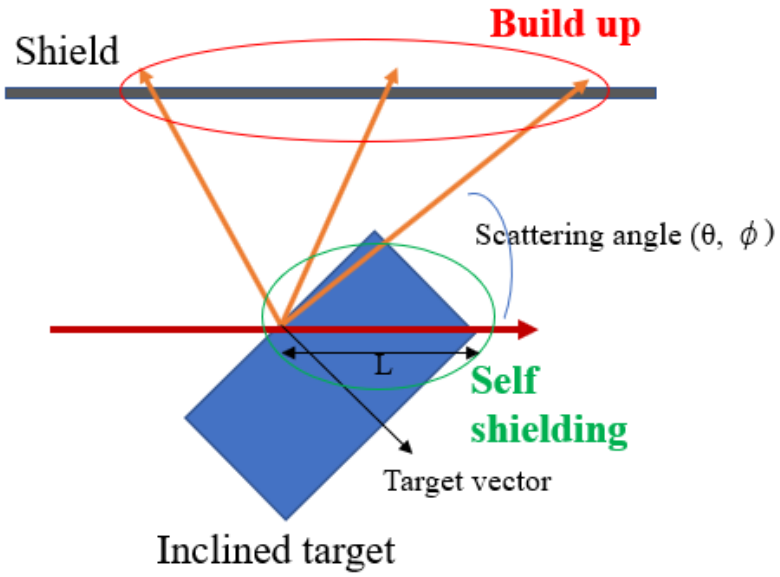

Figure 1: Conceptual illustration of a point kernel method with scattering using STAC8[1].

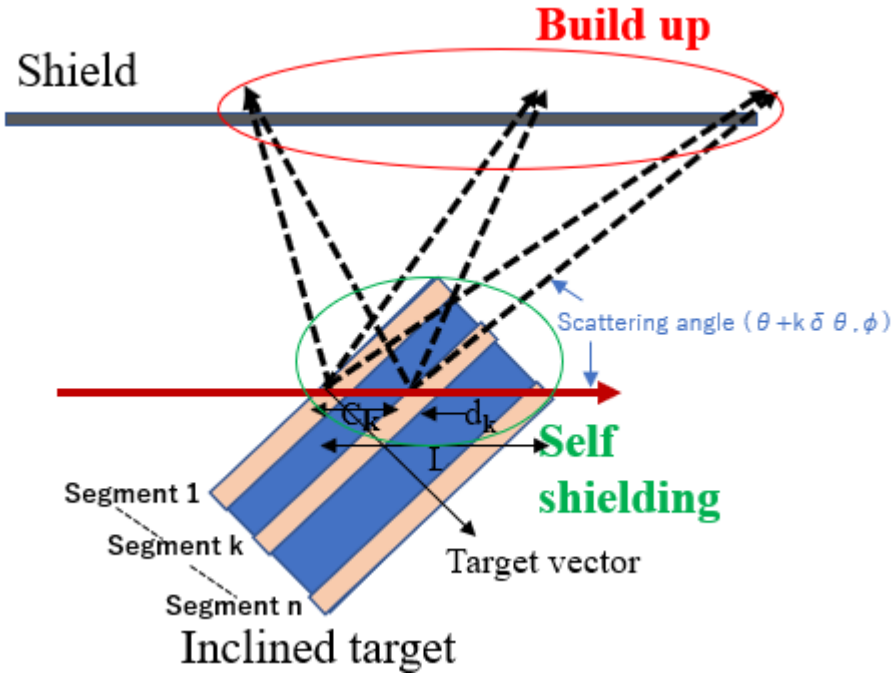

Figure 2: Conceptual illustration of multi-points kernel with scattering method.
"C_k" is the thickness from the surface of the target to the segment k. "d_k" is the effective track length of the segment k with the scattering angle (θ+kδθ, ϕ).

The formula to obtain the leakage dose distribution by using the MPKM method are almost same as formula (1) to (6) fundamentally. The main differences are (1) photon injection points are moved to C_k for the segment k. (2) With this movements, the scattering angle (θ+kδθ, ϕ) depends on each segment k. And (3) Due to the movement of the injection point, the photon spectra are attenuated by the thickness C_k of the target. (4) Due to the movement of the injection point, the self-shielding effect is changed for each segment k. (5) Each leakage dose is summed up by the leakage dose due to each segment k under the consideration of these differences. There are many types of the MPKM method for

synchrotron radiation beamlines. One is the uniform increase in scattering angle ($\delta\theta$=constant). In this case, the effective track length of the segment (d_k) depends on the scattering angle, and this method is reasonable in almost cases because of strong dependence of leakage dose on scattering angle. The other one is the uniform increase in segment effective track length (d_k=constant). In this case, the increment scattering angle of $\delta\theta$ depends on the segment number k , and both methods are almost same, fundamentally.

3 Calculation results using multi-points kernel with scattering method and compare to another method

To verify the effectiveness of the MPKM method, the calculation results of the SLAC SLM beamline [4], [5] have been compared to that of Monte Carlo and point-kernel methods. The SLAC SLM beamline was analysed precisely by the different groups independently and the consistent results were presented. The geometry of SLM is shown in Fig.3. In this case, the target is a silicon mirror with the thickness of 3.8mm and the synchrotron radiation photon beam hits the mirror with the glancing angle of 9 degrees. Two silicon oxide plates are regarded to the shield wall and the distance of the estimation points of leakage doses are 1m far way from the target. The spectrum of the synchrotron radiation photon beam calculated by STAC8 is shown in Fig.4, and the maximum stored electron current is 500mA. In this case, almost photons with over 1keV energy are scattered by this mirror.

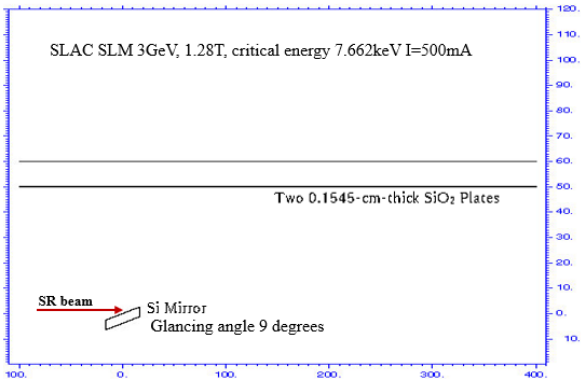

Figure 3: Geometry for the simulation of synchrotron radiation, emitted from the **SPEAR3 bending magnet**, hitting the Si mirror. The mirror is 9 degrees inclined relative to the beam direction (i.e., +Z axis). Polarization vector points toward +X. The shielding is two SiO_2 plates, parallel to the Z axis and each 0.1545 cm thick. The dose is scored at 1 m away from Z axis (i.e., X=100 cm)[4].

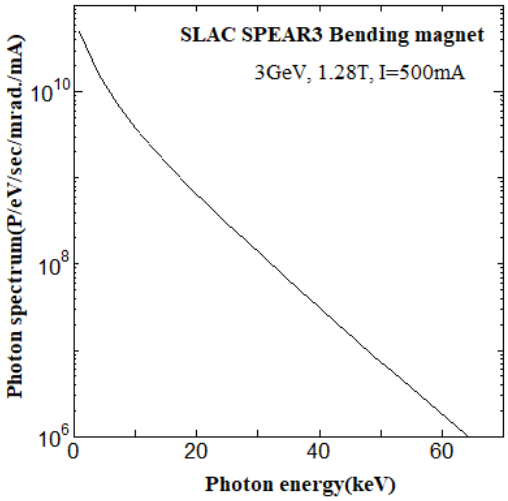

Figure 4: Photon energy spectrum of SPEAR3 bending magnet with the electron energy of 3GeV and the magnetic field strength of 1.28T. The critical energy is 7.662keV.

Figure 5 shows the calculation results using STAC8v25 for one point kernel method and MPKM method with considering photon polarization effect and without considering build up effect including advanced EGS4 (EGS5) [6] simulation results. In this MPKM calculation, the δθ was fixed to 0.1 degrees and k depends on θ from 1 to 22. In these calculations, the results are almost same, however there are some important points. One is that both STAC8v25 and MPKM calculation results of maximum leakage doses are less than that of EGS4 without considering buildup effect. One is that the position of the peak leakage dose by MPKM is moved from that of STAC8v25 to that of EGS4, and this indicates the effectiveness of MPKM to find out the position of the peak leakage dose. The other is the depression distribution of leakage doses at almost 90 degrees with considering photon polarization.

Figure 6 shows the leakage dose calculations with considering the buildup effect. The differences in comparison with and without considering buildup effect are that both leakage dose distributions by using STAC8 and MPKM on P=0 cases obtained almost the same maximum leakage dose level, and both kernel methods with considering buildup effect estimate conservative values in comparison of the EGS4 simulation. In addition, the peak position of the leakage doses by using MPKM is improved and consistent with that of EGS4. These are important for the shielding design of synchrotron radiation beamlines. For the cases of long distance along Z, there are large gaps between the EGS4 results and both STAC8, MPKM results. The slant length of the shield wall is long so that the buildup effect will be overestimated in case of the small angles of scattering such as the large distance along Z in Fig.6, however there are no problems for the shielding design because of low leakage doses.

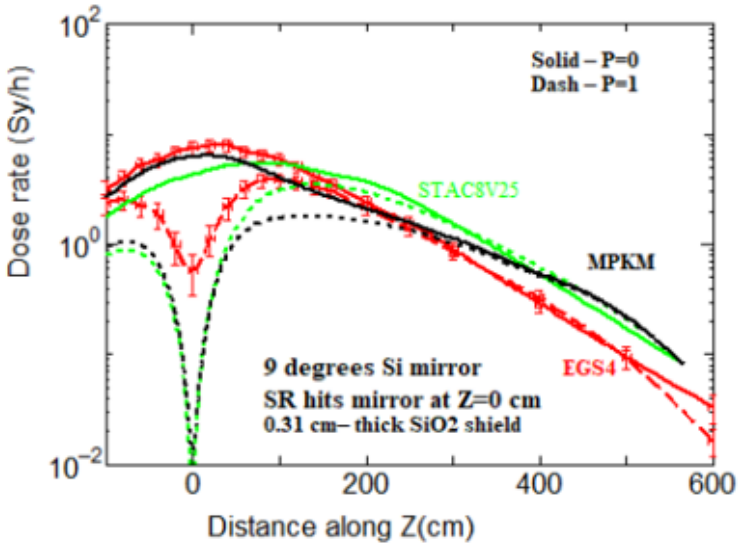

Figure 5: Comparison of the calculation results of leakage dose outside the mirror case of the SLAC SLM beamline. The results of STAC8v25 and MPKM are without considering buildup effect. The solid lines indicate the leakage doses on the parallel direction of the photon polarization vector and the dashed lines are on the perpendicular direction.

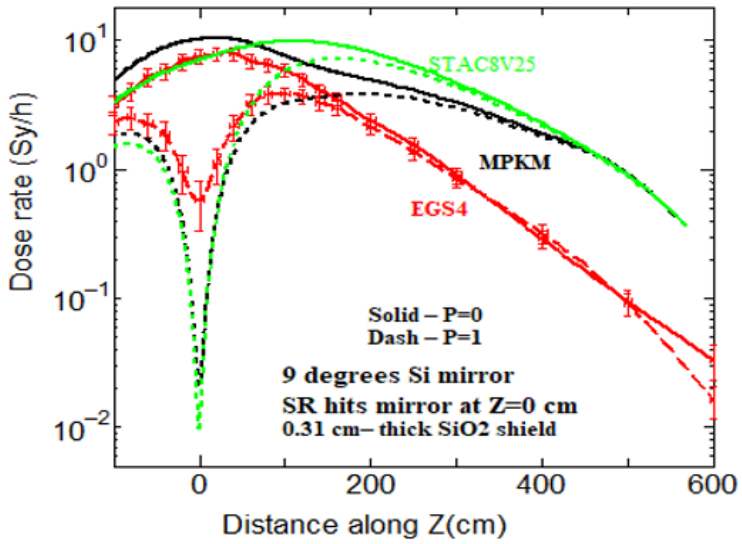

Figure 6: Comparison of the calculation results of leakage dose outside the mirror case of the SLAC SLM beamline with considering build up effect. Others are the same as Fig.5.

4 Summary

Point kernel methods with scattering is useful for designing the shield of synchrotron radiation beamlines with quickly and conservatively. These codes ae focused to use to shielding design of the synchrotron radiation beamlines, however these methods are not general-purpose codes. The point kernel methods with scattering have some limitations for the cases of long target compared to the distance from the target to the estimation points. In the cases, there are some possibilities that the position of the maximum leakage dose outside the shield wall will be shifted. Using segment targets and the multi-points kernel method, the improvements were performed, and the calculations were compared to Monte Carlo code. The results were obtained within good consistency, even though the long calculation times were necessary.

As is well known, there are some special techniques for shielding design of synchrotron radiation beamline to use Monte Carlo codes because of strong attenuation conditions and huge intensity photons. The point kernel methods and the multi-points kernel methods with scattering have some limitations even the Monte Carlo codes so that it is required to compare the methods each other and to use these codes under well-known synchrotron radiation beamline systems, components, and the radiation physics.

References

[1] – Y.Asano, JAERI-Research 2001-006, JAERI (2001).
[2] – A.Ferrari, P.R.Sala, A.Fasso, and J.Ranft, CERN-2005-10(2005), INFN/TC_05/11, SLAC-R-773, (http://www.fluka.org)
[3] – T. Sato, et.al., J. Nucl. Sci. Technol. 55, 684-690 (2018). (https://phits.jaea.or.jp)
[4] – Y Asano and J.C.Liu, Proc. of the 10th EGS4 Workshop on KEK Proceedings 2002-18 p48-54 Tukuba,
[5] – J.C.Liu, A.Fasso, A.Prinz, S.Rokni, and Y.Asano, Radiation Protection Dosimetry Vol. **116** pp.658-661 (2005)
[6] – Y.Namito, and H.Hirayama, LSCAT ;Low Energy-Photon Scattering expansion for EGS4code », KEK Internal 2000-3 (2000)